APPROXIMATION TECHNIQUES FOR SINGLE MODE OPTICAL FIBRES

Conleth Denis Hussey

A thesis submitted for the degree of
Doctor of Philosophy
at the Australian National University,
Canberra

December 1981

PREFACE

This dissertation is an account of work carried out in the Department of Applied Mathematics, Research School of Physical Sciences, Australian National University, during the period between January 1979 and December 1981, for the degree of Doctor of Philosophy.

Part 1, the study of the vector corrections to the scalar wave equation, was carried out under the supervision of Professor Allan W. Snyder and in close collaboration with Drs. J.D. Love and Rowland A. Sammut.

Part 2, which develops and applies the moment characterization of single mode fibres, is the result of a joint effort with Dr. Colin Pask.

None of the work reported here has been submitted to any other institution of learning for any degree.

Conleth D. Hussey

C.D. Hussey

PUBLICATIONS

1. Sammut, R.A., Hussey, C.D., Love, J.D., Snyder, A.W.: "Modal analysis of polarization effects in weakly guiding fibres", *I.E.E. Proc. Part H* 128, 173-187 (1981).

2. Love, J.D., Hussey, C.D., Snyder, A.W., Sammut, R.A.: "Polarization corrections to mode propagation on weakly guiding fibres", *J. Opt. Soc. Am.* (submitted).

3. Hussey, C.D., Pask, C.: "Single mode fibres in a few moments", *Electron. Lett.* 17, 644-645 (1981).

4. Hussey, C.D., Pask, C.: "The theory of the profile moments description of single mode fibres", *I.E.E. Proc. Part H* (submitted).

5. Hussey, C.D., Pask, C.: "Characterization and design of single mode optical fibres", *Opt. & Quantum Electron.* (submitted).

6. Hussey, C.D., Pask, C.: "Waveguide dispersion in single mode fibres with on-axis dips", *J. Opt. Soc. Am.* (submitted).

ACKNOWLEDGEMENTS

It has been my privilege to have carried out my Ph.D research at the Department of Applied Mathematics at the A.N.U.

The enthusiastic and yet relaxed atmosphere of the Department is due predominantly to the personality of its founding guru, Barry Ninham. Barry's hospitality on my initial arrival in Australia and his continued concern throughout my stay has made the writing of this thesis a most enjoyable task, for this I am very grateful.

Allan Snyder's scientific insight and his stress on physical concepts has had a profound influence on the work contained in this thesis.

I owe my greatest thanks to Colin Pask, whose understanding of the subject and readiness to discuss any aspect of the work has helped greatly towards the successful and speedy completion of this thesis.

I would like to thank John Love for his willingness to allow me to take advantage of his mathematical ability, and Rowland Sammut for his endless patience while introducing me to some of the techniques in the field of optical waveguide theory.

Thanks to Norma Chin for the admirable skill and good humour with which she tackled the production of this thesis.

I am sincerely grateful to my parents for the constant interest and encouragement they have shown throughout my studies.

The completion of this thesis on time is due wholly to my wife, Daniela, who drew the figures and proofread the manuscript. Her love and support have kept me sane over the past few months.

Finally, I thank the Australian National University for the award of a Ph.D scholarship.

ABSTRACT

The single mode optical fibre has become recognized as the most promising transmission medium for future high capacity communication. In this thesis we study approximation techniques for analysing propagation on single mode fibres of arbitrary refractive index profile. The subject matter of the thesis falls into two main categories:

(1) the analysis of the accuracy of the weak guidance or scalar approximation and its extension for those parameters for which the scalar theory breaks down; and

(2) the development of accurate approximation techniques within the weak guidance theory which lead to simple formulae, which are useful in engineering applications, for all modal parameters.

In Chapter 1 we provide some necessary background information for the thesis and discuss the weak guidance approximation.

In Part 1, which consists of Chapters 2 - 4, we develop methods which enable us to derive expressions for the vector (or polarization) corrections to the scalar wave equation. These methods avoid the substantial effort required in solving the exact electromagnetic (vector) problem.

In Chapter 2, we introduce the perturbation theory for analysing the vector corrections. The perturbation expansion is such that the scalar wave equation forms the first term. Higher terms are then the required corrections.

In Chapter 3, a full eigenfunction expansion method is presented for determining the higher-order corrections. This uses the full spectrum of scalar modes on the circular fibre to determine expressions for vector (or polarization) corrections on both the circular and non-circular fibre. The analysis is presented in closed

form for the step refractive index case.

In Chapter 4, a power series method is derived for the special case of the power law profiles. This method is simpler and more direct than the eigenfunction method but is restricted in application to this special class of profiles. The results for the infinite parabolic and the step as analysed in Chapter 3 are also presented on graphs. We give a general discussion of the results of Part 1.

Having established the accuracy and limitations of the scalar wave theory in Part 1, we proceed to Part 2 to the development of a characterization of single mode fibres, within the scalar approximation, the aim being to provide simple yet accurate formulae suitable for fibre design.

Chapter 5 contains a general introduction by outlining previous characterizations of single mode fibres. We also produce two numerical techniques for solving the scalar wave equation for arbitrary refractive index profiles. One is a variational method based on the moments of the refractive index profile and the other, a Green's function technique which can be modified for W-type profiles.

In Chapter 6, a universal characterization of single mode fibres is presented. This is based on the first three moments of the refractive index profile. The properties of moments and their relationship to profile shape are examined. We derive simple formulae, in terms of universal parameters for all modal properties of interest.

In Chapter 7, the moment method is applied in some fibre design examples. The moments are related to directly measurable quantities on the fibre or on the preform. These quantities are used in our examples.

In Chapter 8, we examine dispersion in the region where the effective waveguide parameter $\bar{V} \cong 3$. The simple expressions in terms of the moments, as derived in Chapter 6, break down in this region, however, the profile can still be characterized by moments. Our examples deal with step fibres with on-axis dips but the methods presented are general.

In Chapter 9, we examine radiation from the fundamental mode in single mode fibres. Approximation methods are examined and an equivalent step based only on the first moment of the refractive index profile is found to be adequate for analysing the radiation.

C O N T E N T S

PREFACE ii
PUBLICATIONS iii
ACKNOWLEDGEMENTS iv
ABSTRACT v

CHAPTER 1. SINGLE MODE OPTICAL FIBRES

1.1 Introduction 1
1.2 The Single Mode Optical Fibre 4
1.3 The Weak Guidance Approximation 7
1.4 Outline of the Thesis 9
References 12

PART I
VECTOR THEORY OF SINGLE MODE OPTICAL FIBRES

CHAPTER 2. PERTURBATION THEORY FOR POLARIZATION EFFECTS

Preamble 14
2.1 Introduction 14
2.2 The Vector Wave Equation and Exact Modal Parameters 17
2.3 Expansion of the modal Parameters and the Scalar Wave Equation 19
2.4 Governing Equations 20
2.5 Resumé 26
References 27

CHAPTER 3. EIGENFUNCTION METHODS

Preamble 28
3.1 Introduction 28
3.2 Modes of the Scalar Wave Equation 29

3.2.1 Perturbation theory for non-circular fibres 34

3.3 Zeroth Order Modes of the Vector Wave Equation 36

3.3.1 Perturbation theory for the vector wave equation 38

3.4 Vector Corrections for the Step Profile 40

3.5 Birefringence in Waveguides with Elliptical Cross Section 43

3.6 Resumé 44

Appendix — Details of the Contour Integration 45

References 47

CHAPTER 4. POWER SERIES METHODS

Preamble 49

4.1 Introduction 49

4.2 Infinite Parabolic Profile 50

4.3 Clad Power-Law Profiles 52

4.4 Results 57

4.4.1 Propagation constant 57

4.4.2 Group Velocity 57

4.4.3 Waveguide dispersion 60

4.4.4 Modal fields 60

4.5 Discussion 66

References 68

PART II

SCALAR THEORY OF SINGLE MODE OPTICAL FIBRES

CHAPTER 5. APPROXIMATE AND EXACT SOLUTIONS TO THE SCALAR WAVE EQUATION ON SINGLE MODE FIBRES

5.1 Introduction 69

5.2 Characterization Methods 71

5.2.1 The effective waveguide parameter $\bar{V}$ 71

5.2.2 Profile shape dependent methods 72

5.2.3 Theoretically determined equivalent profiles 73

5.2.4 Experimentally defined equivalent profiles 74

5.3 Numerical Methods 75

5.3.1 The scalar wave equation 76

5.3.2 The variational-exact moment method 77

5.3.3 The variational-few moment method 79

5.3.4 Green's function method — standard profile $n(r) \geq n_{cl}$ 81

5.3.5 Green's function method — "W-type" profiles $n(R) < n_{cl}$ for some $R \leq 1$ 82

5.4 Resumé 88

References 88

CHAPTER 6. MOMENTS DESCRIPTION OF SINGLE MODE FIBRES

Preamble 91

6.1 Introduction 91

6.2 Profile Shape Function and Moments 94

6.2.1 Examples 96

6.2.2 Bounds on the moments 99

6.3 Solving the Wave Equation 101

6.4 Fundamental Mode Parameters 104

6.5 Accuracy 106

6.6 Second Mode Cutoff 109

6.7 Qualitative Features of Modal Guidance 111

6.8 Conclusion 118

References 121

CHAPTER 7. FIBRE DESIGN BY THE MOMENT METHOD

Preamble 124

7.1 Introduction 124

7.2 Formalism 127

7.2.1 Modal field and microbending 128

7.2.2 Pulse dispersion 129

7.3 Refractive Index Data 131

7.4 Error Analysis 136

7.5 Fibre Design 137

7.5.1 Choosing m_1 when the Preform is Given 137

7.5.2 Two parameter designs 139

7.6 The Moment Method and Equivalent Steps 140

7.7 Conclusion 142

Appendix — Formulae and Numerical Data for the Step Index Fibre 143

References 146

CHAPTER 8. WAVEGUIDE DISPERSION AT $\bar{V} \simeq 3$

	Preamble	149
8.1	Introduction	149
8.2	Fibre Parameterization	151
8.3	Results	152
8.4	Conclusion	157
	References	158

CHAPTER 9. RADIATION FROM GRADED INDEX OPTICAL FIBRES

	Preamble	160
9.1	Introduction	160
9.2	The Modification Factor for Tubular Sources with $\cos\ell\phi$ Symmetry	161
	9.2.1 The step profile	161
	9.2.2 The graded profile	163
9.3	Sources with Sinusoidal z dependence	163
9.4	Results for the Fundamental HE_{11} Mode ($\ell = 0$)	165
9.5	Approximations	166
	9.5.1 The equivalent step method	170
	9.5.2 The W.K.B. Approximation	170
	9.5.3 Large Angle Approximation	173
	9.5.3.1 Step index fibre	173
	9.5.3.2 Graded index fibre	173
9.6	Resumé	175
	References	175

CHAPTER 1

SINGLE MODE OPTICAL FIBRES

1.1 INTRODUCTION

Light-wave telecommunication systems using glass fibre waveguides are now being manufactured and installed on a regular commercial basis. The low attenuation, high information bandwidth and low projected manufacturing cost of glass waveguides make them an attractive alternative to the coaxial cables and multiple wire pair cables presently in use.

Already optical fibre systems are being integrated into the telecommunication network of many countries. Applications vary from undersea communication links to domestic inter-city links and from urban trunking to data buses for computers [1]. As Charles K. Kao, one of the pioneers in the field has asserted: "The stage is set for an enrichment of life like that following the invention of the steam engine, the light bulb and the transistor" [2].

At Higashi Ikoma, a model town outside Osaka, Japan, this assertion is becoming a reality. There Japan's Ministry of International Trade and Industry has opened Hi-OVIS (Highly Interactive Optical Visual Information System), a computer and transmission centre linked by optical fibre cable with 158 homes [3]. Participants can shop by television at local stores, get stock market quotations, train timetables and weather reports. Two-way

communication channels provide televised home study courses where a computer checks answers and speeds up or slows down course material as required.

The Hi-OVIS managing director, Dr. Masahiro Kawahata, explains: "The immense signal carrying capacity of a few optical fibres makes it possible to provide many more — and more sophisticated — services than could ever be handled by a like amount of copper wire" [2].

Installed cabled systems have shown losses in the vicinity of 4 dB/km, while laboratory fibre samples have shown losses below 0.2 dB/km, and present objectives are for less than 1 dB/km installed [1]. Dispersion limits for the multimode fibres now being produced are governed mainly by the different delay times of different modes, propagating along the waveguide. These would permit a bit rate exceeding 50 Mbits/s for repeater spacings of at least 10 km [1].

For single mode fibres, where intermodal dispersion is removed, this bandwidth can be increased by up to two orders of magnitude. For instance, experimental data from Japan shows that bandwidths of 1.2 and 1.6 Gbits/s at repeater spacings of 23 km and 15 km respectively are being achieved [4].

Although such high data rates do not represent the majority of today's application, the presence of such high capacity cables would permit long-term growth potential particularly for data transfer in the cables to be installed. Cable replacement is costly and involves considerable inconvenience. Therefore, long-term planning suggests the installation of optical cables with excess bandwidth.

When research in optical communication first began in 1966 [5] the main interest was in single mode fibres, since it was thought that the bandwidth of step index multimode fibres would be too restricted

to exploit the immense information carrying capacity promised by optical frequencies following the recent invention of the laser.

With the development of SELFOC and other graded index fibres, a degree of equalization of delay times for different modes became possible, and the bandwidth available with multimode fibres was greatly increased [6].

Interest then shifted away from single mode fibres for two main reasons. Firstly, the small core diameter (i.e. 5-10 μm, compared with 25-150 μm for multimode fibres) made it difficult to achieve the tight mechanical tolerances required for low loss interconnections and it also produced problems in actually launching light into the fibre. Secondly, the lifetimes of semiconductor lasers, the only small and relatively efficient source possible, were too short.

However, the advances in basic component technology over the last decade have now made feasible the production of second generation equipment involving the single mode fibre.

The production of stable semiconductor laser sources [7] and the improved fabrication processes and jointing techniques [8] for single mode fibres have combined to put the single mode fibre back as the most promising transmission medium for long distance, high capacity communication.

A second consideration in favour of single mode communication is the extreme difficulty in switching multimode light. With a single mode it is possible to efficiently modulate and switch optical power in low cross-talk integrated optical modulators and switches [8].

It is the purpose of this thesis to examine the characteristics of mode propagation on the single mode fibre. In particular we examine and extend approximation techniques [9,10,11] currently in use

and we produce a simple characterization [12,13,14] of single mode fibres which gives formulae for propagation parameters very accurate yet simple enough to serve for engineering applications.

1.2 THE SINGLE MODE OPTICAL FIBRE

A fibre is called single moded if it can propagate only one class of bound mode — called the fundamental or HE_{11} mode.

The basic structure upon which we shall examine the HE_{11} mode is the circularly symmetric optical fibre as shown in Fig. 1(a). The fibre has a "core" of radius ρ and refractive index distribution $n(r)$ (where the dielectric permittivity $\varepsilon(r) = \varepsilon_0 n^2(r)$), and an infinite "cladding" region of uniform refractive index n_{cl} as in Fig. 1(b). To describe the fibre we introduce cartesian axes aligned so that the z-axis lies along the axis of the guide.

At this point we would like to remove any confusion associated with the term "single mode fibre". When we refer to a fibre that is single moded we mean that it can propagate only the two polarization states of the fundamental (HE_{11}) mode. We shall study only one polarization state, as the other is identical but polarized in the perpendicular direction. For example, Fig. 2 shows the two polarization states of the fundamental mode of the step index (i.e. $n(r) = n_{co} = \text{const}$) fibre.

Virtually all profiles described in this work will have circular symmetry and uniform cladding refractive index. Any deviation from these will be explicitly mentioned in the text.

Bound modes propagate unattenuated on a non-absorbing cylindrical waveguide, their fields are everywhere finite. Bound modes have a characteristic propagation constant or eigenvalue determined from an

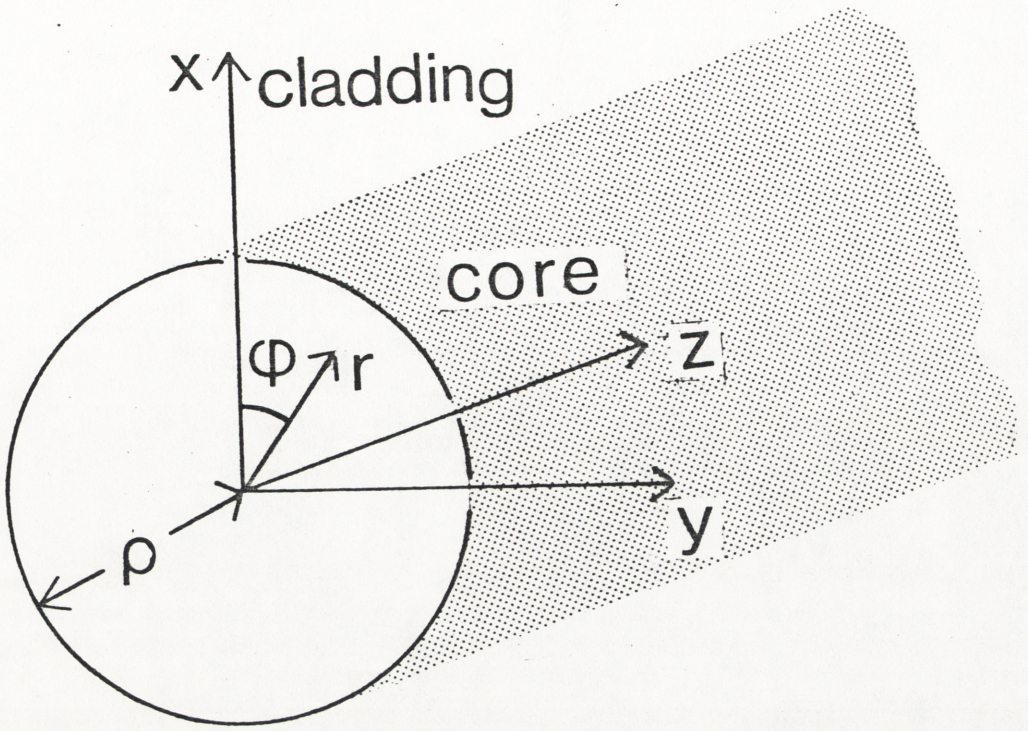

(a)

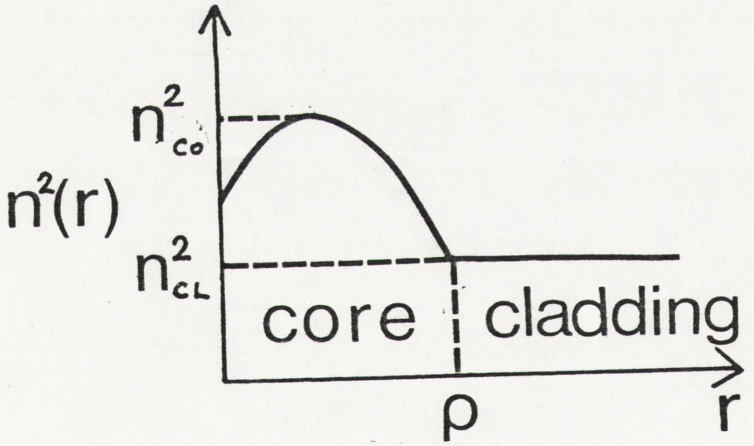

(b)

Fig. 1: (a) Cylindrical polar and cartesian coordinates for describing the fibre. ρ is the core radius.

(b) A typical refractive index profile with n_{co} the maximum core value and n_{cl} the uniform cladding value.

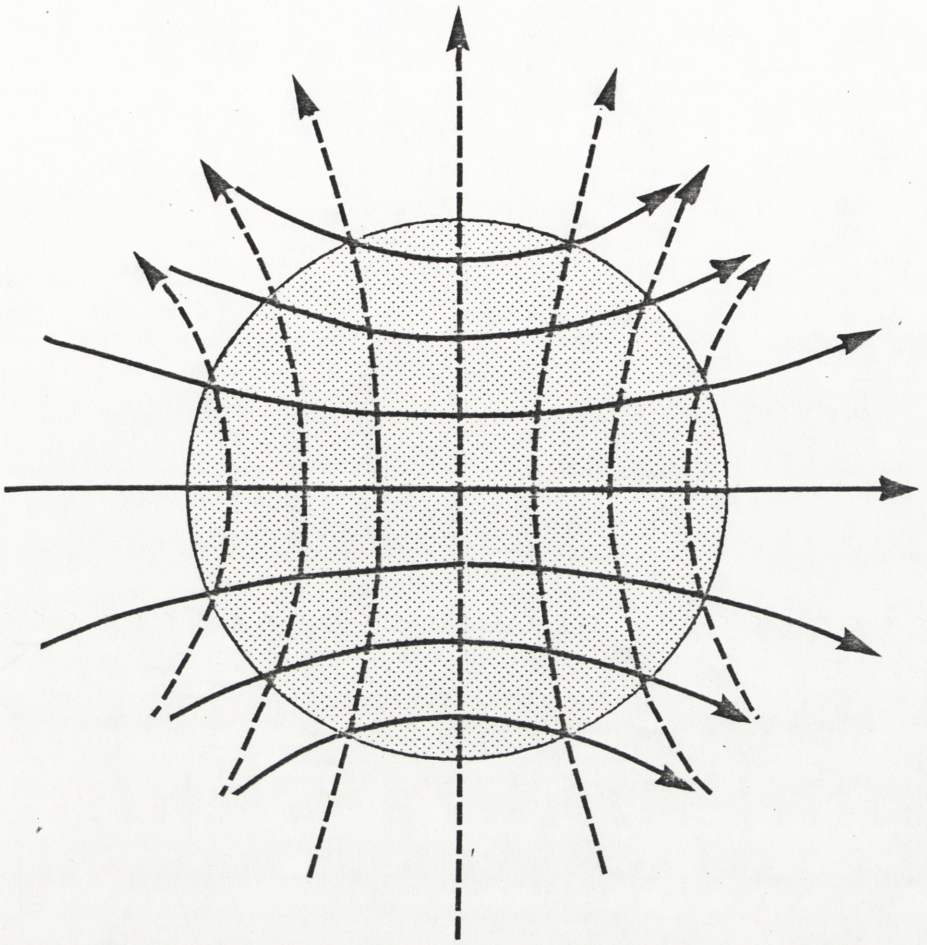

Fig. 2: The two polarization states of the fundamental mode of the step refractive index profile.

eigenvalue equation.

However, although the bound mode fully describes the field far along an ideal non-absorbing fibre, a radiation field is required to describe leakages of power from the core, particularly for power launched into the cladding region and also for power radiated from irregularities and bends. This radiation field can be described in terms of Green's function techniques [15] or by an eigenfunction expansion via the radiation modes [16,17].

1.3 THE WEAK GUIDANCE APPROXIMATION

The only refractive index profile of practical interest for which Maxwell's equations can be solved exactly in analytical form is the step index profile. Even for profiles which can be solved exactly the derivation and representation of the modal fields and propagation constant is often tedious and cumbersome [18,19].

However, the majority of optical fibres used in communication have profiles where the variation in the refractive index between its maximum value n_{co}, and its minimum value n_{cl}, is small, typically less than 1%. This small variation gives rise to what has become known as the $n_{co} \cong n_{cl}$ [9,11] or weak guidance approximation [10] for optical fibres.

Because $n_{co} \cong n_{cl}$, the fields are only weakly influenced by the polarization properties of the fibre structure. This is clear from the elementary result that plane wave reflection from a dielectric interface is almost insensitive to the polarization of the incident wave when the two dielectrics are similar [20].

The weak guidance approximation allows us to reduce Maxwell's equations and their associated vector wave equation to what is recognized to be equivalent to the "Helmholtz" [21] or scalar approximation of wave optics, i.e. the scalar wave equation. This procedure neglects polarization effects. However, Snyder and Young [11] have extended the weak guidance method to include the more important polarization effects.

The electric and magnetic fields of the modes of an optical fibre with cylindrical symmetry have the form

$$\underline{E}(r,\phi,z) = \underline{e}(r,\phi)\ \exp[i(\beta z - \omega t)] \tag{1a}$$

$$\underline{H}(r,\phi,z) = \underline{h}(r,\phi)\ \exp[i(\beta z - \omega t)]\ , \tag{1b}$$

where ω is the angular frequency and β is the propagation constant in the z direction.

The propagation constant β must lie somewhere between the two extremes given by the value of the propagation constant for a z directed plane wave propagating in an infinite medium of refractive index equal to the maximum (n_{co}) or minimum (n_{cl}) value of the refractive index profile; β is then bounded by

$$k_{cl} \leq \beta \leq k_{co} , \tag{2}$$

where $k = 2\pi n/\lambda$ and λ is the wavelength in vacuum.

Since $\beta \cong k_{co}$ the wave vector is nearly parallel to the fibre axis, and the field must be nearly a transverse electromagnetic (T.E.M.) wave. The simplest example is the fundamental mode where the field is polarized in one direction only.

In general the number of bound modes that an optical fibre can sustain depends on the core radius ρ, the wavelength λ and the relative refractive index difference between the core and the cladding, Δ [22], where

$$2\Delta = [n_{co}^2 - n_{cl}^2]/n_{co}^2 . \tag{3}$$

Single mode operation requires approximately that [23]

$$\bar{V} \leq \bar{V}_{co} \simeq 2.405 , \tag{4}$$

where $\bar{V}$ is the effective waveguide parameter defined by

$$\bar{V} = \frac{2\pi}{\lambda} \left\{ 2 \int_0^\infty [n^2(r) - n_{cl}^2) \; r \, dr \right\}^{\frac{1}{2}} . \tag{5}$$

$\bar{V}$ reduces to the usual waveguide parameter V, where

$$V = \frac{2\pi}{\lambda} \rho (n_{co}^2 - n_{cl}^2)^{\frac{1}{2}} \tag{6}$$

for the case of the step profile (i.e. $n(r) = n_{co}$). The number 2.405 is the cutoff value for the second mode of the step profile, for which case $\bar{V}_{co}$ in eq. (4) is exactly equal to 2.405.

The relation defined by Eq. (4) is very useful in characterizing single mode fibres. However, Gambling *et al.* [23] have shown that fibres are effectively single moded for $\bar{V} < 3.0$. This is because a large fraction of the power in the second mode propagates within the cladding for $\bar{V} < 3.0$; therefore, this mode is highly susceptible to cladding absorption and radiation losses due to bends, and hence its presence can usually be ignored. On the other hand, recent trends towards large wavelength sources [24,25] indicate that applications will confine the wavelength to be such that $\bar{V} < 2.405$.

We will return to a more thorough discussion of $\bar{V}$ and extend its use in Part 2 of this thesis.

1.4 OUTLINE OF THE THESIS

Although the weak guidance approximation does simplify the theory of propagation in optical fibres, reducing the original Maxwell's equations to a scalar wave equation, there are, even then, few refractive index profiles for which exact analytic solutions can be obtained for the scalar wave equation. The step and infinite parabolic profile are the most useful.

The aim of this thesis is therefore twofold. Firstly, in Part 1, we examine the accuracy of the weak guidance approximation for those profiles for which the scalar wave equation can be solved exactly using either analytic or simple numerical methods. Secondly, in Part 2, having established the accuracy and limitations of the weak guidance approximation, we discuss approximation methods for the

scalar wave equation.

In detail then, Chapter 2 outlines a perturbation expansion for the vector wave equation and the associated propagation parameters. The perturbation is such that the solution to the scalar wave equation and its associated parameters form the "first terms" in the expansion. This allows us to isolate the polarization effects (or vector corrections to the scalar wave equation) directly.

In Chapter 3 we present a full eigenfunction expansion method for determining the polarization effects. We outline the formal theory for general profiles and we present the step profile as an example, as this is the only profile of any practical interest which can be attempted analytically. Other profiles require numerical methods.

In Chapter 4 we present a power series method for determining the polarization effects for the special case of the clad power-law profiles. This method is simpler and more direct than that of Chapter 3. We consider the infinite parabolic profile which, although it is unphysical since $n^2 \to -\infty$ as $r \to \infty$, gives simple closed-form expressions for all quantities of interest. Results for these profiles and the results for the step profile are presented. We then give a general summary for Part 1.

Part 2 of this thesis is mainly devoted to developing a universal characterization of single mode fibres of arbitrary refractive index profile. We develop simple and accurate formulae for all modal parameters of interest in terms of the first three moments of the refractive index profile. These expressions are suitable for fibre design.

We begin in Chapter 5 by outlining previous characterization attempts, some of which are more fully developed by the moment method.

Chapter 5 also contains a discussion of numerical techniques for solving the scalar wave equation. Two such techniques are presented. The first is a variational scheme where the field solution is obtained in terms of a power series. Each additional term in the power series requires two additional moments of the refractive index profile. We refer to this method as the "exact moment method". The second is a Green's function procedure which can be modified for the case of doubly-clad or "W-type" profiles. The characteristics of such profiles are also discussed.

The theory of the profile moments description of single mode fibres is fully developed in Chapter 6. The properties of moments and their relationship to profile shape are examined. Simple expressions are derived, in terms of universal formulae, for all modal parameters of interest.

In Chapter 7 we consider how the simple formulae derived in the previous chapter can be applied to fibre design. We relate the moments to experimentally measurable quantities — either on the fibre or even on the preform — and use these quantities in our examples.

The moment method is restricted in applicability to the region $\bar{V} \leq 2.405$. In Chapter 8, we concentrate on the region $\bar{V} \cong 3$ since the fibre is effectively single moded to this point. Profiles can still be characterized by moments but we now require *the exact solution for a reference profile possessing the same moments.* We examine the point of zero waveguide dispersion and propose a more useful parameter when comparing dispersion properties of different profiles. Step profiles with on-axis dips are examined in detail although the methods presented are general.

We discuss radiation due to sources in fibres in Chapter 9. We

examine the influence of the perturbing core on the free space radiation pattern and find that, for the purposes of determining radiation, we can adequately characterize the arbitrary profile by using the effective waveguide parameter $\bar{V}$. So that for a given profile height (or critical angle θ_c) only the first moment of the refractive index profile is required. We also examine the accuracy of W.K.B. methods.

REFERENCES

1. Miller, S.E.: "Overview of telecommunications via optical fibres", *Proc. I.E.E.E.* 68, 1173-1174 (1980).

2. Boriako, A.A.: "Harnessing light by a thread", Photos, Ward, F., *National Geographic* 516-535 (1979).

3. Kawahta, M.: "Hi-OVIS (Higashi Ikoma Optical Visual Information System) Development Project", *IOOC* C6-2, 467-471 (1977).

4. Kimura, T.: "Single mode digital transmission technology", *Proc. I.E.E.E.* 68, 1263-1268 (1980).

5. Kao, K.C., Hockham, G.A.: "Dielectric-fibre surface waveguides for optical frequencies", *Proc. I.E.E.* 113, 1151-1158 (1966).

6. Gambling, W.A., Matsumura, H.: "A comparison of single mode and multimode fibres for long distance telecommunications", from *Fibre and Integrated Optics* (ed. Ostrowsky, D.B.), 333-343 (1978).

7. Ladany, I., Ettenberg, M., Lockwood, H.F., Kressel, H.: "Al_2O_3 half-wave films for long life CW lasers", *Appl. Phys. Letters* 30, 87-89 (1977).

8. Giallorenzi, T.G.: "Optical communications research and technology: Fibre optics", *Proc. I.E.E.E.* 66, 744-780 (1978).

9. Snyder, A.W.: "Asymptotic expressions for eigenfunctions and eigenvalues of a dielectric or optical waveguide", *I.E.E.E. Trans.* MTT-17, 1130-1138 (1969).

10. Gloge, D.: "Weakly guiding fibres", *Appl. Opt.* 10, 2252-2258 (1971).

11. Snyder, A.W., Young, W.R.: "Modes of optical waveguides", *J. Opt. Soc. Am.* 68, 297-309 (1978).

12. Hussey, C.D., Pask, C.: "Single mode fibres in a few moments", *Electron. Lett.* 17, 644-645 (1981).

13. Hussey, C.D., Pask, C.: "The theory of the profile moments description of single mode fibres", (to be published).

14. Hussey, C.D., Pask, C.: "Waveguide dispersion in single mode fibres with on-axis dips", (to be published).

15. Snyder, A.W.: "Weakly guiding optical fibers", *J. Opt. Soc. Am.* 70, 405-411 (1980).

16. Snyder, A.W.: "Continuous mode spectrum of a circular dielectric rod", *I.E.E.E. Trans.* MTT-19, 720-727 (1971).

17. Snyder, A.W., Sammut, R.A.: "Radiation modes of optical waveguides", *Electron. Lett.* 15, 4-5 (1979).

18. Clarricoats, P.J.B.: "Propagation along bounded and unbounded dielectric rods", *IEE Monograph* 409E (1960).

19. Snitzer, E.: "Cylindrical dielectric waveguide modes", *J. Opt. Soc. Am.* 51, 491-498 (1961)

20. Landau, L.D., Lifshitz, E.M.: *Electrodynamics of Continuous Media* (Pergamon, New York, 1963), p.285.

21. Arnaud, J.A.: "Transverse coupling in fiber optics. Part II: Coupling to mode sinks", *B.S.T.J.* 53, 676-696 (1974).

22. Pask, C., Snyder, A.W., Mitchell, D.J.: "Number of modes on optical waveguides", *J. Opt. Soc. Am.* 65, 356-357 (1975).

23. Gambling, W.A., Matsumura, H., Ragdale, C.M.: "Wave propagation in a single mode fibre with dip in the refractive index", *Opt. & Quantum Electron.* 10, 301-309 (1978).

24. Lin, C., Cohen, L.G., French, W.G., Presley, H.M.: "Measuring dispersion in single mode fibers in the 1.1-1.3 μm spectral region — A pulse synchronization technique", *I.E.E.E. J.* QE-16, 33-36 (1980).

25. Imoto, N., Kawana, A., Machida, S., Tsuchiya, H.,: "Characteristics of dispersion free single mode fiber in the 1.5 μm wavelength range", *I.E.E.E. J.* QE-16, 1052-1058 (1980).

PART I

VECTOR THEORY OF SINGLE MODE OPTICAL FIBRES

CHAPTER 2

PERTURBATION THEORY FOR POLARIZATION EFFECTS

PREAMBLE

In this chapter we lay the basic theoretical framework for examining the accuracy of the weak guidance approximation. We isolate the vector corrections (i.e. polarization effects) by couching the problem in terms of a perturbation expansion where the scalar wave equation forms the first term. Second order terms essentially give us the polarization effects. We are concerned with isolating the influence of the polarization properties of the fibre on the fields and propagation constants, group velocity and dispersion.

2.1 INTRODUCTION

Most aspects of weakly guiding optical fibres can be analysed completely in terms of the scalar wave equation. However, the subtle differences between the solutions of the scalar wave equation and the full vector wave equation, which we call polarization effects, can occasionally become very significant [1,2].

For instance, the small correction to the propagation constant β due to polarization effects is essential [1], since β appears as $\exp(i\beta z)$ in the expression for the propagating field, where z can be arbitrarily large. Accordingly, when a small percentage error in β is multiplied by a large z, a large error can result.

Another important example is the birefringence in a single mode fibre with an elliptical core caused by the difference in phase velocity between the two polarization states of the fundamental mode [3,4]. In the scalar theory the two polarization states have identical phase velocities and it is only by including vector wave effects that this degeneracy is broken.

This birefringence is significant both in telecommunication systems [3] (where it limits the theoretical bandwidth achievable with monomode fibres by introducing some intermodal dispersion) and also in such devices as the Faraday effect current transducer [4], where it affects the usefulness of the fibre as a transmitter of polarization information.

Other polarization effects include those on the actual field itself. For instance, within the weak guidance approximation the fundamental mode field is a plane wave polarized in one direction only as shown in Fig. 1(a). The actual field, however, has an angular dependence as depicted schematically in Fig. 1(b).

We examine field effects because there is very limited information available for arbitrary refractive index profiles. In particular, there are only two profiles for which exact analytical solutions for Maxwell's equations can be obtained on waveguides of circular symmetry [5], the step profile being the most familiar. Thus it is of basic theoretical interest to know how waveguide polarization influences the modes of more general structures.

Two general methods have been proposed which allow these polarization effects to be determined for arbitrary refractive index profiles. These are the eigenfunction expansion method [6,7] and the Green's function method [8]. In this thesis we give an example of the

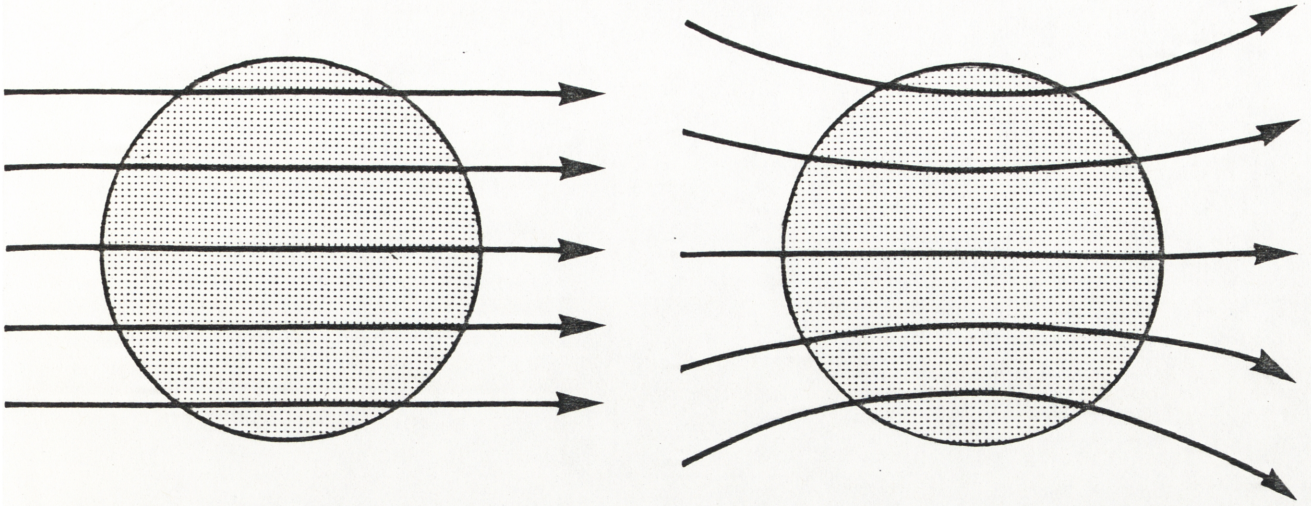

(a) (b)

Fig. 1: Schematic of the transverse electric field lines: (a) in the scalar approximation, and (b) when polarization effects of the fibre are included.

eigenfunction method which requires the full spectrum of scalar (bound and radiation) modes. We also propose a power series method [9] which is more appropriate for clad power-law profiles.

We examine the influence of the polarization properties of the fibre structure on the propagation constant and investigate how this affects group velocity and waveguide dispersion, as these ultimately determine the bandwidth of the single mode fibre.

The polarization effects can be isolated by expanding the modal parameters as a perturbation series in the refractive index difference Δ [1]. This is the parameter which is assumed small in the weak guidance approximation. In this manner the first term in each expansion corresponds to the scalar result, and higher terms show the influence of polarization.

We first define the exact modal fields and governing equations, and then give their expansions within the weak guidance approximation.

2.2 THE VECTOR WAVE EQUATION AND EXACT MODAL PARAMETERS

The electric and magnetic field vectors of a fibre of circular cross-section are expressible in the separable form

$$\underline{E}(R,\phi,z) = \underline{e}(R,\phi)\, e^{i\beta z} \qquad \underline{H}(R,\phi,z) = \underline{h}(R,\phi)\, e^{i\beta z}, \tag{1}$$

where β is the exact propagation constant, (r,ϕ,z) are cylindrical polar coordinates based on the fibre axis in Fig. 1.1(a), and $R = r/\rho$ is the normalized radius. We refer the components of $\underline{e}$ and $\underline{h}$ to *fixed cartesian directions*, so that

$$\underline{e} = e_x\hat{\underline{x}} + e_y\hat{\underline{y}} + e_z\hat{\underline{z}} = \underline{e}_t + e_z\hat{\underline{z}} \tag{2a}$$

$$\underline{h} = h_x\hat{\underline{x}} + h_y\hat{\underline{y}} + h_z\hat{\underline{z}} = \underline{h}_t + h_z\hat{\underline{z}}, \tag{2b}$$

where $\hat{\underline{x}}$, $\hat{\underline{y}}$ and $\hat{\underline{z}}$ are unit vectors parallel to the axes in Fig. 1.1(a), t denotes transverse component, and $e_x \equiv e_x(R,\phi)$, etc. Under this decomposition, $\underline{e}_t$ satisfies the vector wave equation [1]

$$\{\nabla_t^2 + k^2(R)\}\, \underline{e}_t = \beta^2\underline{e}_t - \underline{\nabla}_t\{\underline{e}_t \cdot \underline{\nabla}_t \ln n^2(R)\}, \tag{3}$$

where ∇_t^2 is the transverse part of the *scalar* Laplace operator, i.e.

$$\rho^2\nabla_t^2 = \frac{\partial^2}{\partial R^2} + \frac{1}{R}\frac{\partial}{\partial R} + \frac{1}{R^2}\frac{\partial^2}{\partial\phi^2}, \tag{4a}$$

and the transverse gradient operator $\underline{\nabla}_t$ is expressible as

$$\rho\underline{\nabla}_t = \hat{\underline{x}}\,\rho\frac{\partial}{\partial x} + \hat{\underline{y}}\,\rho\frac{\partial}{\partial y} = \hat{\underline{r}}\,\frac{\partial}{\partial R} + \hat{\underline{\phi}}\,\frac{1}{R}\frac{\partial}{\partial\phi}, \tag{4b}$$

where $\hat{\underline{r}}$ and $\hat{\underline{\phi}}$ are unit vectors in the radial and azimuthal directions. Subsidiary relationships are

$$k(R) = \frac{2\pi}{\lambda}\, n(R) = \omega\{\mu\varepsilon(R)\}^{\frac{1}{2}} \qquad \varepsilon(R) = \varepsilon_0\, n^2(R), \tag{5}$$

where λ is the free-space wavelength, ε_0 the free-space dielectric constant and μ the uniform permeability. The dielectric profile is

given by $\varepsilon(R)$ and the refractive index profile by $n(R)$. All field components contain the implicit time dependence $\exp(-i\omega t)$, where ω is the angular frequency.

Given the solution of Eq. (3), the remaining components of $\underline{e}$ and $\underline{h}$ are expressible through Maxwell's equations in terms of $\underline{e}_t$ by

$$e_z = \frac{i}{\beta}\{\underline{\nabla}_t \cdot \underline{e}_t + \underline{e}_t \cdot \underline{\nabla}_t \ln n^2(R)\}, \tag{6a}$$

$$\underline{h}_t = \frac{1}{\omega\mu}\,\hat{\underline{z}} \times \{\beta \underline{e}_t + i\underline{\nabla}_t\, e_z\}, \tag{6b}$$

$$h_z = \frac{i}{\beta}\,\underline{\nabla}_t \cdot \underline{h}_t . \tag{6c}$$

The modal fields have normalization N defined by

$$N = \tfrac{1}{2}\int_{A_\infty} \underline{e} \times \underline{h}^* \cdot \hat{\underline{z}}\, dA, \tag{7}$$

where A_∞ is the infinite cross-section and * denotes complex conjugate.

The fibre parameter V is defined in terms of the relative refractive index difference Δ by

$$V = \frac{2\pi\rho}{\lambda}(2\Delta)^{\frac{1}{2}} n_{co} \qquad \Delta = \tfrac{1}{2}\,\frac{n_{co}^2 - n_{cl}^2}{n_{co}^2}, \tag{8}$$

where ρ is the core radius, n_{co} the maximum refractive index, and n_{cl} the uniform cladding index or the value of $n(R)$ at $R=1$ for infinite profiles. It is convenient to express the propagation constant in terms of the modal parameter U, where

$$U = \rho(k_{co}^2 - \beta^2)^{\frac{1}{2}} \qquad k_{co} = \frac{2\pi n_{co}}{\lambda} = \frac{V}{\rho(2\Delta)^{\frac{1}{2}}}, \tag{9}$$

and k_{co} is the maximum value of the wavenumber $k(R)$.

2.3 EXPANSION OF THE MODAL PARAMETERS AND THE SCALAR WAVE EQUATION

The exact modal fields depend parametrically on V and Δ of Eq. (8). In the weak guidance approximation $n_{co} \cong n_{cl}$ and consequently $\Delta \ll 1$. We then assume that the fields can be expanded as a power series about $\Delta = 0$, i.e. about the scalar result. This expansion is facilitated if we introduce a small parameter δ defined by

$$\delta = (2\Delta)^{\frac{1}{2}} = (1 - n_{cl}^2/n_{co}^2)^{\frac{1}{2}} , \tag{10}$$

and express the refractive index profile in the general form

$$n^2(R) = n_{co}^2\{1 - 2\Delta f(R)\} , \qquad f(R) \geq 0 . \tag{11}$$

If we substitute Eqs. (8), (9) and (11) into Eq. (3), we obtain the dimensionless equation

$$\{\rho^2\nabla_t^2 + U^2 - V^2 f(R)\}\, \underline{e}_t = -\rho\underline{\nabla}_t\{\underline{e}_t \cdot \rho\underline{\nabla}_t \ln n^2(R)\} . \tag{12}$$

From Eq. (11) we deduce that

$$\rho\underline{\nabla}_t \ln n^2(R) = -\delta^2 \frac{df}{dR} + O(\delta^4) . \tag{13}$$

Consequently $\underline{e}_t$ and U have expansions in powers of δ^2. In section 4 we show that $\underline{h}_t$, and thus the normalization, have similar expansions

$$\underline{e}_t(V,\delta) = \tilde{\underline{e}}_t + \delta^2\, \underline{e}_t^{(2)} + O(\delta^4) , \tag{14a}$$

$$\underline{h}_t(V,\delta) = \tilde{\underline{h}}_t + \delta^2\, \underline{h}_t^{(2)} + O(\delta^4) , \tag{14b}$$

$$N(V,\delta) = \tilde{N} + \delta^2\, N^{(2)} + O(\delta^4) , \tag{14c}$$

where the coefficients of each order depend parametrically only on V. Similarly

$$U = \tilde{U} + \delta^2\, U^{(2)} + O(\delta^4) , \tag{15a}$$

$$\beta = \tilde{\beta} + \delta^3\, \beta^{(3)} + O(\delta^5) , \tag{15b}$$

$$\tilde{U} = \rho(k_{co}^2 - \tilde{\beta}^2)^{\frac{1}{2}} = \left\{\frac{V^2}{\delta^2} - \rho^2\tilde{\beta}^2\right\}^{\frac{1}{2}}, \tag{15c}$$

using Eqs. (9) and (10). The ~ denotes quantities associated with the scalar wave equation, which relates the lowest order terms in Eq. (3) by

$$\mathcal{L}\tilde{\underline{e}}_t \equiv \{\rho^2\nabla_t^2 + \tilde{U}^2 - V^2 f(R)\}\,\tilde{\underline{e}}_t = 0\,. \tag{16}$$

The value of $\tilde{U}$ is found from the eigenvalue equation, i.e. from the condition that $\tilde{\underline{e}}_t$ and its first derivatives be everywhere continuous.

The modal group velocity is defined by

$$v_g = \frac{d\omega}{d\beta} = \frac{c}{n_{co}}\left\{1 + \delta^2\, v_g^{(2)} + \delta^4\, v_g^{(4)} + O(\delta^6)\right\}, \tag{17a}$$

$$= \tilde{v}_g + \frac{c}{n_{co}}\,\delta^4\, v_g^{(4)} + O(\delta^6)\,, \tag{17b}$$

where c is the free-space speed of light. Finally, waveguide dispersion is conveniently expressed in terms of a dimensionless parameter D, where [10]

$$D = \frac{c^2}{\rho\delta^3 n_{co}^2}\frac{d^2\beta}{d\omega^2} = \frac{1}{\delta^2}\frac{d}{dV}\left\{\frac{c/n_{co}}{v_g}\right\}, \tag{18a}$$

$$= \tilde{D} + \delta^2\, D^{(2)} + O(\delta^4)\,, \tag{18b}$$

and we have used Eqs. (8), (9) and (10) to obtain

$$V = k_{co}\,\rho\delta = \frac{\omega}{c}\,\rho\, n_{co}\,\delta \qquad c = \frac{1}{(\mu\varepsilon_0)^{\frac{1}{2}}}. \tag{19}$$

Having defined higher order corrections to the scalar results, we can now derive equations for these corrections on arbitrary profile fibres.

2.4 GOVERNING EQUATIONS

On a circularly symmetric fibre, the scalar components of the transverse electric field of the fundamental mode are given by [1]

$$\tilde{\underline{e}}_t = \Psi\hat{\underline{x}} \qquad e_r = \Psi\cos\phi \qquad e_\phi = -\Psi\sin\phi\,, \tag{20a}$$

if the mode is x-polarized, and by

$$\tilde{\underline{e}}_t = \Psi\hat{\underline{y}} \qquad e_r = \Psi\sin\phi \qquad e_\phi = \Psi\cos\phi\,, \tag{20b}$$

if the mode is y-polarized, where Ψ is the solution of the axisymmetric form of the scalar wave equation, i.e.

$$\left\{\frac{d^2}{dR^2} + \frac{1}{R}\frac{d}{dR} + \tilde{U}^2 - V^2 f(R)\right\}\Psi = 0\,. \tag{21}$$

The values of $\tilde{U}$ are determined from the eigenvalue equation, found by requiring Ψ and $d\Psi/dR$ to be everywhere continuous.

The corresponding values of the scalar propagation constant $\tilde{\beta}$ follow from Eq. (15c). To relate $\tilde{\beta}$ to the exact propagation constant β, we substitute for k_{co} in Eq. (9) from Eq. (19) and generate the expansion

$$\rho\beta = \frac{V}{\delta} - \frac{\tilde{U}^2}{2V}\delta - \frac{\{\tilde{U}^4 + 8\tilde{U}V^2U^{(2)}\}}{8V^3}\delta^3 + O(\delta^5)\,, \tag{22}$$

where U has been replaced by the expansion of Eq. (15a). The corresponding expansion of $\tilde{\beta}$ follows from Eq. (15c) as

$$\rho\tilde{\beta} = \frac{V}{\delta} - \frac{\tilde{U}^2}{2V}\delta - \frac{\tilde{U}^4}{8V^3}\delta^3 + O(\delta^5)\,. \tag{23}$$

On comparing Eqs. (22) and (23) we deduce

$$\rho\beta = \rho\tilde{\beta} - \frac{\tilde{U}U^{(2)}}{V}\delta^3 + O(\delta^5)\,, \tag{24}$$

and a comparison with the expansion of Eq. (15b) leads to

$$\beta^{(3)} = -\frac{\tilde{U}U^{(2)}}{\rho V}\,. \tag{25}$$

It remains to determine $U^{(2)}$.

Higher order corrections to $\tilde{U}$ are found from the formula [1]

$$U^2 - \tilde{U}^2 = \frac{\int_{A_\infty} (\rho \underline{\nabla}_t \cdot \underline{\tilde{e}}_t)(\underline{e}_t \cdot \rho \underline{\nabla}_t) \ln n^2(R)\, dA}{\int_{A_\infty} \underline{\tilde{e}}_t \cdot \underline{e}_t\, dA}, \tag{26}$$

where A_∞ is the infinite cross-section of the fibre. This expression is derived by taking the scalar products of Eq. (12) with $\underline{\tilde{e}}_t$ and Eq. (16) with $\underline{e}_t$, subtracting, and then integrating over A_∞. Green's theorem shows that the area integral over terms involving ∇_t^2 is equivalent to a line integral at infinity, which vanishes since $\underline{e}_t$ and $\underline{\tilde{e}}_t$ are exponentially small as $R \to \infty$. An integration by parts leads to the above result. We substitute the expansions of $\rho \underline{\nabla}_t \ln n^2(R)$, $\underline{e}_t$ and U from Eqs. (13), (14a) and (15a), and equate terms of order δ^2 to obtain

$$U^{(2)} = - \frac{\int_{A_\infty} (\rho \underline{\nabla}_t \cdot \underline{\tilde{e}}_t)\, \tilde{e}_r \frac{df}{dR}\, dA}{2\tilde{U} \int_{A_\infty} \underline{\tilde{e}}_t^2\, dA}. \tag{27}$$

If we express the area integral in terms of cylindrical coordinates and substitute the fundamental mode fields of Eq. (20), we can perform the ϕ integration and find that the polarization correction is the same for either polarization [7]

$$U^{(2)} = - \frac{\int_0^\infty R\Psi \frac{d\Psi}{dR} \frac{df}{dR}\, dR}{4\tilde{U} \int_0^\infty R\Psi^2\, dR}. \tag{28}$$

Thus, if $\tilde{U}$ is prescribed, $U^{(2)}$ is given explicitly.

The group velocity v_g is expressed in terms of the angular frequency ω and the propagation constant β by Eq. (17a). However, it is more convenient to work in terms of the dimensionless fibre

parameter V of Eq. (19) and the modal parameter U of Eq. (9). Hence

$$v_g = \frac{c}{n_{co}} \frac{(V^2 - \delta^2 U^2)^{\frac{1}{2}}}{V - \frac{\delta^2}{2}\frac{dU^2}{dV}} . \tag{29}$$

If we substitute the expansion for U in Eq. (15a), expand in powers of δ and compare with Eq. (17a), we deduce

$$v_g^{(2)} = \frac{1}{2}\frac{d}{dV}\left\{\frac{\tilde{U}^2}{V}\right\}, \tag{30a}$$

$$v_g^{(4)} = \left\{\frac{\tilde{U}}{V}\frac{d\tilde{U}}{dV}\right\}^2 - \frac{1}{8V^4}\frac{d}{dV}(\tilde{U}^4 V) + \frac{d}{dV}\left\{\frac{\tilde{U}}{V}U^{(2)}\right\}, \tag{30b}$$

which require the first derivatives of $\tilde{U}$ and $U^{(2)}$. For the infinite parabolic profile we differentiate the eigenvalue equation to determine $d\tilde{U}/dV$, but for the clad profiles it is simpler to use the following integral expression.

Consider the scalar wave equation at frequency $\omega = \omega_0$, and denote the corresponding values of $\tilde{U}$, V and $\tilde{\underline{e}}_t$ by $\tilde{U}_0$, V_0 and $\tilde{\underline{e}}_{t0}$ respectively. Thus Eq. (16) becomes

$$\{\rho^2\nabla_t^2 + \tilde{U}_0^2 - V_0^2 f(R)\}\,\tilde{\underline{e}}_{t0} = 0 . \tag{31a}$$

Likewise at frequency $\omega = \omega_1$ the corresponding equation is

$$\{\rho^2\nabla_t^2 + \tilde{U}_1^2 - V_1^2 f(R)\}\,\tilde{\underline{e}}_{t1} = 0 . \tag{31b}$$

We take the scalar products of Eq. (31a) with $\tilde{\underline{e}}_{t1}$ and Eq. (31b) with $\tilde{\underline{e}}_{t0}$, subtract and integrate over the infinite cross-section. For reasons given below Eq. (26), terms involving ∇_t^2 vanish and we are left with

$$(\tilde{U}_0^2 - \tilde{U}_1^2)\int_{A_\infty} \tilde{\underline{e}}_{t0}\cdot\tilde{\underline{e}}_{t1}\, dA = (V_0^2 - V_1^2)\int_{A_\infty} f(R)\,\tilde{\underline{e}}_{t0}\cdot\tilde{\underline{e}}_{t1}\, dA . \tag{32}$$

If we divide $V_0^2 - V_1^2$ and take the limit $\omega_1 \to \omega_0 = \omega$, we find

$$\frac{d\tilde{U}}{dV} = \frac{V}{\tilde{U}} \frac{\int_{A_\infty} f(R)\ \tilde{\underline{e}}_t^2\ dA}{\int_{A_\infty} \tilde{\underline{e}}_t^2\ dA} . \tag{33}$$

For either polarization of the fundamental mode fields of Eq. (20) we deduce

$$\frac{d\tilde{U}}{dV} = \frac{V}{\tilde{U}} \frac{\int_0^\infty R\Psi^2\ f(R)\ dR}{\int_0^\infty R\Psi^2\ dR} . \tag{34}$$

Consequently $d\tilde{U}/dV$ is given explicitly once $\tilde{U}$ is prescribed.

The derivative $dU^{(2)}/dV$ is obtained by differentiating Eq. (28) and substituting for $d\tilde{U}/dV$.

The dispersion parameter D is defined by Eq. (18a). If we substitute the expansion for v_g of Eq. (17a) and compare with Eq. (18b) we find

$$\tilde{D} = - \frac{dv_g^{(2)}}{dV} , \tag{35a}$$

$$D^{(2)} = \frac{d}{dV} \left\{ \left(v_g^{(2)} \right)^2 - v_g^{(4)} \right\} . \tag{35b}$$

These expressions involve the second derivatives of $\tilde{U}$ and $U^{(2)}$, which are generated by taking the derivative of Eq. (34) and the second derivative of Eq. (28). By repeated application we can express $\tilde{D}$ and $D^{(2)}$ in terms of $\tilde{U}$.

The transverse field correction $\underline{e}_t^{(2)}$ satisfies the equation found by substituting Eqs. (13), (14a) and (15a) into Eq. (12) and equating terms of order δ^2

$$\mathcal{L}\underline{e}_t^{(2)} = - 2\tilde{U}U^{(2)}\ \tilde{\underline{e}}_t + \rho\underline{\nabla}_t \left\{ \tilde{e}_r \frac{df}{dR} \right\} , \tag{36}$$

where the operator $\mathcal{L}$ is defined by Eq. (16) and the right side is

prescribed. If we substitute the x-polarized fundamental mode field of Eq. (20a), the component equations reduce to

$$\mathcal{L}e_x^{(2)} = -2\tilde{U}U^{(2)}\Psi + \frac{1}{2R}\frac{d}{dR}\left\{R\Psi\frac{df}{dR}\right\} + \frac{R}{2}\frac{d}{dR}\left\{\frac{\Psi}{R}\frac{df}{dR}\right\}\cos 2\phi\,, \tag{37a}$$

$$\mathcal{L}e_y^{(2)} = \frac{R}{2}\frac{d}{dR}\left\{\frac{\Psi}{R}\frac{df}{dR}\right\}\sin 2\phi\,. \tag{37b}$$

The corresponding equations for the y-polarized mode are obtained by making the transformation $\phi \to \phi + \pi/2$, $e_x^{(2)} \to e_y^{(2)}$, $e_y^{(2)} \to -e_x^{(2)}$.

Given $\tilde{\underline{e}}_t$ and $\underline{e}_t^{(2)}$, the remaining field components correct to third order in δ are given by Table 1, where the exact longitudinal field components have the expansions

$$e_z = \delta e_z^{(1)} + \delta^3 e_z^{(3)} + O(\delta^5)\,, \tag{38a}$$

$$h_z = \delta h_z^{(1)} + \delta^3 h_z^{(3)} + O(\delta^5)\,. \tag{38b}$$

The field relationships in Table 1 are obtained by substituting the expansions of Eqs. (14a), (14b), (24) and (38) into Eq. (6), using Eq. (19) to replace $\omega\mu$ by $(\mu/\varepsilon_{co})^{\frac{1}{2}}(V/\rho\delta)$, and then equating powers of δ.

The normalization expressions in Table 1 are similarly obtained by substituting Eqs. (14a) and (14b) into Eq. (7), comparing with Eq. (14c) and then expressing $\tilde{\underline{h}}_t$ and $\underline{h}_t^{(2)}$ in terms of $\tilde{\underline{e}}_t$ and $\underline{e}_t^{(2)}$. For the fundamental modes we have prescribed the scalar normalization by choosing $\Psi = 1$ at $R = 1$. We deduce from Eq. (20) and Table 1 that

$$\tilde{N} = \pi\left(\frac{\varepsilon_{co}}{\mu}\right)^{\frac{1}{2}}\int_0^\infty R\Psi^2\,dR\,, \tag{39}$$

assuming Ψ real. The polarization correction $\underline{e}_t^{(2)}$ is defined to be the solution of Eq. (37) which satisfies $N^{(2)} = 0$. For the x-polarized fundamental mode, we deduce from Table 1 and Eq. (21) that this is equivalent to requiring

$$\tilde{\underline{h}}_t = \left(\frac{\varepsilon_{co}}{\mu}\right)^{\frac{1}{2}} \hat{\underline{z}} \times \tilde{\underline{e}}_t \qquad e_z^{(1)} = i\,\frac{\rho}{V}\,\underline{\nabla}_t \cdot \tilde{\underline{e}}_t$$

$$h_z^{(1)} = i\,\frac{\rho}{V}\,\underline{\nabla}_t \cdot \tilde{\underline{h}}_t = -i\,\frac{\rho}{V}\left(\frac{\varepsilon_{co}}{\mu}\right)^{\frac{1}{2}} \hat{\underline{z}} \cdot \underline{\nabla}_t \times \tilde{\underline{e}}_t$$

$$\underline{h}_t^{(2)} = \left(\frac{\varepsilon_{co}}{\mu}\right)^{\frac{1}{2}} \hat{z} \times \left(\underline{e}_t^{(2)} - \frac{\tilde{U}^2}{2V^2}\,\tilde{\underline{e}}_t - \frac{\rho^2}{V^2}\,\underline{\nabla}_t(\underline{\nabla}_t \cdot \tilde{\underline{e}}_t)\right)$$

$$e_z^{(3)} = i\,\frac{\rho}{V}\left(\underline{\nabla}_t \cdot \underline{e}_t^{(2)} + \frac{\tilde{U}^2}{2V^2}\,\underline{\nabla}_t \cdot \tilde{\underline{e}}_t - \tilde{\underline{e}}_t \cdot \underline{\nabla}_t\, f\right)$$

$$h_z^{(3)} = i\,\frac{\rho}{V}\left(\frac{\varepsilon_{co}}{\mu}\right)^{\frac{1}{2}} \hat{\underline{z}} \cdot \underline{\nabla}_t \times \underline{e}_t^{(2)} = i\,\frac{\rho}{V}\left(\underline{\nabla}_t \cdot \underline{h}_t^{(2)} + \frac{\tilde{U}^2}{2V^2}\,\underline{\nabla}_t \cdot \tilde{\underline{h}}_t\right)$$

$$N = \frac{1}{2}\left(\frac{\varepsilon_{co}}{\mu}\right)^{\frac{1}{2}} \int_{A_\infty} \tilde{\underline{e}}_t^2\, dA$$

$$N^{(2)} = \frac{1}{2}\left(\frac{\varepsilon_{co}}{\mu}\right)^{\frac{1}{2}} \int_{A_\infty} \left(2\tilde{\underline{e}}_t \cdot \underline{e}_t^{(2)} - \frac{\tilde{U}^2}{2V^2}\,\tilde{\underline{e}}_t^2 - \frac{1}{V^2}\,(\tilde{\underline{e}}_t \cdot \rho\underline{\nabla}_t)(\rho\underline{\nabla}_t \cdot \tilde{\underline{e}}_t)\right) dA$$

Table 1: Field components and normalization up to third order in terms of $\tilde{\underline{e}}_t$ and $\tilde{\underline{e}}_t^{(2)}$, assumed real.

$$\int_0^\infty Rf(R)\,\Psi^2\,dR = \frac{2}{\pi}\int_0^{2\pi}\int_0^\infty R\Psi\, e_x^{(2)}\, dR\, d\phi\,. \tag{40}$$

The general solution of Eq. (37a) consists of a particular solution plus a constant multiple of the complementary solution of Eq. (20a). This constant is determined by Eq. (40).

2.5 RESUMÉ

In this chapter we have introduced the perturbation expansion terms which describe polarization effects on the single mode fibre.

We did this by considering the vector wave equation as a perturbation about the scalar wave equation where the $\underline{\nabla}_t \ln[n^2(R)]$ term is the perturbation which introduces polarization effects. In the following chapters we quantify these effects for arbitrary profiles.

REFERENCES

1. Snyder, A.W., Young, W.R.: "Modes of optical waveguides", *J. Opt. Soc. Am.* 68, 297-309 (1978).

2. Tjaden, D.L.A.: "First order correction to 'weak guidance' approximation in fibre optics theory", *Philips J. Res.* 33, 103-112 (1978).

3. Tsuchiya, H., Imoto, N.: "Dispersion-free single mode fibre in 1.5 μm wavelength region", *Electron. Lett.* 15, 476-478 (1979).

4. Norman, S.R., Payne, D.N., Adams, M.J., Smith, A.M.: "Fabrication of single-mode fibres exhibiting extremely low polarization birefringence", *Electron. Lett.* 15, 309-311 (1979).

5. Love, J.D.: "Optical waveguides with exact vector field solutions", *I.E.E.E. J. Quantum Electron.* (submitted).

6. Sammut, R.A.: "Birefringence in graded index monomode fibres with elliptical cross section", *Electron. Lett.* 16, 156-157 (1980).

7. Sammut, R.A., Hussey, C.D., Love, J.D., Snyder, A.W.: "Modal analysis of polarization effects in weakly guiding fibres", *I.E.E. Proc. Part H* 128, 173-187 (1981).

8. Snyder, A.W., Love, J.D., Sammut, R.A.: "Green's function methods for analysing optical fibre perturbations", (submitted).

9. Love, J.D., Hussey, C.D., Snyder, A.W., Sammut, R.A.: "Polarization corrections to mode propagation on weakly guiding fibres", (submitted).

10. Snyder, A.W., Sammut, R.A.: "Dispersion in graded single mode fibres", *Electron. Lett.* 15, 269-271 (1979).

CHAPTER 3

EIGENFUNCTION METHODS

PREAMBLE

In this chapter we review the derivation of the complete set of modes of the scalar wave equation and then present the application of these modes to perturbation problems on optical waveguides. In particular we derive expressions for the polarization effects for the fundamental mode as described in Chapter 2. The step is used to demonstrate the method. We indicate how analogous methods can be used to determine the birefringence on slightly non-circular fibres.

3.1 INTRODUCTION

Our intention in this chapter is to demonstrate the use of the complete set of modes derived from the scalar wave equation as a basis for perturbation analysis on optical waveguides [1]. It is relatively easy to find the complete set of eigenfunctions (discrete and continuous) for arbitrary refractive index profiles. These are obtained numerically in most cases, although analytic expressions can be obtained for the step refractive index profile.

In the following section we review the derivation of the scalar modes [1,2,3] on fibres of circular cross-section and indicate how these modes can be used as a basis to construct the scalar modes of the slightly non-circular fibre.

For a perturbation theory of the vector wave equation (eq. 2.12) for the fundamental mode as outlined in Chapter 2, the zeroth order modes of the vector wave equation are required. These are derived from the scalar modes in section 3.

As an example, we apply the methods of section 3 to the fundamental mode of the step index fibre in section 4. The vector correction for the step-profile can be found by a limiting process from the known exact solution [4]. However, we present the perturbation method for the step profile, since it can be written down in closed form. The solution for the graded profile is obtained by a straightforward generalization of the methods presented for the step profile. For the power-law profiles considered in Part 1 of this thesis, however, we present a simpler and more direct method of solution in Chapter 4 [5].

In section 5 we indicate how the methods presented in section 2 can be used to determine the birefringence of slightly elliptical monomode fibres [6].

3.2 MODES OF THE SCALAR WAVE EQUATION

In this section we give a complete set of eigenfunctions, or modes, of the scalar wave equation on a waveguide with circular cross section. These eigenfunctions, $\psi^{(0)}(r,\phi)$ satisfy the scalar wave equation

$$\left(\frac{\partial^2}{\partial r^2} + \frac{1}{r}\frac{\partial}{\partial r} + \frac{1}{r^2}\frac{\partial^2}{\partial \phi^2} + k^2(r) - \beta^2\right)\psi^{(0)} = 0 , \tag{1}$$

where

$$k^2(r) = k_{co}^2[1 - \delta^2 f(r)] \tag{2}$$

and $f(r) \equiv 1$ in the cladding region, defined by $r \geq \rho$.

The boundary conditions imposed on $\psi^{(0)}$ by the fact that Eq. (1)

applies *everywhere* are that both $\psi^{(0)}$ and its derivative with respect to r be continuous everywhere. If we also demand that $\psi^{(0)}$ be finite at $r=0$ and satisfy the Sommerfeld radiation condition at infinity, then we obtain the discrete spectrum of bound modes which decay exponentially with radius. On a dielectric waveguide, there is only a finite number of such modes and these do not form a complete set. However, relaxing the radiation condition and assuming only that $\psi^{(0)}$ remain finite everywhere leads to a continuous spectrum of radiation modes which, when added to the discrete spectrum, *do* form a complete set.

To derive the modes, we note that $\psi^{(0)}(r,\phi)$ is expressible in the form

$$\psi^{(0)}(r,\phi) = F_m(U,R)\ \Theta_{sm}(\phi)\ , \tag{3}$$

where $\Theta_{sm}(\phi)$ is $\cos m\phi$ if $s=+1$ and $\sin m\phi$ if $s=-1$ (m being a positive integer) and F_m satisfies

$$\left(\frac{d^2}{dR^2} + \frac{1}{R}\frac{d}{dR} + U^2 - V^2 f - \frac{m^2}{R^2}\right) F_m = 0\ , \tag{4}$$

where $R=r/\rho$ is the normalized radius, $V=\rho(k_{co}^2 - k_{cl}^2)^{\frac{1}{2}}$ is a dimensionless parameter characterizing the waveguide and $U=\rho(k_{co}^2 - \beta^2)^{\frac{1}{2}}$ is the modal eigenvalue. Solutions of Eq. (4) which are evanescent in the cladding have propagation constants in the range $k_{cl}^2 < \beta^2 \le k_{co}^2$. Thus the cladding field of a discrete mode has the form

$$F_m(U,R) = \frac{K_m(WR)}{K_m(W)}\ , \qquad R \ge 1\ , \tag{5}$$

where $W=(V^2 - U^2)^{\frac{1}{2}}$ and the field has been normalized so that $F_m(1)=1$. The field in the core cannot, in general, be written down analytically but is a solution of Eq. (4) which remains finite at $R=0$. In the particular case of the step-index fibre, where $f=0$ in the core,

$$F_m(U,R) = \frac{J_m(UR)}{J_m(U)}, \qquad R \le 1, \tag{6}$$

but, in general, we denote the numerical solution of Eq. (4) by $f_m(U,R)$, i.e.

$$F_m(U,R) = f_m(U,R), \qquad R \le 1, \tag{7}$$

where $f_m(U,1) = 1$. The arguments U,R will only be explicitly stated when they are required to avoid confusion between two modes with the same m but different U.

Now imposition of the boundary conditions at $R = 1$ leads to the eigenvalue equation

$$\left.\frac{\partial f_m}{\partial R}\right|_{R=1} = \frac{WK_m'(W)}{K_m(W)}, \tag{8}$$

where the prime indicates differentiation with respect to the argument of the Bessel function. This equation determines the discrete values of W, and hence of β and U, which correspond to bound modes of the waveguide. (Note that, except when $m = 0$, each eigenvalue corresponds to two modes, one with $\cos m\phi$ and the other with $\sin m\phi$ variation.) At any finite value of V there will be a finite number ($n = 1,2,\ldots,N_m$) of distinct real solutions to Eq. (8) (where n denotes the radial order of the mode), and also a maximum value, M, of the azimuthal order, m, for which any solutions exist. It is because this finite collection of modes cannot form a complete set that the modes of the continuous spectrum are required.

To derive the continuum modes, we return to Eq. (4) and remove the restriction that $\beta^2 > k_{cl}^2$, so that the fields are no longer evanescent as $R \to \infty$. The general solution of this equation in the cladding can then be written in the form

$$F_m(U,R) = a_m J_m(QR) + b_m H_m^{(1)}(QR), \tag{9}$$

where $H_m^{(1)} = J_m + iY_m$, $Q = \rho(k_{cl}^2 - \beta^2)^{\frac{1}{2}}$ and the constants a_m and b_m are found by matching F_m and its derivative at the core-cladding boundary. In fact, Eq. (9) could have been written as a combination of J_m and Y_m functions but the particular combination shown is convenient for reasons which will become clear later.

In the core region, F_m has precisely the same form as do the bound modes (Eq. (6) or (7)) so that matching fields at the boundary gives

$$a_m = \frac{\pi i}{2} D_m \tag{10a}$$

and

$$b_m = -\frac{\pi i}{2} C_m a_m , \tag{10b}$$

where

$$D_m = H_m^{(1)}(Q) \left.\frac{\partial f_m}{\partial R}\right|_{R=1} - QH_m^{(1)\prime}(Q) \tag{11a}$$

and

$$C_m = J_m(Q) \left.\frac{\partial f_m}{\partial R}\right|_{R=1} - QJ_m'(Q) . \tag{11b}$$

In Eqs. (11), primes denote differentiation with respect to the argument of the functions.

Note that for these modes, because of the relaxation of the boundary condition at infinity, there is no eigenvalue equation so that Q, and therefore U and β, are continuous variables. If we choose the positive branch of the square-root for Q, then we see that Q may vary from zero to infinity and that Eq. (9) is written in the form of a free-space field, $J_m(Q)$, plus an outward-travelling wave, $H_m^{(1)}(Q)$.

Finally, we must consider the orthogonality and normalization properties of these modes. The bound modes are orthogonal to the modes of the continuous spectrum and, amongst themselves, also satisfy the orthogonality condition

$$\langle \psi_p^{(0)*} \psi_{p'}^{(0)} \rangle \equiv \int_{A_\infty}\int \psi_p^{(0)*} \psi_{p'}^{(0)} \, dA \tag{12}$$

$$= N_p^s \, \delta_{pp'} \, , \tag{13}$$

where A_∞ represents the infinite cross section and the asterisk denotes complex conjugation. The single subscript, p, is a shorthand notation for the set of mode parameters m, n and s and is used wherever clarity allows. Similarly, $\delta_{pp'}$ is an abbreviation for $\delta_{mm'}$, $\delta_{nn'}$, $\delta_{ss'}$ where δ is the usual Kronecker delta. The normalization constant, N_p^s, is given by

$$N_p^s = \frac{\pi\rho^2}{2} (1+\delta_{m,o}) \left(\frac{K_{m-1}(W) \; K_{m+1}(W)}{K_m^2(W)} - 1 + 2 \int_0^1 f_m^2(U,R) \; R \, dR \right) . \tag{14}$$

The modes of the continuous spectrum, because they do not satisfy the radiation condition at infinity, are not normalizable in the sense of Eqs. (12) and (13) and satisfy a different type of orthogonality condition. It can be shown fairly simply [7] that the cross integral $\langle \psi_p^{(0)*} \psi_{p'}^{(0)} \rangle$ between two radiation modes in the presence of the waveguide is identical with this same integral evaluated in the absence of the scattered term represented by $b_m H_m^{(1)}(QR)$ in Eq. (9). Noting also that we are only interested in the dominant part of the normalization integral, we see that

$$\langle \psi_p^{(0)*} \psi_{p'}^{(0)} \rangle = \pi\rho^2 (1+\delta_{m,o}) \; \delta_{mm'} \; \delta_{ss'} |a_m|^2 \int_c^\infty J_m(QR) \; J_m(Q'R) \; R \, dR \, ,$$

where c is some positive constant. Evaluating this integral asymptotically, we find

$$\langle \psi_p^{(0)*} \psi_{p'}^{(0)} \rangle = N_p^s \, \delta_{mm'} \, \delta_{ss'} \, \delta(Q-Q') \, , \tag{15a}$$

where, for these radiation modes,

$$N_p^s = \pi\rho^2 (1+\delta_{m,o}) \; |a_m|^2/Q \tag{15b}$$

and $\delta(Q-Q')$ is a Dirac delta function.

3.2.1 Perturbation Theory for Non-Circular Fibres

We now have a complete set of eigenfunctions of the scalar wave equation on a waveguide with circular cross section together with the orthogonality relations required to use these as a basis for perturbation analysis of the scalar wave equation on waveguides with non-circular symmetry. However, it must be noted that, except when $m=0$, there are two degenerate modes for each value of β. If this degeneracy is removed in first order by the non-circular perturbation, then appropriate linear combinations of the zeroth order functions must be used such that each of these new zeroth-order functions goes over continuously to one of the non-degenerate first-order functions. If the degeneracy persists in first order but is removed in second order, then linear combinations must be formed of the unperturbed first order functions. And so on. For example, in the elliptical fibre which we refer to in section 5 [1], only the $m=1$ mode pair has its degeneracy split to first order in the eccentricity. Modes with $m>1$ are less strongly affected by the ellipticity and so remain degenerate to a higher order in the perturbation.

To simplify the examples in this chapter, however, we will be restricting our attention to the fundamental mode ($m=0$, $n=1$) in which case a given value of β corresponds to a unique scalar function. For this mode, if the perturbation of the circular fibre is described as

$$f = f^{(0)}(r) + \kappa f^{(1)}(r,\phi) ,$$

where r,ϕ are circular polar coordinates, f is defined in Eq. (2) and $f^{(0)}$ corresponds to the circular structure. Then the scalar wave

equation becomes

$$\left(\rho^2\nabla_t^2 + U_0^2 - V^2(f^{(0)} + \kappa f^{(1)})\right)\psi_0 = 0 , \tag{16}$$

where ψ_0 is the eigenfunction corresponding to the fundamental mode on the non-circular fibre and U_0 is its eigenvalue. Since $|\kappa f^{(1)}| << |f^{(0)}|$ we seek a solution to Eq. (16) of the form

$$\psi_0 = \psi_0^{(0)} + \kappa\psi_0^{(1)} + O(\kappa^2) \tag{17}$$

and

$$U_0 = U_0^{(0)} + \kappa U_0^{(1)} + O(\kappa^2) , \tag{18}$$

where $\psi_0^{(0)}$ and $U_0^{(0)}$ are the corresponding eigenfunction and eigenvalue on the circular fibre. Since the modes of the circular fibre form a complete set, we can expand the first-order correction $\psi_0^{(1)}$ in the form

$$\psi_0^{(1)} = \sum_{s=\pm 1}\left\{\sum_{m=0}^{M}\sum_{n=1}^{N_m} A_p\,\psi_p^{(0)} + \sum_{m=0}^{\infty}\int_0^{\infty} A_p\,\psi_p^{(0)}\,d\Omega\right\} , \tag{19a}$$

where the first term in the brackets extends over *all allowed bound modes* and the second term represents an integral over the radiation modes. Where there is no danger of ambiguity, we write Eq. (19) in the abbreviated form

$$\psi_0^{(1)} = \sum_p A_p\,\psi_p^{(0)} , \tag{19b}$$

where the summation symbol represents all the summations and the integration in Eq. (19).

Then substituting Eqs. (17) - (19) into Eq. (16) and equating terms of equal order in κ, we find

$$\sum_p A_p\left(U_0^{(0)\,2} - U_p^{(0)\,2}\right)\psi_p^{(0)} + \left(2U_0^{(0)}\,U_0^{(1)} - V^2\,f^{(1)}\right)\psi_0^{(0)} = 0 , \tag{20}$$

where it must be recalled that, for the radiation modes, $U_p^{(0)}$ is

actually a continuous variable in the range (V,∞).

Using the mode orthogonality relations, we then derive the first order correction to U_0 as

$$U_0^{(1)} = \frac{V^2 \langle \psi_0^{(0)*} \; f^{(1)} \; \psi_0^{(0)} \rangle}{2U_0^{(0)} \; N_0^s} \tag{21}$$

and the amplitude coefficients, A_p, are given by

$$A_p = \frac{V^2 \langle \psi_p^{(0)*} \; f^{(1)} \; \psi_0^{(0)} \rangle}{\left(U_0^{(0)2} - U_p^{(0)2}\right) N_p^s} \; . \tag{22}$$

By substituting back into Eqs. (17) - (19), we then have the perturbed eigenvalue and eigenfunction on the non-circular waveguide, within an arbitrary multiple of $\kappa\psi_0^{(0)}$. The coefficient of $\psi_0^{(0)}$ in Eq. (19) is not determined by Eq. (22) but can be arbitrarily chosen depending on the normalization of the perturbed field.

3.3 ZEROTH ORDER MODES OF THE VECTOR WAVE EQUATION

To construct vector fields from the scalar functions, ψ, derived in section 2, it is necessary to add some polarization information. Since in zeroth order, where δ is assumed to be zero, the cartesian component of any transverse modal field individually satisfy the scalar wave equation, for any value of β, we can write four degenerate vector fields (except in the case $m = 0$ where only "even" modes exist):

$$\begin{aligned} \underline{e}_{xe} &= F_m(U,R) \cos m\phi \; \hat{\underline{x}} \qquad & \underline{e}_{ye} &= F_m(U,R) \cos m\phi \; \hat{\underline{y}} \\ \underline{e}_{xo} &= F_m(U,R) \sin m\phi \; \hat{\underline{x}} \qquad & \underline{e}_{yo} &= F_m(U,R) \sin m\phi \; \hat{\underline{y}} \; . \end{aligned} \tag{23}$$

Because of the degeneracy of these modes, any linear combination of them is also an eigenfunction of the scalar wave equation. However,

only certain particular combinations are valid zeroth-order modes of the vector wave equation since it is a basic assumption of the perturbation theory that the $\delta = 0$ modes go over continuously into modes of the $\delta \neq 0$ waveguide [8]. The appropriate linear combinations are therefore those which incorporate the waveguide symmetry imposed by the $\underline{\nabla}_t \ln n^2(R)$ term in the vector wave equation (2.12). It is shown in [2] that these are the symmetric and antisymmetric combinations of the fields given in Eq. (23):

$$\begin{aligned} \underline{e}_{1t}^{(0)} &= \underline{e}_{xe} + \underline{e}_{yo} & \underline{e}_{2t}^{(0)} &= \underline{e}_{xe} - \underline{e}_{yo} \\ \underline{e}_{3t}^{(0)} &= \underline{e}_{xo} + \underline{e}_{ye} & \underline{e}_{4t}^{(0)} &= \underline{e}_{xo} - \underline{e}_{ye} . \end{aligned} \tag{24}$$

Since radiation modes do not have discrete eigenvalues, the problem of degeneracy does not arise and it is not really necessary to form the combinations given in Eq. (24) — the modes given by Eq. (23) would serve equally well. However, for the sake of uniformity, we shall use the same combinations for all modes. Note also that for the $m = 0$ case, the "appropriate" combinations are simply the original $\hat{\underline{x}}$ and $\hat{\underline{y}}$ polarized fields themselves.

Assuming that δ is small, the remaining field components can be derived from Eqs. (24) using the relations (2.6).

We conclude our derivation of the zeroth-order vector modes by writing down the normalization and orthogonality properties which they satisfy. Where there is no ambiguity, we use the single subscript "p" to represent the set of mode parameters j (labelling the polarization states in Eq. (24), m (the azimuthal mode number) and either n (the radial mode number for bound modes) or Q (the transverse wave number for radiation modes). From Eqs. (12) - (15), we then find that the bound modes satisfy

$$\langle \underline{e}_{pt}^{(0)*} \cdot \underline{e}_{p't}^{(0)} \rangle = N_p \, \delta_{pp'} \, , \tag{25a}$$

where

$$N_p = \frac{2}{1+\delta_{m,o}} N_p^s \tag{25b}$$

and

$$\delta_{pp'} = \delta_{jj'} \, \delta_{mm'} \, \delta_{nn'} \tag{25c}$$

while the radiation modes satisfy

$$\langle \underline{e}_{pt}^{(0)*} \cdot \underline{e}_{p't}^{(0)} \rangle = N_p \, \delta_{jj'} \, \delta_{mm'} \, \delta(Q-Q') \, , \tag{26a}$$

where

$$N_p = \frac{2\pi\rho^2 |a_m|^2}{Q} \tag{26b}$$

and a_m is given by Eq. (10a).

3.3.1 Perturbation Theory for the Vector Wave Equation

We are now in a position to use these vector modes as a basis for perturbation of the vector wave equation in a similar manner to that outlined for the scalar wave equation in section 2. Assuming circular symmetry, we rewrite the vector wave equation (2.12) for the mode $\underline{e}_p$ in the form

$$[\rho^2\nabla_t^2 + U_p^2 - V^2 f] \, \underline{e}_{pt} = - \delta^2 \rho^2 \underline{\nabla}_t [\underline{e}_{pt} \cdot \underline{\nabla}_t \, ln \, n^2(R)] \tag{27}$$

and seek a solution of the form

$$\underline{e}_{pt} = \underline{e}_{pt}^{(0)} + \delta^2 \, \underline{e}_{pt}^{(2)} + O(\delta^4) \tag{28}$$

$$U_p = U_p^{(0)} + \delta^2 \, U_p^{(2)} + O(\delta^4) \, , \tag{29}$$

where $\delta^2 \, \underline{e}_{pt}^{(2)}$ represents the second-order correction to the modal field and $\delta^2 \, U_p^{(2)}$ the change in the modal eigenvalue due to the non-zero value of δ.

Substituting Eqs. (28) and (29) into Eq. (27) and equating terms of equal order in δ, we deduce that the higher order perturbation in U_p due to the finite value of δ is given by

$$U_p^{(2)} = \frac{\rho^2 \langle \underline{e}_{pt}^{(0)*} \cdot \underline{\nabla}_t [\underline{e}_{pt}^{(0)} \cdot \underline{\nabla}_t \ln n^2(R)] \rangle}{2U_p^{(0)} N_p} \tag{30a}$$

so that the propagation constant, to second order in δ, is given by

$$\beta_p^2 = \beta_p^{(0)2} - \frac{4\Delta}{\rho^2} U_p^{(0)} U_p^{(2)} . \tag{31}$$

If we insert the specific forms of Eqs. (23) and (24) into Eq. (30a), we find that for a circularly-symmetric fibre with arbitrary refractive-index profile, $U_{jmn}^{(2)}$, is given by

$$U_{1mn}^{(2)} = \frac{(1+\delta_{m,1}) \int_0^\infty F_m^2 [Rf'' - (2m-1) f'] \, dR}{8U_p^{(0)} \int_0^\infty F_m^2 R \, dR} \tag{30b}$$

$$U_{2mn}^{(2)} = U_{3mn}^{(2)} = \frac{\int_0^\infty F_m^2 [Rf'' + (2m+1) f'] \, dR}{8U_p^{(0)} \int_0^\infty F_m R \, dR} \tag{30c}$$

and

$$U_{4mn}^{(2)} = (1-\delta_{m,1}) U_{1mn}^{(2)} , \tag{30d}$$

where $p \equiv (j,m,n)$. These results show the interesting fact that TM_{om} and TE_{om} modes [$p = (1,1,n)$ and $(4,1,n)$, respectively] have an "accidental" degeneracy on an infinite parabolic profile, where $f = R^2$ and $U_{11n}^{(1)} = U_{41n}^{(1)} = 0$. Accidental degeneracies also occur between other mode types when $f = R^6$ and $f = R^{-2}$ but these are of less practical interest.

To find the higher-order correction to the field itself, we can expand $\underline{e}_{pt}^{(2)}$ in the form

$$\underline{e}_{pt}^{(2)} = \sum_{j'=1}^{4} \left\{ \sum_{m=0}^{M} \sum_{n=1}^{N_m} A_{p'} \underline{e}_{p't}^{(0)} + \sum_{m=0}^{\infty} \int_0^{\infty} A_{p'} \underline{e}_{p't}^{(0)} \, dQ \right\}$$

$$= \sum_{p'} A_{p'} \underline{e}_{p't}^{(0)} , \tag{32}$$

where we have introduced a generalized summation symbol as in Eq. (19). From Eq. (27) and the orthogonality conditions, we find that the expansion coefficients $A_{p'}$ $(p' \neq p)$ are given by

$$A_{p'} = \frac{\langle \underline{e}_{p't}^{(0)*} \cdot \underline{\nabla}_t [\underline{e}_{pt}^{(0)} \cdot \underline{\nabla}_t \ln n^2(R)] \rangle}{(U_p^{(0)2} - U_{p'}^{(0)2}) \, N_{p'}} . \tag{33}$$

As in the scalar case the coefficient A_p is determined only by the normalization chosen for the perturbed field.

We now proceed to consider some specific examples of the application of sections 2 and 3.

3.4 VECTOR CORRECTIONS FOR THE STEP PROFILE

The step refractive profile is defined by

$$f(R) = 0 \qquad 0 \leq R \leq 1 \tag{34a}$$

$$= 1 \qquad 1 \leq R \leq \infty \tag{34b}$$

and df/dR is a delta function at the core-cladding boundary. The fundamental mode is given by Eq. (6) with $m = 0$, i.e.

$$\tilde{\underline{e}}_t = \frac{J_0(\tilde{U}R)}{J_0(\tilde{U})} \hat{\underline{x}} \qquad 0 \leq R \leq 1 \tag{35a}$$

$$= \frac{K_0(\tilde{W}R)}{K_0(\tilde{W})} \hat{\underline{x}} \qquad 1 \leq R \leq \infty , \tag{35b}$$

where we have resumed the notation of Chapter 2 for the fundamental mode $\tilde{U} = U_0^{(0)}$ and $\tilde{W} = W_0^{(0)}$. Continuity of $\tilde{\underline{e}}_t$ and its derivative at the

core cladding boundary leads to the eigenvalue equation

$$\frac{\tilde{U}\ J_1(\tilde{U})}{J_0(\tilde{U})} = \frac{\tilde{W}\ K_1(\tilde{W})}{K_0(\tilde{W})} \tag{36}$$

which allows us to solve for $\tilde{U}$. Substitution of $\underline{\tilde{e}}_t$ into Eq. (30a), which reduces to Eq. (2.28), leads to the following expression for the eigenvalue correction,

$$U^{(2)} = \frac{1}{2}\frac{\tilde{W}^2}{V^2}\frac{J_0(\tilde{U})}{J_1(\tilde{U})} . \tag{37}$$

Similarly from Eq. (2.34), we find

$$\frac{d\tilde{U}}{dV} = \frac{\tilde{U}}{V} - \frac{\tilde{W}^2}{\tilde{U}V}\left(\frac{J_0(\tilde{U})}{J_1(\tilde{U})}\right)^2 . \tag{38}$$

Using these expressions in Eqs. (2.30) and (2.35) yields analytic expressions for $v_g^{(2)}$, $v_g^{(4)}$, $\tilde{D}$ and $D^{(2)}$. These parameters are plotted in Figs. 4.3 and 4.4, where they are also obtained by allowing the exponent q of the power-law profiles to go to infinity.

The modal field correction $\underline{e}_t^{(2)}$ is given directly by Eqs. (32) and (33). On the single mode fibre the summation over the discrete spectrum in Eq. (32) includes only the fundamental mode $\underline{\tilde{e}}_t$. The term $\underline{\nabla}_t[\underline{\tilde{e}}_t \cdot \underline{\nabla}_t \ln n^2(R)]$ is required to evaluate the coefficients A_p of Eq. (33). For the step index where $[\underline{\nabla}_t \ln n^2(R)]$ is a delta function, we require only the value of the field $\underline{\tilde{e}}_t$ in the core. The expression then becomes

$$\begin{aligned}\underline{\nabla}_t[\underline{\tilde{e}}_t \cdot \underline{\nabla}_t \ln n^2(R)] = -\frac{1}{2J_0(\tilde{U})}\Bigg\{\Bigg(\Bigg(\frac{1}{R}J_0(\tilde{U}R) - \tilde{U}\ J_1(\tilde{U}R)\Bigg)\ \delta(R-1) \\ + J_0(\tilde{U}R)\ \delta'(R-1)\Bigg)\ \underline{\hat{x}} + \Bigg(\Bigg(-\frac{1}{R}J_0(\tilde{U}R) - \tilde{U}\ J_1(\tilde{U}R)\Bigg)\ \delta(R-1) \\ + J_0(\tilde{U}R)\ \delta'(R-1)\Bigg)\ \Big(\cos 2\phi\underline{\hat{x}} + \sin 2\phi\underline{\hat{y}}\Big)\Bigg\} .\end{aligned} \tag{39}$$

Observation of this expression indicates that we require only the two

radiation modes (1) $m=0$ and with x component only and (2) $m=2$ with even-x and odd-y components. If we label the coefficients corresponding to these two modes A_1 and A_2 respectively we find from Eqs. (33) and (26) that

$$A_1 = -\frac{2}{\pi^2}\frac{Q\ U\ J_1(U)}{(Q-\tilde{Q}^2)\ J_0(U)\ (D_0)^2} \tag{40a}$$

and

$$A_2 = \frac{2}{\pi^2}\frac{Q\ U\ J_1(U)}{(Q-\tilde{Q}^2)\ J_2(U)\ (D_2)^2}, \tag{40b}$$

where

$$D_m = -\frac{1}{J_m(U)}\left[U\ J_{m+1}(U)\ H_m(Q) - Q\ H_{m+1}(Q)\ J_m(U)\right]. \tag{41}$$

The expression for $\underline{e}_t^{(2)}$ is then obtained from Eq. (32).

On evaluating the integral over the continuous spectrum using contour-integration methods described in the Appendix, we find that for the mode with x-polarized zeroth-order term,

$$\begin{aligned}\underline{e}_{ot}^{(2)} &= \frac{1}{J_0(\tilde{U})}\Big\{\hat{\underline{x}}[A_0J_0(\tilde{U}R) + U^{(2)}(CJ_0(\tilde{U}R) - RJ_1(\tilde{U}R) - \tfrac{1}{2}\tilde{U}J_2(\tilde{U}R)\ \cos 2\phi)] \\ &\quad - \hat{\underline{y}}[\tfrac{1}{2}\tilde{U}U^{(2)}\ J_2(\tilde{U}R)\ \sin 2\phi]\Big\} \qquad R \le 1 \\ &= \frac{1}{K_0(\tilde{W})}\Big\{\hat{\underline{x}}\Big[A_0K_0(\tilde{W}R) + U^{(2)}\Big[CK_0(\tilde{W}R) + \frac{\tilde{U}}{\tilde{W}}RK_1(\tilde{W}R) + \tfrac{1}{2}\tilde{U}K_2(WR)\ \cos 2\phi\Big]\Big] \\ &\quad + \hat{\underline{y}}[\tfrac{1}{2}UU^{(2)}\ K_2(\tilde{W}R)\ \sin 2\phi]\Big\} \qquad R \ge 1\end{aligned} \tag{42a}$$

where $C = (\tilde{W}^2 - \tilde{U}^2)/(\tilde{U}\tilde{W}^2)$. In terms of cylindrical coordinate directions

$$\begin{aligned}\underline{e}_{ot}^{(2)} &= \frac{1}{J_0(\tilde{U})}\Big\{\hat{\underline{r}}\ \cos\phi[A_0J_0(\tilde{U}R) + U^{(2)}(CJ_0(\tilde{U}R) - RJ_1(\tilde{U}R) - \tfrac{1}{2}\tilde{U}J_2(\tilde{U}R)] \\ &\quad - \hat{\underline{\phi}}\sin\phi[A_0J_0(\tilde{U}R) + U^{(2)}(CJ_0(\tilde{U}R) - RJ_1(\tilde{U}R) + \tfrac{1}{2}\tilde{U}J_2(\tilde{U}R))]\Big\} \qquad R \le 1 \\ &= \frac{1}{K_0(\tilde{W})}\Big\{\hat{\underline{r}}\ \cos\phi\Big[A_0K_0(\tilde{W}R) + U^{(2)}\Big[CK_0(\tilde{U}R) + \frac{\tilde{U}}{\tilde{W}}RK_1(\tilde{W}R) + \tfrac{1}{2}\tilde{U}K_2(\tilde{W}R)\Big]\Big] \\ &\quad - \hat{\underline{\phi}}\sin\phi\Big[A_0K_0(\tilde{W}R) + U^{(2)}\Big[CK_0(\tilde{W}R) + \frac{\tilde{U}}{\tilde{W}}RK_1(\tilde{W}R) - \tfrac{1}{2}\tilde{U}K_2(\tilde{W}R)\Big]\Big]\Big\} \qquad R \ge 1\,.\end{aligned} \tag{42b}$$

Similar expressions can be found for the y-polarized form.

The coefficient A_0 is determined only by normalization. When A_0 is equal to zero, $\langle \underline{e}^*_{ot} \cdot \underline{e}_{ot} \rangle = N_0 + O(\delta^2)$. Alternatively, if we choose to normalize the perturbed field as in Chapter 2, so that modal power is unchanged in first order, i.e. $\langle \underline{e}_{ot} \times \underline{h}^*_{ot} \cdot \hat{\underline{z}} \rangle = (\varepsilon/\mu)^{\frac{1}{2}} N_0 + O(\delta^4)$, then

$$A_0 = U^{(2)} \left\{ C + \tfrac{1}{2} \left(\frac{\tilde{U}^2 J_1^2}{\tilde{W}^2 J_0^2} - 1 \right) \frac{J_0}{J_1} \right\} .$$

The latter is the normalization chosen in Figs. 4.5 which illustrates the radial and tangential components of $\underline{e}^{(1)}_{ot}$ when $V = 2.4$. Note that the $\hat{\underline{\phi}}$-component is continuous at $R = 1$ as required by the boundary conditions.

3.5 BIREFRINGENCE IN WAVEGUIDES WITH ELLIPTICAL CROSS SECTION

In a fibre with circular cross section, the two polarization states of the fundamental mode (modes $\underline{e}_{xe}$ and $\underline{e}_{ye}$ of Eq. (23) with $m = 0$) obviously have identical propagation constants for all δ since there is no physical difference between the two polarizations. If the core is deformed in such a way that its cross section becomes elliptical, with the major axis aligned in the x-direction, then to zeroth order in δ, the two polarization states remain degenerate. However, when δ is non-zero, this degeneracy is lifted so that an elliptical monomode fibre is birefringent — light polarized in the direction of the major axis has a smaller phase velocity than that polarized along the minor axis.

In this section we will use Eq. (32) to determine the expression for the phase difference, $\delta\beta$, between the two orthogonally polarized modes in monomode fibres with slightly elliptical cross section. The

two modes have zeroth order transverse fields of the form

$$\underline{E}_x = \psi\hat{\underline{x}} \quad \text{and} \quad \underline{E}_y = \psi\hat{\underline{y}}\,, \tag{43}$$

where ψ satisfies the scalar wave equation for the elliptical fibre. Thus, from Eqs. (31), (12) and (13)

$$\delta\beta^2 \equiv \beta_x^2 - \beta_y^2$$

$$= \frac{\delta}{\langle \phi^*\phi \rangle} \langle \underline{E}_y^*.\nabla_t[\underline{E}_y.\underline{\nabla}_t \ln n^2(R)] - \underline{E}_x^*.\nabla_t[\underline{E}_x.\underline{\nabla}_t \ln n^2(R)] \rangle .$$

Using Eqs. (43) and (2.13) and integrating by parts, we then find that

$$\delta\beta^2 = \frac{2\Delta}{\langle \phi^2 \rangle} \langle \phi \left(\frac{\partial\phi}{\partial x}\frac{\partial f}{\partial x} - \frac{\partial\phi}{\partial y}\frac{\partial f}{\partial y}\right) \rangle \tag{44a}$$

$$= \frac{\Delta}{\langle \phi^2 \rangle} \langle f \left(\frac{\partial^2}{\partial y^2} - \frac{\partial^2}{\partial x^2}\right) \phi^2 \rangle , \tag{44b}$$

where we have used the fact that, for a bound mode, ψ is a real function. Since all bound modes on a weakly-guiding fibre satisfy $\rho\beta \simeq \rho\, k_{co} = V\,\delta^{-1}$, we can write

$$\delta\beta \simeq \frac{\rho\delta}{2V}\,\delta\beta^2 . \tag{44c}$$

All we require to determine the degree of birefringence is therefore the eigenfunction of the scalar wave equation corresponding to the fundamental mode on the elliptical waveguide, which can be determined using the methods presented in section 2.

3.6 RESUMÉ

We have shown how a complete set of modes of the scalar wave equation on a circularly symmetric fibre of arbitrary refractive-index profile can be used as a basis for perturbation analyses of a range of optical waveguide problems. This approach has enabled us to generalize in a systematic way methods of obtaining results which have

previously been known only for the step-index fibre, such as (i) the vector correction to the field of the fundamental mode, and (ii) the difference in phase velocity between the two polarization states of the fundamental mode on a fibre with slightly elliptical cross section when account is taken of the non-zero difference between the refractive-indices of the core and cladding. Although the method is general, we have demonstrated the method only for the step index case. For the power law profiles considered in Part 1 of this thesis, we present a simpler and more direct method in the following chapter.

APPENDIX

DETAILS OF THE CONTOUR INTEGRATION

The expression for $\underline{e}_t^{(2)}$ in the core can be written as

$$\underline{e}_t^{(2)} = A_0 \, \underline{\tilde{e}}_t - \frac{2}{\pi^2} \left[G_0 \underline{\tilde{x}} + G_2 (\cos 2\phi \underline{\hat{x}} + \sin 2\phi \underline{\hat{y}}) \right] , \tag{45}$$

where

$$G_m = \int_0^\infty \frac{Q \, I_m \, J_m(UR)}{(Q - \tilde{Q}^2) \, J_m(U) \, |D_m|^2} \, dQ \tag{46}$$

$$I_0 = \frac{U \, J_1(U)}{J_0(U)} \quad \text{and} \quad I_2 = - \frac{U \, J_1(U)}{J_2(U)} \tag{47}$$

and D_m is given by Eq. (41). It is the purpose of this section to evaluate the integrals G_m analytically. In the above Eq. (46) we have omitted the summation over the higher order bound mode terms since on the single mode fibre these do not propagate. Using similar arguments it is clear that while D_m has zeros corresponding to the eigenvalues of the higher order bound modes, we can neglect calculating the

residues for these since they do not exist on the single mode fibre. In general, on the multimode fibre, the contributions both from the additional bound modes and the residue terms obtained from the integral will cancel. We need, therefore, only calculate the residue at the pole $Q = \pm\tilde{Q}$. To evaluate the integral we extend the range of integration to $(-\infty,\infty)$. We note that for real Q

$$\frac{1}{|D_m|^2} = \tfrac{1}{4}\pi i\left(\frac{H_m^{(2)}(Q)}{D_m^*} - \frac{H_m^{(1)}(Q)}{D_m}\right) . \tag{48}$$

This expression is useful when evaluating the integrals involved in determining the cladding field on the circular and the birefringence on the non-circular fibre. However, if we use Eq. (48) to extend the range of integration to $(-\infty,\infty)$ for the core field, as before, then we arrive at

$$G_m = -\tfrac{1}{4}\pi i \int_{-\infty}^{\infty} \frac{Q\ I_m(U)\ H_m^{(1)}(Q)\ f_m(UR)}{(Q^2 - \tilde{Q}^2)\ D_m}\, dQ \tag{49}$$

$$= \tfrac{1}{4}\pi i \int_{-\infty}^{\infty} \frac{UQ\ J_1(U)\ H_m^{(1)}(Q)\ J_m(UR)}{(Q^2 - \tilde{Q}^2)\ J_m(U)\ (UJ_1 H_m^{(1)} - QH_1^{(1)}\ J_m)}\, dQ \tag{50}$$

so that the integrand of G_m has an infinite number of poles at the zeros of $J_m(U)$, as well as those at the bound-mode eigenvalues. This problem can be overcome by noting that Eq. (48) can be rewritten in the alternative form

$$\frac{1}{|D_m|^2} = \frac{\pi i}{4(m + f_m')}\left(\frac{QH_{m-1}^{(2)}(Q)}{D_m^*} - \frac{QH_{m-1}^{(1)}(Q)}{D_m}\right) . \tag{51}$$

Using this relationship, Eqs. (49) and (50) are replaced by

$$G_m = -\tfrac{1}{4}\pi i \int_{-\infty}^{\infty} \frac{Q^2\ I_m(U)\ H_{m-1}^{(1)}(Q)\ f_m(UR)}{(Q^2 - \tilde{Q}^2)\ D_m(m + f_m')}\, dQ \tag{52}$$

$$= \mp\tfrac{1}{4}\pi i \int_{-\infty}^{\infty} \frac{Q^2 \; H_1^{(1)}(Q) \; J_m(UR)}{(Q^2 - \tilde{Q}^2) \; (UJ_1 H_m^{(1)} - QH_1^{(1)} \; J_m)} \, dQ \, , \tag{53}$$

where the upper sign applies to $m = 0$ and the lower sign to $m = 2$. We now close the contour of integration with an infinite semi-circle in the upper half plane. In this representation, the integrand only has poles at the bound mode eigenvalues (for the step-index case). Evaluation of the residue at the pole $Q = \tilde{Q}$ [9] gives the result for the core field in Eq. (42).

Of course the two representations for G_m are identical, the connection between them being the Fourier-Bessel expansion

$$\frac{J_m(\tilde{U}R)}{J_m(\tilde{U})} = 2 \sum_{\nu} \frac{U_\nu J_m(U_\nu R)}{(\tilde{U}^2 - U_\nu^2) \; J_{m-1}(U_\nu)} \, ,$$

where the sum extends over the positive zeros of J_m.

REFERENCES

1. Sammut, R.A., Hussey, C.D., Love, J.D., Snyder, A.W.: "Modal analysis of polarization effects in weakly guiding fibres", *I.E.E. Proc. Part H* 128, 173-187 (1981).

2. Snyder, A.W., Young, W.R.: "Modes of optical waveguides", *J. Opt. Soc. Am.* 68, 297-309 (1978).

3. Snyder, A.W., Sammut, R.A.: "Radiation modes of optical waveguides", *Electron. Lett.* 15, 4-5 (1979).

4. Snyder, A.W.: "Asymptotic expressions for eigenfunctions and eigenvalues of a dielectric or optical waveguide", *I.E.E.E. Trans.* MTT-17, 1130-1138 (1969).

5. Love, J.D., Hussey, C.D., Snyder, A.W., Sammut, R.A.: "Polarization corrections to mode propagation on weakly-guiding fibres" (submitted).

6. Sammut, R.A.: "Birefringence in graded index monomode fibres with elliptical cross section", *Electron. Lett.* 16, 156-157 (1980).

7. Friedman, B.: *Principles and Techniques of Applied Mathematics* (Wiley, New York, 1956), 251-252.

8. Borowitz, S.: *Fundamentals of Quantum Mechanics* (Benjamin, New York, 1967), Section 14-6.

9. Carrier, G.F., Krook, M., Pearson, C.E.: *Functions of a Complex Variable* (McGraw-Hill, New York, 1966).

CHAPTER 4

POWER SERIES METHODS

PREAMBLE

We present the results for the polarization corrections as defined in Chapter 2 for the infinite parabolic profile and the class of clad power-law profiles. The infinite parabolic profile leads to simple analytic expressions and, although it is unphysical, it does provide a reasonable model for some fibre parameters. For the power law profiles we solve the eigenvalue correction in terms of the power series solution of the fundamental mode. The second order field corrections are solved using a power series trial function, matching the boundary conditions and using the normalization defined in Chapter 2. We finally give an overall discussion of the results of Part 1.

4.1 INTRODUCTION

We examine the effects of polarization on the modal properties of fibres with either the infinite parabolic profile or one of the family of clad power-law profiles. The former leads to simple expressions for all quantities of interest and the latter is analysed using a power series expansion [1]. This method is simpler and more direct than the eigenfunction expansion methods of Chapter 3 [2] or the Green's function method [3], but is restricted in application to the special case of clad power law profiles.

We consider the infinite parabolic profile

$$n^2(R) = n_{co}^2(1 - 2\Delta R^2) , \qquad 0 \le R < \infty , \tag{1a}$$

or

$$f(R) = R^2 , \qquad 0 \le R < \infty , \tag{1b}$$

and the family of clad power-law profiles

$$n^2(R) = n_{co}^2(1 - 2\Delta R^q) , \qquad 0 \le R \le 1 , \tag{2a}$$

or

$$f(R) = R^q , \qquad 0 \le R \le 1 , \tag{2b}$$

$$n^2(R) = n_{cl}^2 = n_{co}^2(1 - 2\Delta) , \qquad 0 \le R < \infty , \tag{2c}$$

or

$$f(R) = 1 , \qquad 1 \le R < \infty , \tag{2d}$$

These profiles are illustrated in Fig. 1. The infinite parabolic profile coincides with the clad parabolic profile ($q = 2$) for $0 \le R \le 1$, and the step profile corresponds to the limit $q \to \infty$.

The infinite parabolic profile is unphysical since $n^2(R) \to -\infty$ as $R \to \infty$ and the weak guidance approximation is inaccurate where there are large variations in profile. However, if we restrict attention to larger values of V, mode power is then confined close to the fibre axis and the effect of the region $R \gg 1$ becomes insignificant. The advantage of this profile is that it leads to simple expressions for all scalar and higher order corrections, and is a reasonable model for a class of practical fibres.

4.2 INFINITE PARABOLIC PROFILE

We first consider the profile defined by Eq. (1), which leads to simple expressions for all the quantities introduced in Chapter 2, and thus provides qualitative insight into the polarization effects of the fibre. As explained in section 1, the profile is unphysical as $R \to \infty$, but the results are physically relevant provided V is not too small.

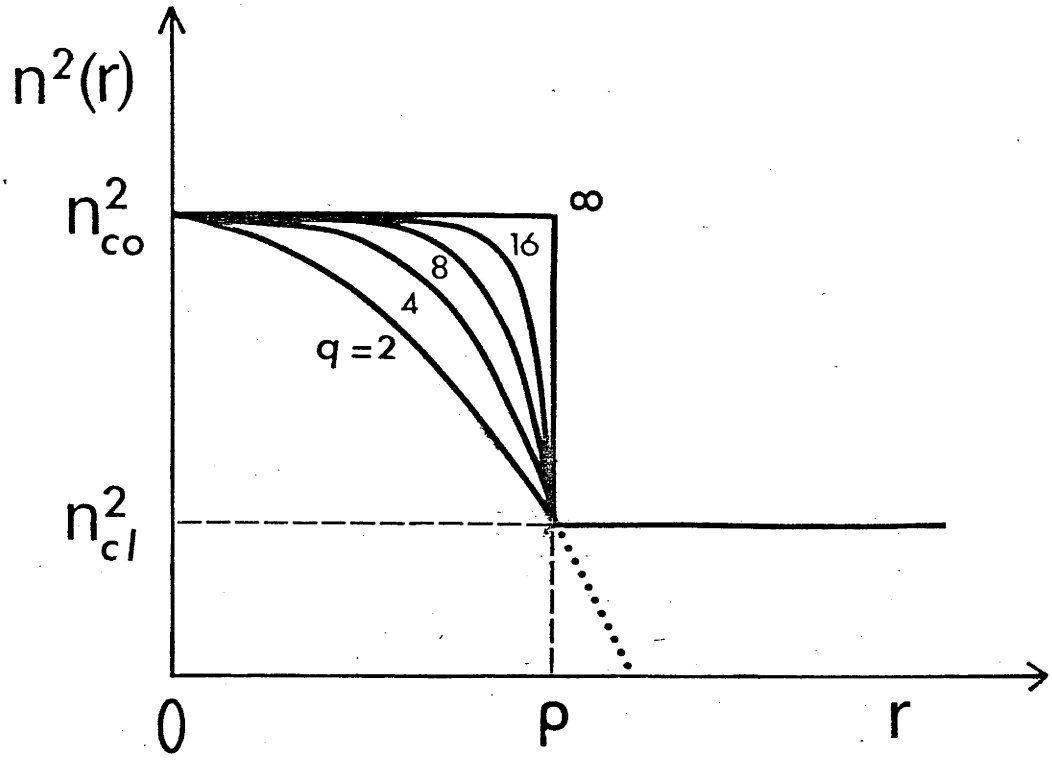

Fig. 1: Plots of the clad power-law profiles of Eq. (2) and the infinite parabolic profile of Eq. (1), the latter coinciding with the $q = 2$ profile for $0 \le R \le 1$.

If we substitute Eq. (1) into the scalar wave equation (2.21), it is readily verified that the fundamental mode amplitude Ψ satisfying $\Psi = 1$ at $R = 1$ is given by

$$\Psi = \exp\left(-\frac{V}{2}(R^2 - 1)\right), \tag{3}$$

and the corresponding modal parameter and propagation constant are

$$\tilde{U} = (2V)^{\frac{1}{2}} \qquad \tilde{\beta} = \frac{V}{\rho\delta}\left(1 - \frac{2\delta^2}{V}\right)^{\frac{1}{2}}. \tag{4}$$

It follows from Eqs. (2.28) and (2.25) that the corrections are given by

$$U^{(2)} = \frac{1}{(8V)^{\frac{1}{2}}} \qquad \beta^{(3)} = -\frac{1}{2\rho V}. \tag{5}$$

The group velocity components of Eq. (2.30) follow from Eqs. (4) and

(5) as

$$v_g^{(2)} = 0 \qquad v_g^{(4)} = -\frac{1}{V^2}, \tag{6}$$

and the dispersion parameter expressions of Eq. (2.35) give

$$\tilde{D} = 0 \qquad D^{(2)} = -\frac{2}{V^3}. \tag{7}$$

The transverse field solution of Eq. (2.37) which satisfies the normalization condition of Eq. (2.40) is found by inspection to be

$$e_x^{(2)} = \frac{R^2}{2}\Psi\cos 2\phi \qquad e_y^{(2)} = \frac{R^2}{4}\Psi\sin 2\phi, \tag{8a}$$

in terms of Eq. (3). Relative to the radial and azimuthal directions this solution takes the simpler form

$$e_r^{(2)} = \frac{R^2}{2}\Psi\cos\phi \qquad e_\phi^{(2)} = 0. \tag{8b}$$

The remaining field components and normalization in Table 2.1 give

$$\tilde{\underline{h}}_t = \left(\frac{\varepsilon_{co}}{\mu}\right)^{\frac{1}{2}}\Psi\hat{\underline{y}} \qquad e_z^{(1)} = -iR\Psi\cos\phi \qquad h_z^{(1)} = -i\left(\frac{\varepsilon_{co}}{\mu}\right)^{\frac{1}{2}}R\Psi\sin\phi, \tag{9a}$$

$$\underline{h}_t^{(2)} = -\frac{R^2}{2}\Psi\cos\phi\hat{\underline{\phi}} \qquad e_z^{(3)} = -\frac{i}{2V}R\Psi(3+VR^2)\cos\phi, \tag{9b}$$

$$h_z^{(3)} = -\frac{i}{2V}\left(\frac{\varepsilon_{co}}{\mu}\right)^{\frac{1}{2}}R^2\Psi\sin\phi \qquad \tilde{N} = \frac{\pi}{2}\left(\frac{\varepsilon_{co}}{\mu}\right)^{\frac{1}{2}}\frac{e^V}{V}. \tag{9c}$$

4.3 CLAD POWER-LAW PROFILES

The clad profiles are defined by Eq. (2) and illustrated in Fig. 1. For the fundamental mode the solution of the scalar wave equation (2.21) is expressible as a power series in the core, and is proportional to the zero-order modified Hankel function of the second kind in the cladding [4,5,6]. Hence

$$\Psi = \sum_{n=0}^{\infty} a_n R^n \qquad 0 \le R \le 1 , \tag{10a}$$

$$= \frac{K_0(\tilde{W}R)}{K_0(\tilde{W})} \qquad 1 \le R < \infty , \tag{10b}$$

where $\tilde{W} = (V^2 - \tilde{U}^2)^{\frac{1}{2}}$, and the coefficients are related by

$$a_{2m} = -\frac{\tilde{U}^2}{4m^2} a_{2m-2} \qquad 2 \le 2m < q+2 , \tag{11a}$$

$$a_n = \frac{1}{n^2}(V^2 a_{n-q-2} - \tilde{U}^2 a_{n-2}) \qquad q+2 \le n < \infty . \tag{11b}$$

The value of a_0 is chosen to satisfy $\Psi = 1$ at $R = 1$, i.e. continuity of Ψ. If $q \to \infty$ the series reduces to the step-profile result $J_0(\tilde{U}R)/J_0(\tilde{U})$, where J_0 is the Bessel function of the first kind. Continuity of Ψ and $d\Psi/dR$ at the interface leads to the eigenvalue equation

$$\sum_{n=0}^{\infty} n a_n = -\tilde{W}\frac{K_1(\tilde{W})}{K_0(\tilde{W})} , \tag{12}$$

and the left side reduces to $-\tilde{U}J_1(\tilde{U})/J_0(\tilde{U})$ as $q \to \infty$.

If we substitute Eq. (10) into Eqs. (2.27) and (2.34), we find

$$U^{(2)} = -\frac{1}{4\tilde{U}}\frac{A}{B+C} \qquad \frac{d\tilde{U}}{dV} = \frac{V}{\tilde{U}}\frac{C+F}{B+C} , \tag{13a}$$

where C involves a standard Bessel function integral [9], and

$$A = q\sum_{m=0}^{\infty}\sum_{n=0}^{\infty}\frac{n a_m a_n}{m+n+q} \qquad B = \sum_{m=0}^{\infty}\sum_{n=0}^{\infty}\frac{a_m a_n}{m+n+2} , \tag{13b}$$

$$C = \frac{1}{2}\left(\frac{K_1^2(\tilde{W})}{K_0^2(\tilde{W})} - 1\right) \qquad F = \sum_{m=0}^{\infty}\sum_{n=0}^{\infty}\frac{a_m a_n}{m+n+q+2} . \tag{13c}$$

We differentiate the expressions in Eq. (13a) to obtain other derivatives of $U^{(2)}$ and $\tilde{U}$ occurring in Eqs. (2.30) and (2.35). Since the coefficients in Eq. (10a) depend implicitly on $\tilde{U}$, we need to evaluate terms like $da_n/d\tilde{U}$ and $d^2a_n/d\tilde{U}^2$. This is achieved by

differentiating Eq. (11) with respect to $\tilde{U}$ and solving the resulting recurrence relations with $da_0/d\tilde{U} = d^2a_0/d\tilde{U}^2 = 0$. A check on the values is provided by numerical differentiation of the values of $\tilde{U}$ obtained from the eigenvalue equation as V varies.

The transverse electric field corrections for the x-polarized fundamental mode follow by substituting Eq. (10) into Eq. (2.37). Within the core $f(R) = R^q$, and

$$\mathcal{L}e_x^{(2)} = \sum_{n=0}^{\infty} a_n\left(-2\tilde{U}U^{(2)}R^n + \frac{q}{2}(n+q)\,R^{n+q-2} + \frac{q}{2}(n+q-2)\,R^{n+q-2}\cos 2\phi\right), \tag{14a}$$

$$\mathcal{L}e_y^{(2)} = \frac{q}{2}\sum_{n=0}^{\infty} a_n(n+q-2)\,R^{n+q-2}\sin 2\phi\,. \tag{14b}$$

Within the cladding $f(R) = 1$, and

$$\mathcal{L}e_x^{(2)} = -2\tilde{U}U^{(2)}\frac{K_0(\tilde{W}R)}{K_0(\tilde{W})} \qquad \mathcal{L}e_y^{(2)} = 0\,. \tag{15}$$

To solve Eq. (14) we express $e_x^{(2)}$ and $e_y^{(2)}$ as power series

$$e_x^{(2)} = \sum_{n=0}^{\infty}(c_n + b_n\cos 2\phi)\,R^n\,, \tag{16a}$$

$$e_y^{(2)} = \sum_{n=0}^{\infty} b_n\,R^n\sin 2\phi \tag{16b}$$

and substitute. Recalling $\mathcal{L}$ of Eq. (2.16) and equating powers of R gives

$$b_0 = b_1 = 0 \qquad b_{2m} = -\frac{\tilde{U}^2}{4m^2-4}\,b_{2m-2} \qquad 4 \le 2m < 2q\,, \tag{17a}$$

$$b_n = \frac{1}{2n^2-8}\left[q(n-2)\,a_{n-q} - 2\tilde{U}^2\,b_{n-2}\right] \qquad q \le n < q+2\,, \tag{17b}$$

$$b_n = \frac{1}{2n^2-8}\left[2V^2\,b_{n-q-2} + q(n-2)\,a_{n-q} - 2\tilde{U}^2\,b_{n-2}\right] \qquad q+2 \le n < \infty\,, \tag{17c}$$

$$c_1 = 0 \qquad c_{2m} = -\frac{1}{4m^2}\left(\tilde{U}^2 c_{2m-2} + 2\tilde{U}U^{(2)} a_{2m-2}\right) \qquad 2 \le 2m < 2q\,, \tag{18a}$$

$$c_n = \frac{1}{2n^2}\left(qna_{n-q} - 4\tilde{U}U^{(2)} a_{n-2} - 2\tilde{U}^2 c_{n-2}\right) \qquad q \le n < q+2\,, \tag{18b}$$

$$c_n = \frac{1}{2n^2}\left(2V^2 c_{n-q-2} + qna_{n-q} - 4\tilde{U}U^{(2)} a_{n-2} - 2\tilde{U}^2 c_{n-2}\right) \qquad q+2 \le n < \infty\,, \tag{18c}$$

where b_2 and c_0 are to be determined, and govern the admixture of particular and complementary solutions of Eq. (16). The corresponding solution of Eq. (15) has the form

$$e_x^{(2)} = \frac{\tilde{U}U^{(2)}}{\tilde{W}} R \frac{K_1(\tilde{W}R)}{K_0(\tilde{W})} + d\frac{K_0(\tilde{W}R)}{K_0(\tilde{W})} + f\frac{K_2(\tilde{W}R)}{K_2(\tilde{W})}\cos 2\phi\,, \tag{19a}$$

$$e_y^{(2)} = f\frac{K_2(\tilde{W}R)}{K_2(\tilde{W})}\sin 2\phi\,, \tag{19b}$$

where d and f are to be determined, and the first term on the right of Eq. (19a) is a particular solution of Eq. (15) as may be verified.

We use normalization and the boundary conditions for the vector fields at $R=1$ to evaluate b_2, c_0, d and f. If we substitute Eqs. (16a) and (19a) into Eq. (2.40), the condition $N^{(2)}=0$ gives

$$4Cd + 4G = F + C - 2\frac{\tilde{U}U^{(2)}}{\tilde{W}^2}(2C+1)\,, \tag{20}$$

using $dK_0(z)/dz = -K_1(z)$, where C and F are defined by Eq. (13c) and G denotes B of Eq. (13b) with $a_m a_n$ replaced by $a_m c_n$. In applying the boundary conditions, and in the presentation of results it is convenient to work with the radial and azimuthal components, where from Eqs. (16) and (19) we have

$$e_r^{(2)} = \cos\phi \sum_{n=0}^{\infty} (b_n + c_n) R^n \qquad 0 \le R < 1\,, \tag{21a}$$

$$= \cos\phi \left\{ f\frac{K_2(\tilde{W}R)}{K_2(\tilde{W})} + d\frac{K_0(\tilde{W}R)}{K_0(\tilde{W})} + \frac{\tilde{U}U^{(2)}}{\tilde{W}} R \frac{K_1(\tilde{W}R)}{K_0(\tilde{W})} \right\} \qquad 1 < R < \infty\,, \tag{21b}$$

$$e_\phi^{(2)} = \sin\phi \sum_{n=0}^{\infty} (b_n - c_n)\, R^n \qquad 0 \le R \le 1\,, \quad (21c)$$

$$= \sin\phi \left\{ f \frac{K_2(\tilde{W}R)}{K_2(\tilde{W})} - d \frac{K_0(\tilde{W}R)}{K_0(\tilde{W})} - \frac{\tilde{U}U^{(2)}}{\tilde{W}} R \frac{K_1(\tilde{W}R)}{K_0(\tilde{W})} \right\} \qquad 1 \le R < \infty\,. \quad (21d)$$

Continuity of $e_\phi^{(2)}$ leads to

$$\sum_{n=0}^{\infty} (b_n - c_n) = f - d - \frac{\tilde{U}U^{(2)}}{\tilde{W}} \frac{K_1(\tilde{W})}{K_0(\tilde{W})}\,. \quad (22)$$

In Table 2.1, continuity of $h_\phi^{(2)}$ is equivalent to continuity of $e_r^{(2)} - V^{-2}\, d^2\Psi/dR^2$ since Ψ is continuous. From Eqs. (10) and (21) we deduce that at $R = 1$

$$\sum_{n=0}^{\infty} (b_n + c_n) - \frac{1}{V^2} \sum_{n=0}^{\infty} n(n-1)\, a_n = f + d + \frac{\tilde{U}U^{(2)}}{\tilde{W}} + \frac{\tilde{W}^2}{V^2} + \frac{\tilde{W}}{V^2} \frac{K_1(\tilde{W})}{K_0(\tilde{W})}\,, \quad (23)$$

using recurrence relations for the K's [9]. The final relationship follows from continuity of $e_z^{(3)}$ at $R = 1$, which is equivalent to continuity of $R^{-2}\, \partial(Re_r^{(2)})/\partial R - df/dR \cos\phi$ since $e_z^{(1)}$ and $e_\phi^{(2)}$ are continuous. Hence

$$\sum_{n=0}^{\infty} (n+1)(b_n + c_n) - q = d\left\{1 - \frac{\tilde{W}K_1(\tilde{W})}{K_0(\tilde{W})}\right\} - f\left\{1 + \frac{\tilde{W}K_1(\tilde{W})}{K_2(\tilde{W})}\right\} + \frac{\tilde{U}U^{(2)}}{\tilde{W}} \left\{1 - \frac{K_1(\tilde{W})}{K_0(\tilde{W})}\right\}. \quad (24)$$

The solutions of the recurrence relations in Eqs. (17) and (18) for b_n and c_n in terms of b_2 and c_0 respectively are substituted into Eqs. (20) and (22) - (24). The resulting set of equations is then solved for b_2, c_0, d and f, and the transverse electric field correction follows from Eq. (21). All remaining field components are found by substituting Eqs. (10) and (20) into Table 2.1.

4.4 RESULTS

4.4.1 Propagation Constant

The x- and y-polarized fundamental modes on a circular fibre have the same scalar propagation constant $\tilde{\beta}$. In Fig. 2(a) we plot the corresponding values of $\tilde{U}$ of Eq. (2.15c) against the fibre parameter V. For the step and power-law profiles, $\tilde{U}$ is determined numerically from the eigenvalue equation given by Eq. (12), and for the infinite parabolic profile $\tilde{U}$ is given explicitly by Eq. (4). The values of $\tilde{U}$ for the clad and infinite parabolic profiles merge as V increases, as virtually all modal power is concentrated within $R = 1$. The polarization correction $U^{(2)}$ of Eq. (2.15a) is given explicitly by Eqs. (5) and (13a), and is plotted in Fig. 2(b). As we might expect intuitively, the plots show that for smaller values of V, when modal power is spread into the cladding, the effect of the polarization term $\underline{\nabla}_t \ln n^2(R)$ on the clad profiles is most pronounced for the step profile. In fact, as shown in Chapter 3, this term is proportional to the Dirac delta function $\delta(R-1)$ for the step profile. However, as V increases and modal power is confined mainly to $R < 1$, the situation is reversed and polarization effects are most significant for the clad profile with the smallest value of q, since $\underline{\nabla}_t \ln n^2(R)$ is then largest in the neighbourhood of $R = 0$. In Fig. 2(b), the clad parabolic profile suggests this behaviour, which is seen more clearly in the plots of $U^{(2)}/\tilde{U}$ in Fig. 9 of reference 2.

4.4.2 Group Velocity

Within the scalar approximation, the group velocity $\tilde{v}_g$ is given by the first two terms of the expansion in Eq. (2.17a). Plots of $v_g^{(2)}$ against V are given in Fig. 3(a). For the infinite parabolic profile $v_g^{(2)} = 0$, and for the step and power-law profiles $v_g^{(2)}$ is evaluated

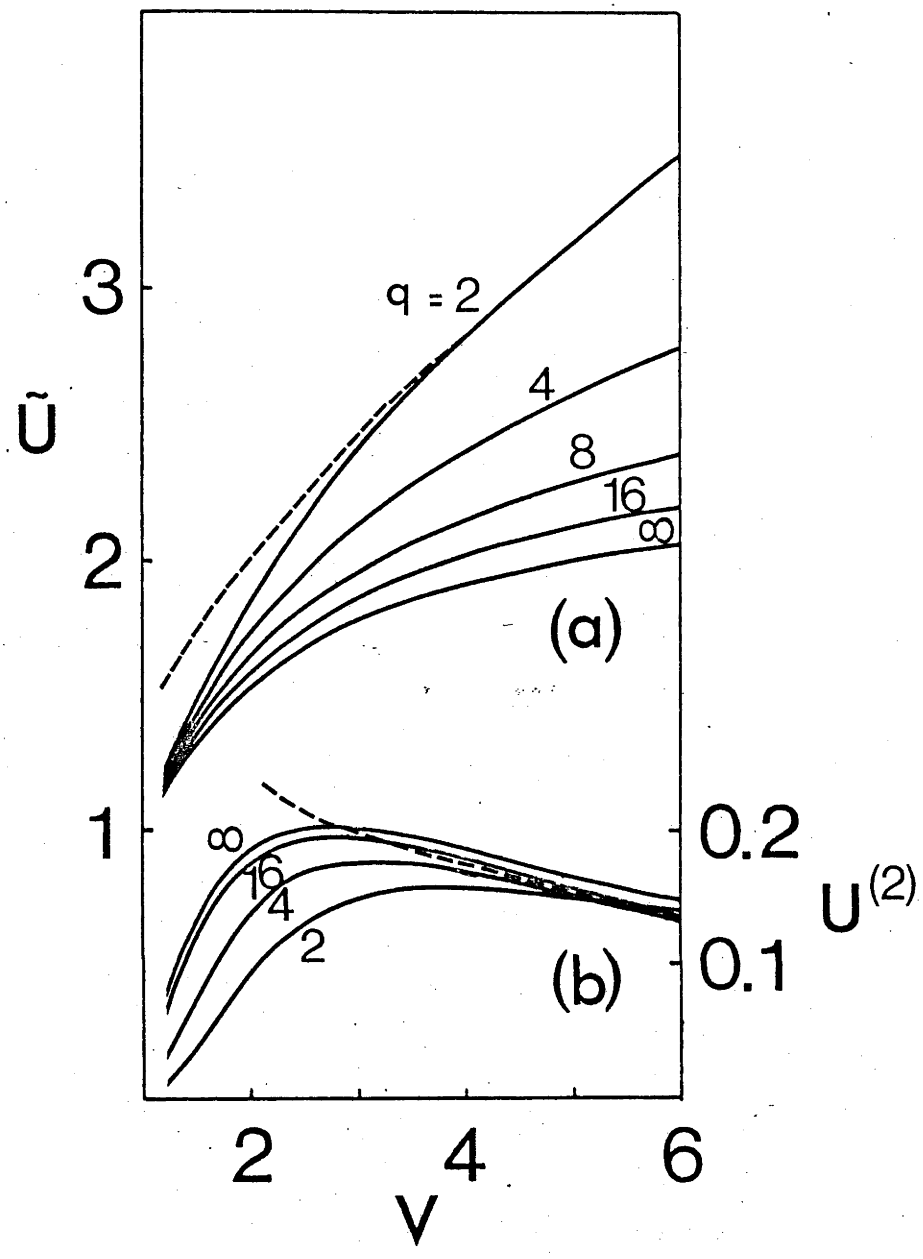

Fig. 2: Plots of (a) $\tilde{U}$ and (b) $U^{(2)}$ against V for the clad power-law profiles and the infinite parabolic profile (shown dashed).

from Eqs. (2.30a) and (13a). The first correction to group velocity due to the polarization properties of the fibre is given by $v_g^{(4)}$ in Eq. (2.17a), which is plotted in Fig. 3(b). For the infinite parabolic profile $v_g^{(4)}$ is given explicitly by Eq. (6), while for the step and clad power-law profiles it is calculated in the manner

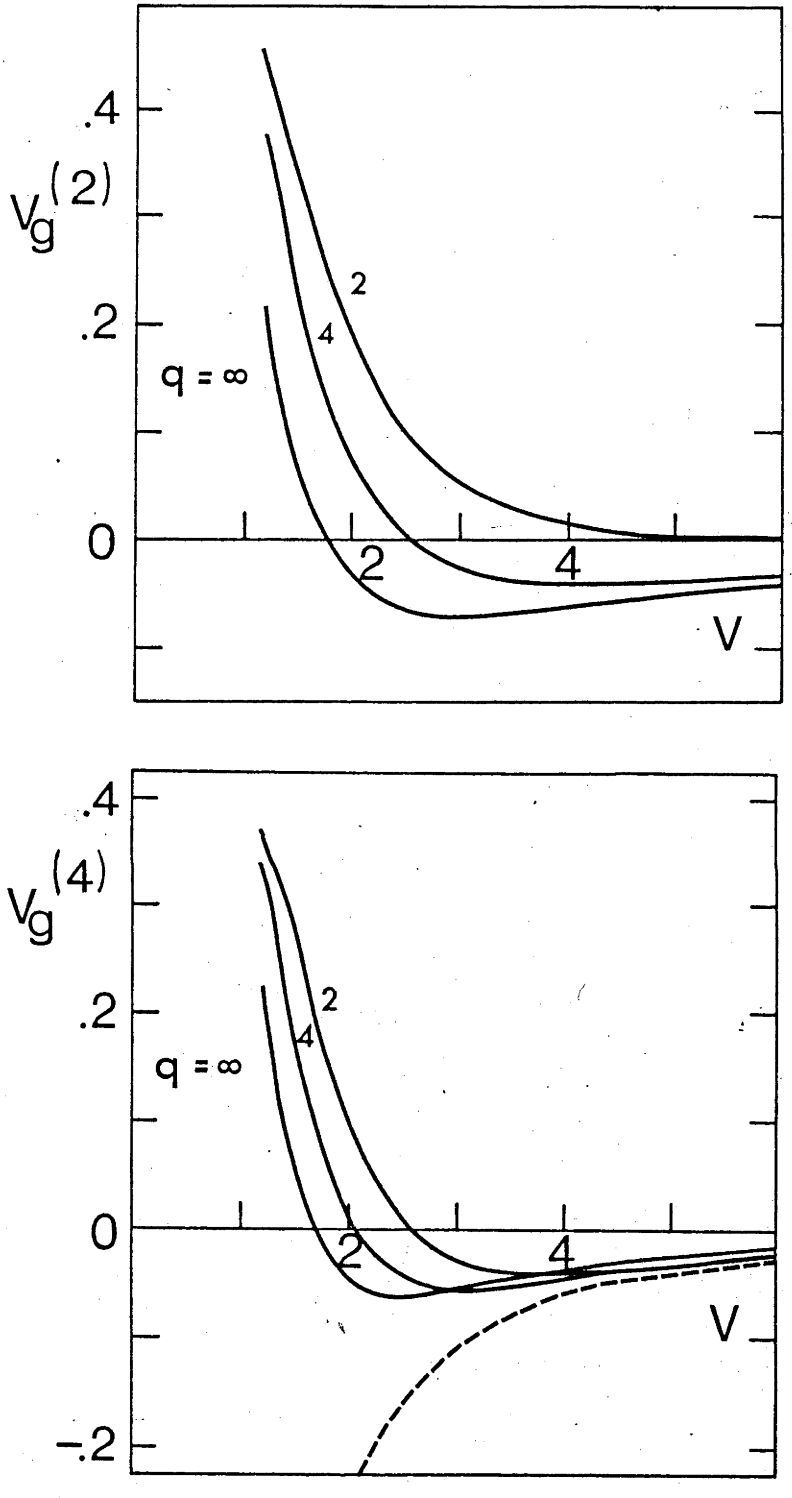

Fig. 3: Plots of (a) $v_g^{(2)}$ and (b) $v_g^{(4)}$ against V for the clad power-law profiles and the infinite parabolic profile (shown dashed).

explained in section 3. We note the similarity between the shape of the curves of $v_g^{(2)}$ and $v_g^{(4)}$ for each clad profile.

4.4.3 Waveguide Dispersion

If the fibre is circularly symmetric and single-moded, then only the fundamental mode can propagate and the only contributions to pulse dispersion are due to material dispersion and waveguide dispersion. The contribution from waveguide dispersion is due to the variation in group velocity with wavelength, and can be conveniently described by the dimensionless parameter D of Eq. (2.18a). The first term in Eq. (2.18b) gives the value of D within the scalar approximation. Plots of $\tilde{D}$ are presented in Fig. 4(a) for the step and clad power-law profiles, following the evaluation described in section 3. For the infinite parabolic profile $\tilde{D} = 0$. The zeros of $\tilde{D}$ correspond to the minima of $v_g^{(2)}$ in Fig. 3(a), and give the values of V for which there is no waveguide dispersion within the scalar approximation [7]. Plots of the polarization correction $D^{(2)}$ are shown in Fig. 4(b), taken from Eq. (7) for the infinite parabolic profile and evaluated as described in section 3 for the clad profiles. Apart from the infinite parabolic profile, the plots are similar in shape to those of $\tilde{D}$. Accordingly the absolute correction to $\tilde{D}$ is minute when $\delta \ll 1$. Polarization effects slightly reduce the value of V for which there is zero waveguide dispersion when $q > 2$. If $q \leq 2$, then $\tilde{D} \to 0$ only as $V \to \infty$, but in Fig. 4(b) we see that $D^{(2)} < 0$ for $q = 2$, so that D may have a zero, depending on the value of δ.

4.4.4 Modal Fields

Within the scalar approximation, the components of the transverse

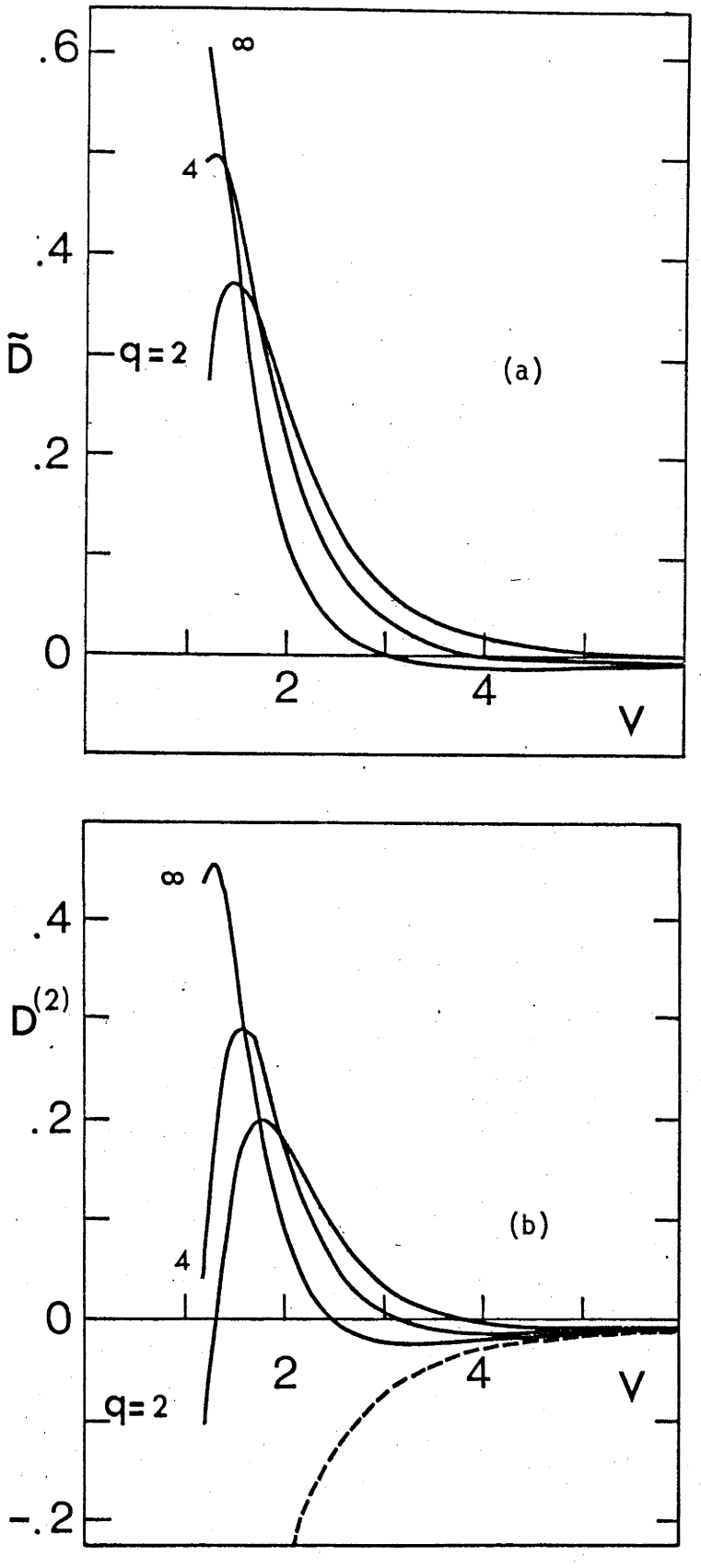

Fig. 4: Plots of (a) $\tilde{D}$ and (b) $D^{(2)}$ against V for the clad power-law profiles and the infinite parabolic profile (shown dashed).

electric field $\tilde{\underline{e}}_t$ for each mode are constructed from linear combinations of solutions to the scalar wave equation which satisfy the symmetry properties of the fibre [8]. With reference to Table 2.1, the transverse magnetic field $\tilde{\underline{h}}_t$ is given in terms of $\tilde{\underline{e}}_t$. To first order in δ there are longitudinal field components $e_z^{(1)}$ and $h_z^{(1)}$ expressed in terms of the scalar fields $\tilde{\underline{e}}_t$ and $\tilde{\underline{h}}_t$. The polarization correction $\underline{e}_t^{(2)}$ is found by iterating Eq. (2.12), as shown in section 3, and the remaining second order terms together with the third order terms are expressible in terms of $\underline{e}_t^{(2)}$ and $\tilde{\underline{e}}_t$. Finally, Table 2.1 gives the components of normalization in Eq. (2.14c) correct to order δ^2. Our main interest here is in the polarization corrections to the fundamental mode fields.

On circularly symmetric fibres the transverse electric field of the x- or y-polarized HE_{11} mode is parallel to the x or y axis respectively in Fig. 1.1(a), and is given by Eq. (2.20). The fundamental mode amplitude Ψ satisfies the scalar wave equation given by Eq. (2.21), and is plotted in Fig. 5 against R for $V = 2.4$, 3.5 and 6 and various fibre profiles. The first two values are close to the cutoff value of V for the second mode on step and clad parabolic profiles respectively. The infinite parabolic profile solution is given by Eq. (3) and the clad profiles by Eq. (10). The value of $\tilde{U}$ is taken from Fig. 2 and we assume $\Psi = 1$ at $R = 1$. Each curve shows how the field amplitude close to the axis increases as V increases, corresponding to the concentration of modal power towards the centre of the fibre.

The polarization correction $\underline{e}_t^{(2)}$ of Eq. (2.14a) is most conveniently expressed in terms of the ratios $e_r^{(2)}/\cos\phi$ and $e_\phi^{(2)}/\sin\phi$, where $e_r^{(2)}$ and $e_\phi^{(2)}$ are the radial and azimuthal components of $\underline{e}_t^{(2)}$.

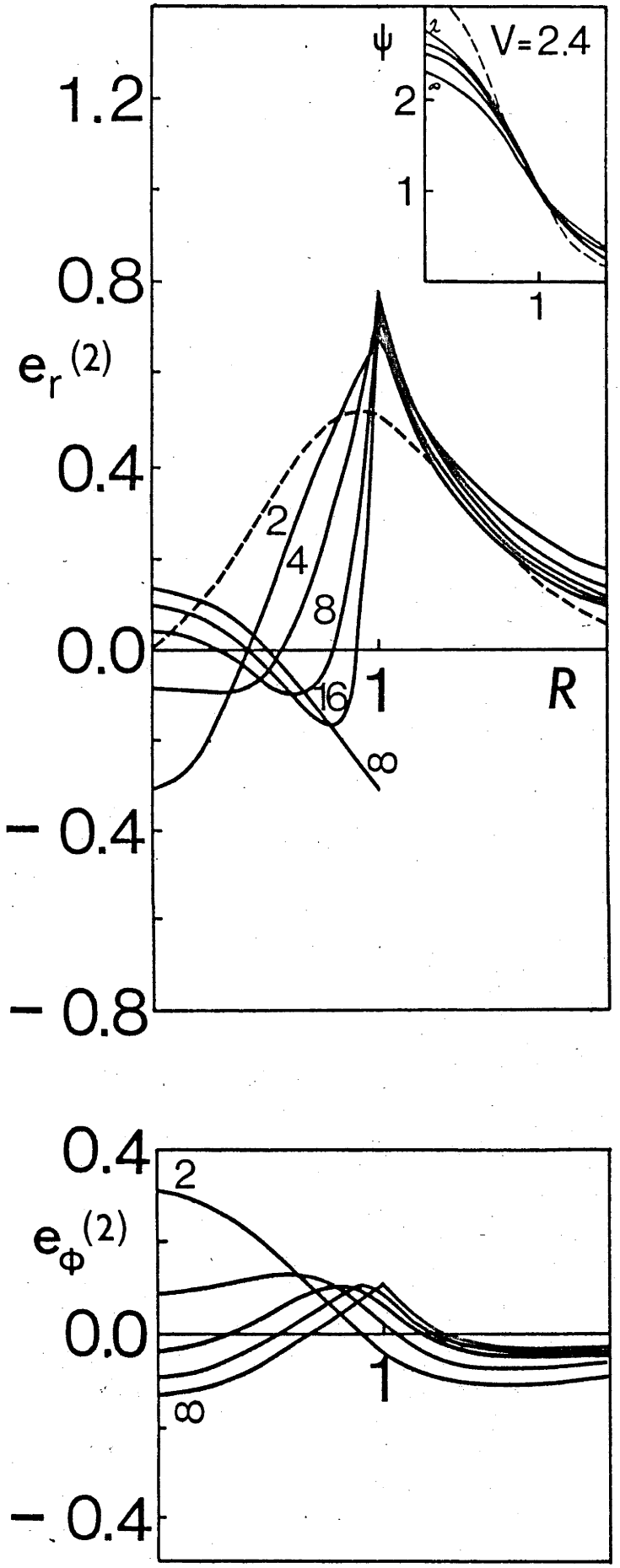

Fig. 5(a): Plots of $e_r^{(2)}/\cos\phi$, $e_\phi^{(2)}/\sin\phi$ and Ψ in the inset for the clad power-law profiles and infinite parabolic profile (shown dashed) at $V = 2.4$.

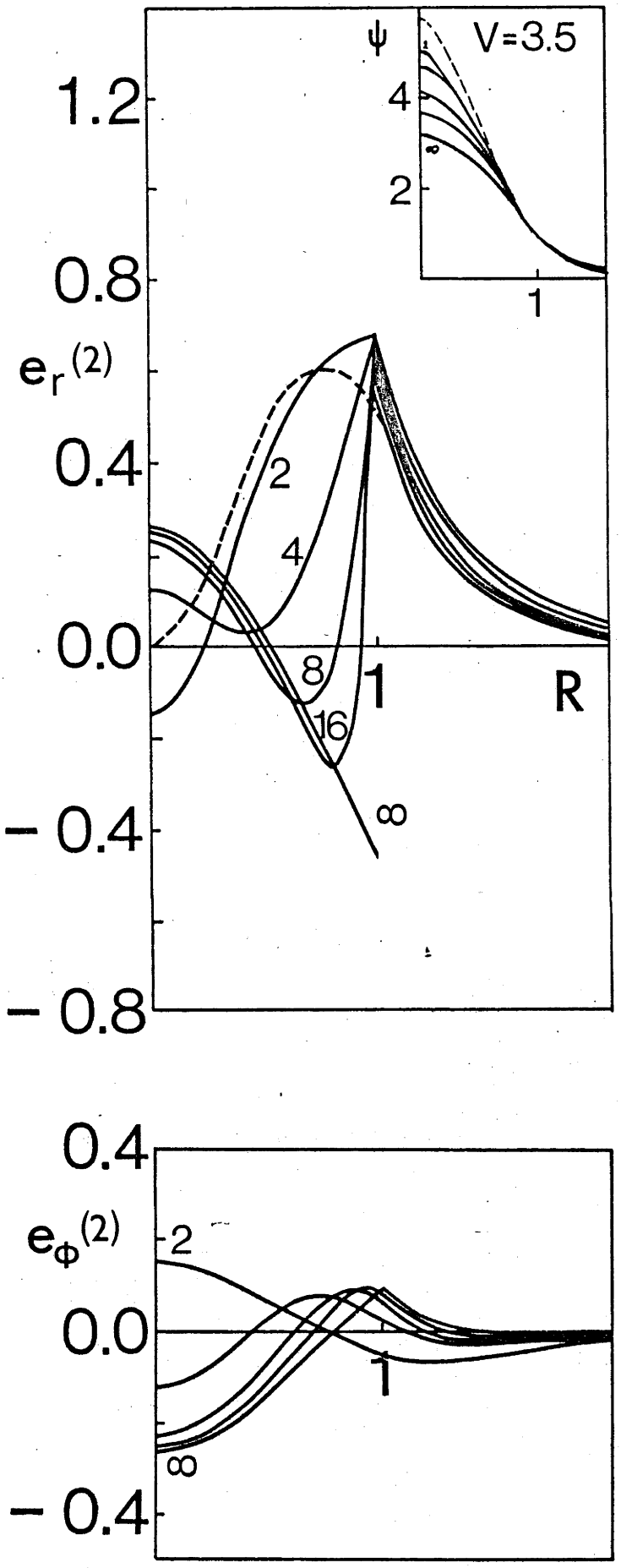

Fig. 5(b): As in Fig. 5(a) at V = 3.5.

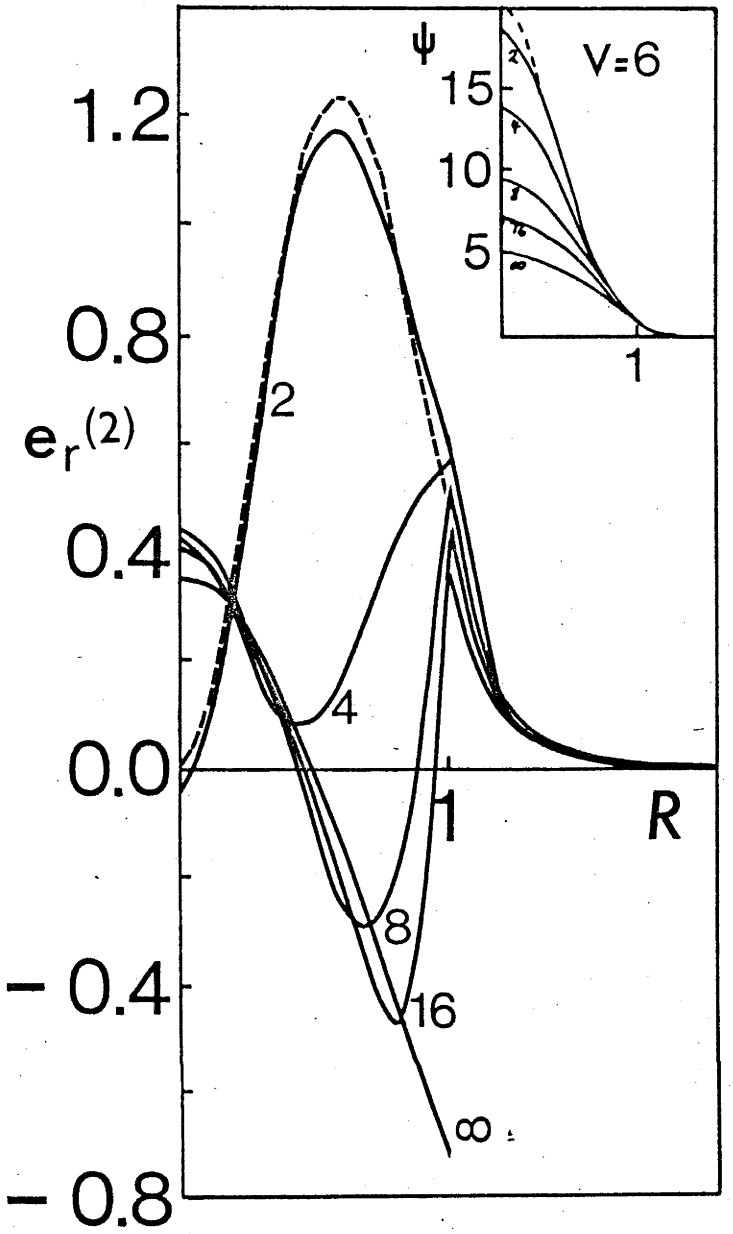

Fig. 5(c): As in Fig. 5(a) at V = 6.0.

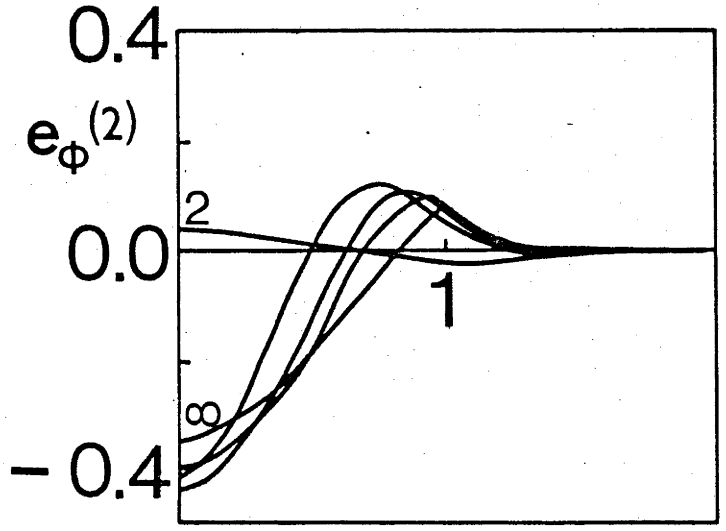

These ratios depend only on the radial coordinate R, and for the x-polarized mode of the infinite parabolic and clad profiles are given by Eqs. (8b) and (21) respectively. Plots are given in Fig. 5 for the values of V given above. In each case the normalization is the same as for the scalar fields, i.e. $N^{(2)} = 0$ in Eq. (2.14c). At the interface there is a discontinuity in $e_r^{(2)}$ for the step profile. As V increases the field amplitude beyond the interface decreases. Modal power is confined to the core and the core fields peak both at the interface ($e_r^{(2)}$) and on axis ($e_\phi^{(2)}$) for $q > 2$. The components of $e_r^{(2)}$ and $e_\phi^{(2)}$ in the y direction account for the slight curvature of the field lines in Fig. 2.1(b).

4.5 DISCUSSION

Part 1 of this thesis has been devoted to the development of techniques for perturbation analyses on optical fibres. Our aim has been to use these techniques to establish the accuracy of the scalar or weak-guidance approximation on the circularly symmetric single mode fibre with general refractive index profile.

For those parameters for which the scalar approximation is not adequate, these methods provide more accurate expressions which avoid the substantial effort required in solving the exact electromagnetic problem. Expanding the modal fields and eigenvalues as asymptotic power series in terms of δ of Eq. (2.10), a measure of the relative refractive index difference, has enabled us to isolate the vector corrections for all of the modal parameters. All of the correction terms are then of order δ^2.

A special case is the birefringence on slightly non-circular fibres since in the scalar theory the lower order terms do not exist. It is only by including the vector wave effects that we can break the

degeneracy between the two polarization states of the fundamental mode. In Chapter 3 we elaborated techniques to deal with this problem. It has been beyond the time frame and scope of this thesis to quantify these results; the reader is referred to Reference 2 for their full elucidation.

The other important case where the scalar theory may not be adequate is in the value of the eigenvalue. While the expression for the correction in terms of the scalar field and eigenvalue have been known, they have only been evaluated previously for the step refractive index profile. We found in the single mode region that the eigenvalue correction was largest for the step profile. This is as "expected" since the influence on the modal behaviour of the perturbation term (Eq. 2.13), which is a delta function for the step, can be expected to be greater than that due to the more "spread out" function due to the power-law profiles. As V increases above the single mode region, the field becomes more concentrated in the core and the influence of profile shape begins to dominate. The eigenvalue correction for power-law profiles can then become larger than that for the step.

The results for the vector corrections to group velocity and dispersion are significant by their insignificance! We have found that the waveguide dispersion on single mode fibres — a key parameter in determining bandwidth — is virtually unaffected by polarization. It is adequately described in terms of the scalar approximation.

The vector corrections for the field have been evaluated for the circularly symmetric fibre. While they are mainly of theoretical interest in this case, the methods presented can be used to determine the field corrections necessary in evaluating the birefringence on

non-circular fibres as discussed earlier. For the long distance communication systems envisaged in future, the first order correction to the eigenvalue may not be adequate and further corrections would require the field corrections derived here.

REFERENCES

1. Love, J.D., Hussey, C.D., Snyder, A.W., Sammut, R.A.: "Polarization corrections to mode propagation on weakly guiding fibres" (submitted).

2. Sammut, R.A., Hussey, C.D., Love, J.D., Snyder, A.W.: "Modal analysis of polarization effects in weakly guiding fibres", *I.E.E. Proc. Part H* 128, 173-187 (1981).

3. Snyder, A.W., Love, J.D., Sammut, R.A.: "Green's function methods of analysing optical fibre perturbations" (submitted).

4. Dil, J.G., Blok, H.: "Propagation of electromagnetic surface waves in a radially inhomogeneous optical waveguide", *Opto-Electron.* 5, 415-428 (1973).

5. Gambling, W.A., Payne, D.N., Matsumura, H.: "Cut-off frequency in radially inhomogeneous single-mode fibres", *Electron. Lett.* 13, 139-140 (1977).

6. Love, J.D.: "Power series solutions of the scalar wave equation for cladded, power-law profiles of arbitrary exponent", *Opt. & Quantum Electron.* 11, 464-466 (1979).

7. Snyder, A.W., Sammut, R.A.: "Dispersion in graded single mode fibres", *Electron. Lett.* 15, 269-271 (1979).

8. Snyder, A.W., Young, W.R.: "Modes of optical waveguides", *J. Opt. Soc. Am.* 68, 297-309 (1978).

9. Abramowitz, M., Stegun, I.A. (eds.): *Handbook of Mathematical Functions*, Washington, D.C.: GPO (1964).

PART II

SCALAR THEORY OF SINGLE MODE OPTICAL FIBRES

CHAPTER 5

APPROXIMATE AND EXACT SOLUTIONS TO THE SCALAR WAVE EQUATION ON SINGLE MODE FIBRES

5.1 INTRODUCTION

We have established in Part 1 of this thesis that, subject to certain adjustments, the scalar wave equation provides adequate accuracy for determining modal propagation parameters on optical fibres as used for communication.

Numerical methods are required to solve the scalar wave equation exactly for arbitrary refractive index profiles. Although these techniques have been refined and simplified in recent years [1,2] (and we present two such techniques in this chapter), they do not lead to the type of methods which one would wish to have for fibre design work. For this reason attempts have been made to characterize the single mode fibre in a manner which would provide simple expressions for modal parameters suitable for engineering applications.

Characterizations have been mainly based on matching certain parameters which are either experimentally measurable or theoretically defined, with the equivalent parameters of a profile for which an exact analytic solution is known. These fall into two main categories:

(a) a Gaussian field type approximation [3,4]; this essentially defines, for the given profile, an equivalent infinite parabolic profile with its Gaussian field solution, and

(b) an equivalent step approximation [5,6].

The cornerstone around which these characterizations are built is the remarkable fact that the electric fields of the HE_{11} mode are nearly identical, irrespective of the shape of the refractive index profile [5]. However, as Stewart comments, this fact has not been fully exploited and

> treatments of optical fibres have tended to start from exact profile data and work, with some approximation, to a solution of the field. The problem with this approach is that the exact profile is not often known. However since it is known that the lowest order modes of many guiding structures are similar, it seems more sensible to start from this point and use as little profile data as possible, thus avoiding the need to treat numerous special and perhaps unrepresentative cases. [7]

Previous characterizations, which are discussed more fully in the following section, have another common drawback. That is, while they may give accurate expressions for spot size and eigenvalue, they do not provide accurate expressions for waveguide dispersion — a key parameter in fibre design as it ultimately determines the bandwidth of the fibre.

In the following chapters we develop a new characterization of single mode fibres which is, following Stewart [7], based on the moments of the refractive index profile and overcomes the above problems. We furnish simple expressions for all modal parameters of interest. We suggest how the profile moments, or related quantities, can be experimentally measured from the fibre or even the preform and we use these quantities in some design examples.

In this chapter we review different characterization methods of single mode fibres, some of which have properties which are incorporated into the moment method of later chapters.

We also discuss exact numerical techniques which are crucial in determining the accuracy of characterization methods. In particular

we present two different numerical procedures for solving the scalar wave equation on circularly symmetric fibres. One is a variational technique which we refer to as the "exact moment method" (a term which will become clear after section 3.2, and particularly in light of Chapter 6). This uses a polynomial trial function in the core and yields simple analytic formulae when an elementary trial function is used. The other is a Green's function technique. This latter has the advantage that, while it can be applied to profiles for which $n(r) > n_{cl}$ always, it can with slight modification also be applied to "W-type" profiles (i.e. $n(R) < n_{cl}$ for some $R \leq 1$). For this case the exact moment method breaks down. We will discuss the merits of such profiles later.

5.2 CHARACTERIZATION METHODS

Characterizations based on the Gaussian field approximation or the equivalent step can be determined either by theoretical methods or, more importantly, by elementary measurements of the spot size or radiation pattern. Some of these methods are more fully developed by the moment scheme presented in later chapters, while others reveal the limitations of examining exact profile shape.

5.2.1 The Effective Waveguide Parameter $\bar{V}$

A first attempt at including "bulk" profile properties and not exact profile shape is to use the effective waveguide parameter $\bar{V}$, defined in Chapter 1. $\bar{V}$ is related to the usual waveguide parameter V through Ω_0, the first moment of the refractive index shape function s(r), which is the "degree of guidance" discussed in [8], as follows

$$\bar{V} = \sqrt{2\Omega_0}\, V , \tag{1}$$

where Ω_0 is

$$\Omega_0 = \int_0^\infty s(r)\, r\, d(r) \tag{2}$$

and s(r) is defined by

$$n^2(r) = n_{cl}^2 + (n_o^2 - n_{cl}^2)\, s(r)\,, \tag{3}$$

where n_o is the maximum core refractive index and n_{cl} the uniform cladding value. The properties of Ω_0 are discussed more fully in Chapter 6.

Using this parameter allows the cutoff value of the second mode for arbitrary profiles to be expressed very simply as [8]

$$\bar{V}_{co} \simeq 2.405\,, \tag{4}$$

a formula which is accurate to a few per cent for all profiles of interest.

Snyder [5] makes a similar observation for the class of "smoothed out" profiles when he says "profiles with the same maximum height, and the same area in cross section $2\pi \int_0^\infty r\, s(r)\, dr$ taking $s(r) = 1$ at maximum, have approximately the same spot size and cutoff V for the second mode."

Normalizations which are based on "cutoff values" essentially reduce to the effective $\bar{V}$, to within a multiplying factor. For instance, V/V_{co} [9] is approximately equivalent to $\bar{V}/2.405$. Similarly, experimental measurements [10,11,12] of spot size at cutoff can be used to describe an equivalent step with the same $\bar{V}$. We return to this concept later.

5.2.2 Profile Shape Dependent Methods

Considerable effort has been spent on analysing the effects of grading on modal parameters. Grading has been approximated by power law profiles where the exponent q varies with the extent of the

grading [13,8]. On-axis dips and rounding at the core-cladding boundary have been characterized by this method. These models can then be solved by power series methods and the modal parameters charted as functions of grading. This model has been used for fibre design [4].

Marcuse [3] has developed a Gaussian field approximation for those power law profiles which model rounding at the core-cladding boundary. He provides formulae in terms of the exponent q which yield accurate expressions for modal spot size and eigenvalue. This has the advantage that once the formulae are known we do not require a computer to evaluate the power series solution of the field. However, as mentioned earlier, the disadvantage of this method is that waveguide dispersion, which relies on the second derivative of the eigenvalue, cannot be determined accurately. The value of waveguide dispersion is of special interest in the region $\bar{V} \simeq 3$, where it has a zero for the step index fibre. Although the second waveguide mode propagates in this region, it is highly susceptible to losses which make the guide effectively single moded in practice [15]. The point of zero waveguide dispersion has been found exactly for a range of profiles [16,17] and is very sensitive to shape. In most profiles of interest this point lies beyond the region of effective single mode operation. For this reason we propose a more useful parameter in Chapter 8.

5.2.3 Theoretically Determined Equivalent Profiles

Using a stationary expression for the modal propagation constant and standard variational methods, both equivalent step [5] and Gaussian field [4] approximations can be produced. The Gaussian

approximation yields simple expressions, which can be solved using elementary numerical methods, for the spot size for profiles of arbitrary shape, and analytical expressions for the step, Gaussian and "smoothed out" profiles. This method is useful for understanding propagation on single mode fibres as it produces a good qualitative insight. Because the Gaussian field approximation corresponds to the infinite parabolic profile which is unphysical in the cladding it is inadequate for describing evanescent field effects such as absorption, bending loss and crosstalk [5].

The equivalent step approximation overcomes this difficulty as it provides the correct field behaviour in the cladding. Unfortunately, this procedure needs to be recalculated at each V value for each profile and does not give general formulae [5].

5.2.4 Experimentally Defined Equivalent Profiles

Experimentally defined profiles mostly fall into the equivalent step category. These overcome the problem of requiring the exact profile. Certain key parameters are measured and then matched to the step result so that exact profile data is not needed.

Experimental techniques are mainly centred on spot size measurements. Brinkmeyer [10,11] produces an equivalent step with what can be recognized to be approximately the same $\bar{V}$. The core radius ρ is determined from the position of the first minimum of the diffraction pattern of a laser beam transversely incident on the fibre which is immersed in index matching fluid. Using this equivalent step, the spot size curves become virtually coincident for the class of power law profiles considered. The degree to which the curves are coincident depends on the definition of spot size.

Pask and Sammut [18] suggest an experimental technique which determines equivalent V and ρ parameters of a step profile from the far field radiation pattern of arbitrary index profiles.

Matsumura and Sugamura [6] define another equivalent step profile. In this case the equivalent V and ρ are determined by a transformation which optimizes the match of the spot size curve of the profile to that of a step, for certain chosen V values.

Millar [12] produces yet another equivalent step. This is defined in such a manner that the measured spot size at cutoff matches the spot size of the equivalent step. This method produces a step fibre with the same $\bar{V}$, as does Brinkmeyer, but now with a core radius determined by the spot size at cutoff. Millar's equivalent step is further discussed in Chapter 7 as it is directly related to the moment method to be developed later.

5.3 NUMERICAL METHODS

Numerical techniques can vary in complexity according to cross sectional geometry and profile shape.

Finite element methods [19] are usually required for fibres of arbitrary cross section. Simplifications do occur when solving the circularly symmetric fibre, and methods range from finite difference [20] to simple power series solutions for power law profiles [8,13,21] and to phase function techniques [1,2] which can even reduce to a pocket calculator level of computation.

In this chapter we develop two numerical schemes; a variational scheme based on the moments of the refractive index profile and a Green's function method which leads to an interesting non-linear problem when dealing with "W-type" profiles.

5.3.1 The Scalar Wave Equation

Using the weak guidance approximation as described in Chapter 1 for communication fibres, the modal fields for a circularly symmetric fibre aligned with the z axis are of the form

$$\psi(r) \begin{Bmatrix} \cos\ell\phi \\ \sin\ell\phi \end{Bmatrix} \exp[i(\beta t - \omega t)] ,$$

where β is the propagation constant, and

$$\frac{d^2\psi}{dr^2} + \frac{1}{r}\frac{d\psi}{dr} - \frac{\ell^2}{r^2}\psi + (k^2n^2 - \beta^2)\psi = 0 , \tag{5}$$

where ℓ is the azimuthal modal label. In terms of V, s (eqn. 3) and $R = r/\rho$,

$$\frac{d^2\psi}{dR^2} + \frac{1}{R}\frac{d\psi}{dR} - \frac{\ell^2}{R^2}\psi + V^2 s(R)\psi = W^2\psi , \tag{6}$$

where the modal eigenvalue W (or U) is given by

$$W^2 = \rho^2(\beta^2 - k^2n_{cl}^2) \tag{7a}$$

$$= V^2 - \rho^2(k^2n_o^2 - \beta^2) \tag{7b}$$

$$= V^2 - U^2 . \tag{7c}$$

For a given profile we require to construct the β versus V or W versus V curve and find the modal field ψ. Occasionally the value of V giving a certain value of W is required, e.g. V_{co} to give $W = 0$, and in fact there is no reason why we cannot construct the W versus V curve by specifying a set of W values and finding the appropriate V's. Obviously by iterating we could then find the W giving any particular V of interest.

The advantage of the above point of view is that for $R \geq 1$ the field is known: $\psi = K_\ell(WR)$. Thus the procedure of finding V for a given W reduces to the following mathematical problem:

$$-\frac{d^2\psi}{dR^2} - \frac{1}{R}\frac{d\psi}{dR} + \frac{\ell^2\psi}{R^2} + W^2\psi = V^2 s(R)\psi \tag{8a}$$

and boundary conditions

$$\psi(0) \quad \text{finite}, \tag{8b}$$

$$\psi'(1)/\psi(1) = -WK'_\ell(W)/K_\ell(W) \equiv -\kappa_\ell(W) . \tag{8c}$$

Equation (8) defines an eigenvalue problem for V involving only the interval $0 \le R \le 1$.

Both formalisms, Eqs. (7) and (8) are standard Sturm-Liouville problems and many techniques are available for their solution [22]. In this chapter we solve the second formalism, Eq. (8), in two different ways. In Chapter 6 we find the formalism of Eq. (5) more convenient for developing the moment characterization.

5.3.2 The Variational-Exact Moment Method

We begin by introducing the moments, Ω_m, of the refractive index profile, where

$$\Omega_m = \int_0^\infty s(r) r^{m+1} dr \tag{9}$$

and the normalized moments $\bar{\Omega}_m$ are simply Ω_m/Ω_o.

We now consider Eq. (8) where we only need to find $\psi(R)$ in the core, i.e. for $0 \le R \le 1$. We set

$$\psi = \sum_{m=0}^{M} c_m R^{2m} \tag{10}$$

and choose the coefficients c_m by applying the variational principle which gives

$$V \le V_{calc}, \tag{11}$$

where for a suitable trial function ψ_t,

$$V^2_{calc} = \int_0^1 \psi_t D_\ell \psi_t RdR \Big/ \int_0^1 \psi_t^2 s(R) RdR \tag{12a}$$

and

$$D_\ell \psi_t \equiv \left\{ - \frac{d^2}{dR^2} - \frac{1}{R}\frac{d}{dR} + \frac{\ell^2}{R^2} + W^2 \right\} \psi_t \, . \tag{12b}$$

This method has two advantages: as more moments are taken as known an exact answer is generated, and it is very clear that only profile moments are needed and enter simply into the answers. We deal with the $\ell = 0$, fundamental mode.

We construct the variational solution to Eq. (8) using Eqs. (11)-(12), but replace the polynomial trial function of Eq. (10) by the form

$$\psi_t = \sum_{j=1}^{M} a_j \, \psi_{tj} , \tag{13}$$

where

$$\psi_{tj} = R^{2(j-1)} (1 - c_j R^2) \, . \tag{14}$$

This allows us to choose c_j so that the ψ_{tj} individually satisfy the boundary conditions, Eq. (8c), and

$$c_j = \{2(j-1) + \kappa_0\}/\{2j + \kappa_0\} \, , \tag{15}$$

where $\kappa_0(W)$ is defined in Eq. (8c). The linear coefficients a_j are chosen by the standard Rayleigh-Ritz procedure to obtain V_{calc}, the best approximation to V for a given M. Then since the polynomials form a complete set, as $M \to \infty$, $V_{calc} \to V$.

Using the set of trial functions defined in Eq. (14) we note that each increment in j requires an additional 2 even moments. In fact for a given M we require the first $(2M - 1)$ even moments of the refractive index profile. In practice, accuracy in V of around 6 decimal places is achieved with $M = 10$, the error being due to numerical methods rather than inaccuracies inherent in the mathematical method itself.

5.3.3 The Variational-Few Moment Method

If our information regarding the profile is limited to Ω_0, Ω_2 and Ω_4, then we can choose two possible trial functions to give an estimate of V for a given W. These are $\psi_t = \psi_{t1}$ from Eq. (14), or a different type of trial function:

$$\phi_t = [1 - e_1 R^2 + e_2 (1 - R^2)^2]^{\frac{1}{2}} , \tag{16a}$$

$$e_1 = \kappa_0/(1 + \kappa_0) , \tag{16b}$$

where e_1 has been chosen to match the boundary conditions, Eq. (8c). The result is immediately cast into the form

$$\bar{V}^2_{calc} = \frac{2 \int_0^1 \psi_t \, D_0 \, \psi_t \, RdR}{A_0 + A_2 \bar{\Omega}_2 + A_4 \bar{\Omega}_4} \tag{17}$$

which gives $\bar{V}$ in terms of $\bar{\Omega}_2$ and $\bar{\Omega}_4$ for the specified W. In Eq. (17),

$$\begin{aligned} A_0, A_1, A_2 &= 1, -2c_1, c_1^2 , & \psi_t &= \psi_{t1} \\ &= (1 + e_2), -(e_1 + 2e_2), e_2 , & \psi_t &= \phi_t . \end{aligned} \tag{18}$$

The integral in Eq. (17) is straightforward to evaluate and provides an analytical formula for $\bar{V}_{calc}$ when $\psi_t = \psi_{t1}$. When ϕ_t is used we have the additional parameter e_2 to specify and this allows us to obtain a better answer as the variational principle tells us to choose e_2 so that $d\bar{V}^2_{calc}/de_2 = 0$.

These formulae produce an explicit relationship between W, $\bar{V}$, $\bar{\Omega}_2$ and $\bar{\Omega}_4$ and they are particularly useful for small $\bar{V}$ fibres. In Fig. 1 we plot the U versus $\bar{V}$ curves for three separate profiles using the exact moment method and the two trial functions ψ_{t1} and ϕ_t. Although the accuracy of these formulae is good they are not as suitable or as accurate as the expressions to be derived in the next chapter for

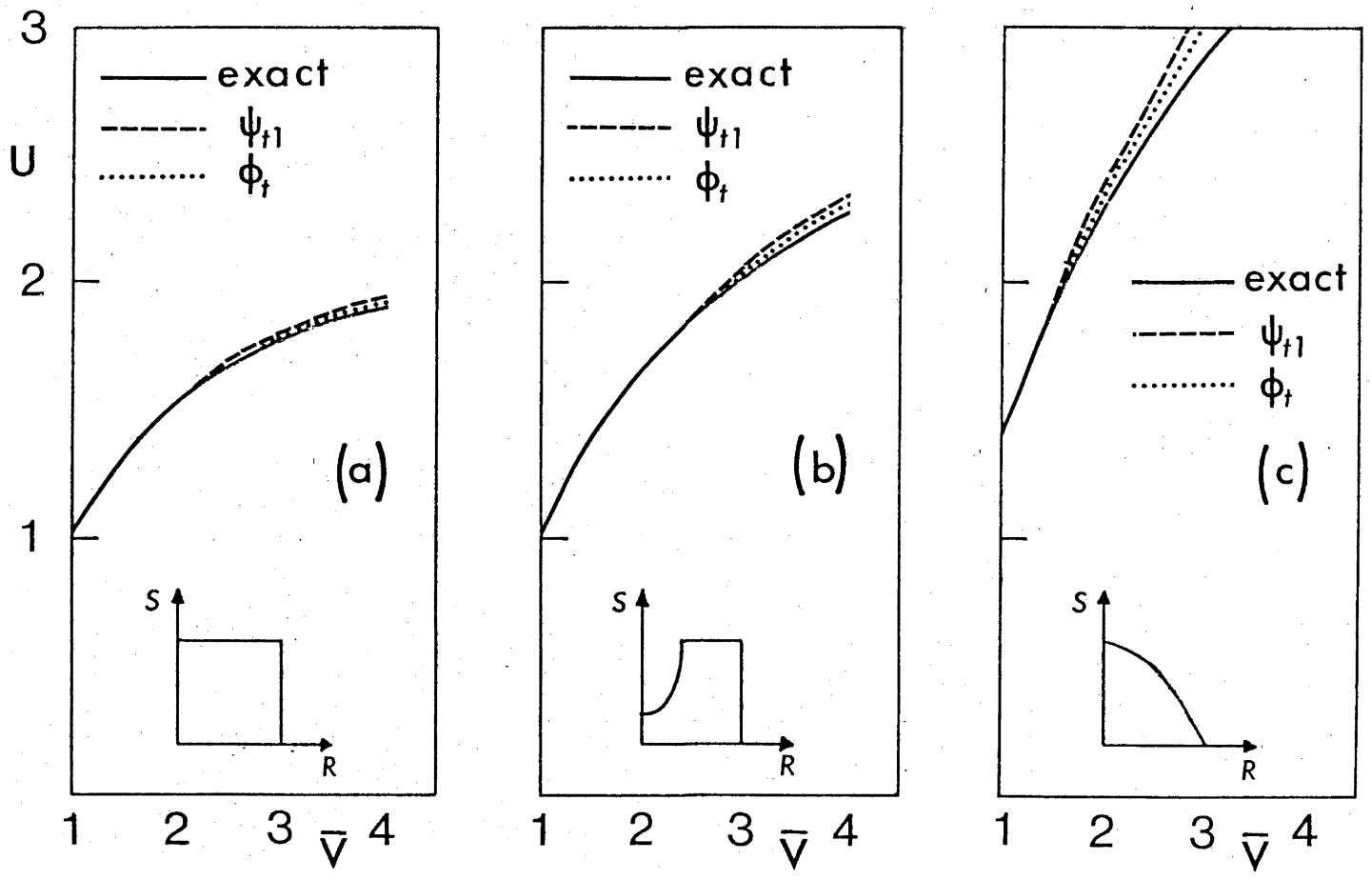

Fig. 1: Plots of the eigenvalue U (Eq. 7) versus $\bar{V}$ curves using the exact moment method (solid curve) and the two trial functions ϕ_t (Eq. 14) (dotted curve) and ψ_{t1} (Eq. 16) (dashed curve) for (a) the step profile, (b) a step with dip, and (c) the clad parabolic profile as shown inset.

going on to find pulse dispersion parameters. For this reason we do not exploit them further in this thesis.

5.3.4 Green's Function Method — Standard Profile $n(r) \geq n_{cl}$

Equation (6) is now transformed into an integral equation in terms of a Green's function [22] as follows:

$$\psi(R) = V^2 \int_0^1 G(R,\xi)\ s(\xi)\ \xi\ \psi(\xi)\ d\xi\ . \tag{19}$$

The Green's function which satisfies the boundary conditions, Eq. (8b,c), is in this case [24]

$$G(R,\xi) = I_0(WR)\ K_0(W\xi) \qquad 0 \leq R \leq \xi \tag{20a}$$

$$= I_0(W\xi)\ K_0(WR) \qquad \xi \leq R \leq 1\ , \tag{20b}$$

where I_0 and K_0 are modified Bessel functions of the first and second kind respectively.

To facilitate solution we symmetrize this equation by defining

$$\phi(R) = \psi(R)\sqrt{s(R)\ R} \tag{21}$$

and

$$K(R,\xi) = \sqrt{s(R)\ R}\ G(R,\xi)\sqrt{s(\xi)\ \xi}\ . \tag{22}$$

Equation (19) can then be written as

$$\phi(R) = V^2 \int_0^1 K(R,\xi)\ \phi(\xi)\ d\xi\ , \tag{23}$$

where

$$K(R,\xi) = K(\xi,R)\ . \tag{24}$$

We now apply the quadrature rule, which has the general form

$$\int_0^1 f(x)\ dx \simeq \sum_{i=0}^{N} w_i f_i \qquad f_i = f(x_i)\ , \tag{25}$$

where w_i are suitable weighting factors. (We use the trapezoidal rule which has

$$w_j = 1/2N \qquad j = 0,N\,, \qquad\qquad w_j = 1/N \qquad j \neq 0,N\,, \tag{26}$$

for the results obtained later.) The discrete form of Eq. (23) is then

$$\phi(R_j) \simeq V^2 \sum_{i=0}^{N} K(R_j,\xi_i)\ \phi(\xi_i)\ w_i \tag{27}$$

which we again symmetrize to get

$$\Phi(R_j) \simeq V^2 \sum_{i=0}^{N} M_{ji}\ \Phi_i\,, \tag{28}$$

where

$$\Phi_j = \sqrt{w_j}\ \phi_j \tag{29}$$

and

$$M_{ji} = \sqrt{w_j}\ K(R_j,\xi_i)\ \sqrt{w_i}\,. \tag{30}$$

Fig. 3(a) shows the U - V curve for the profiles shown in Fig. 2(a) solved by the above method. The profiles of Fig. 2(b) require a modified technique in order to keep the matrices symmetrical. This is discussed next.

5.3.5 Green's Function Method — "W-type" Profiles $n(R) < n_{cl}$ for some $R \leq 1$

Doubly-clad optical fibres have been developed which widen the low dispersion spectral range in the single mode region [25,26]. An example of this type of fibre is shown in Fig. 2(b), i.e. they contain a region for which $n(R) < n_{cl}$ just inside the uniform cladding. This fibre has stronger confinement properties than the singly clad profile. This leads to the following important properties for optical communications [27].

(1) As compared with a singly clad fibre, the largest core area for single mode operation is almost double.

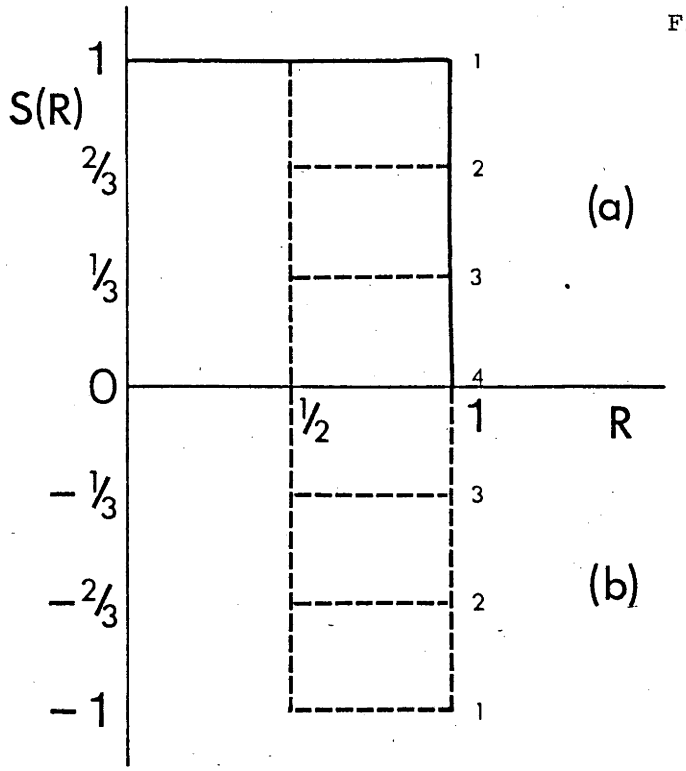

Fig. 2: The shape function s(R) (R = r/ρ) example used in (a) Green's function method, (b) modified Green's function method.

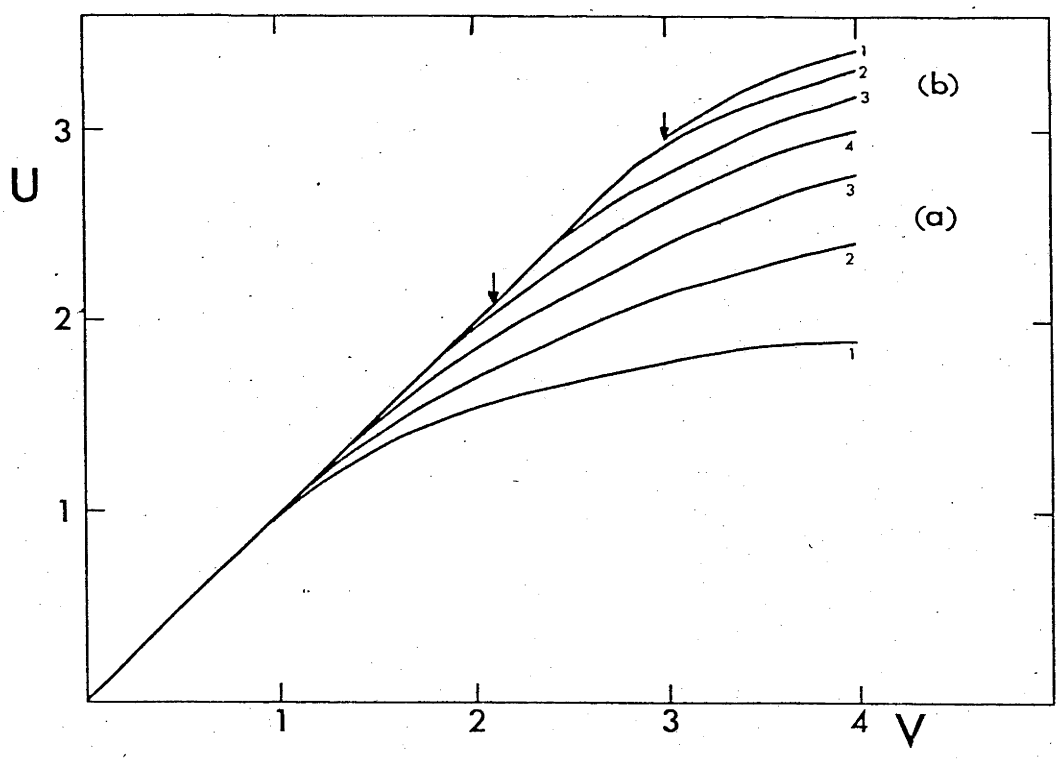

Fig. 3: Eigenvalue of the profiles considered in Fig. 2(a) and (b). The arrow indicates the cutoff point for the fundamental mode.

(2) Total dispersion can be reduced to a minimum over an extended spectral range which coincides with the low loss region [25, 26].

(3) The field is much more tightly confined within the core as compared with singly clad fibres. This minimizes the extra attenuation due to absorption in the cladding.

A consequence of considering profiles which allow $s(R) < 0$ is that negative values of Ω_0 of Eq. (2) are now possible. If $\Omega_0 \leq 0$ then as $V \to 0$ the first mode will cease to propagate [27,28]. At the same time, however, the cutoff frequency of the second mode is also increased so that the range of single mode operation may be extended by careful fibre design [28].

Modal properties of these types of fibres have been studied by finite element methods [25,26], by exact analytical methods for piecewise homogeneous profiles [27,28] and by phase methods [1]. Here we propose an alternative scheme whereby the Green's function technique of the previous section is extended so that the problem can remain symmetrical. However, we do require the additional solution to a nonlinear equation using a linear iteration scheme.

When the profile shape function $s(R)$ goes negative as in Fig. 4(a) we define a new shape function $s(R)$, normalized so that it is always positive as shown in Fig. 4(b). The new normalization is defined by $\gamma > 1$ such that

$$s_c(R) = \frac{s(R) + \gamma\, s_{min}}{1 + \gamma\, s_{min}}, \tag{31}$$

where the minimum value of $s(R)$ is $-s_{min}$. This defines a new eigenvalue problem

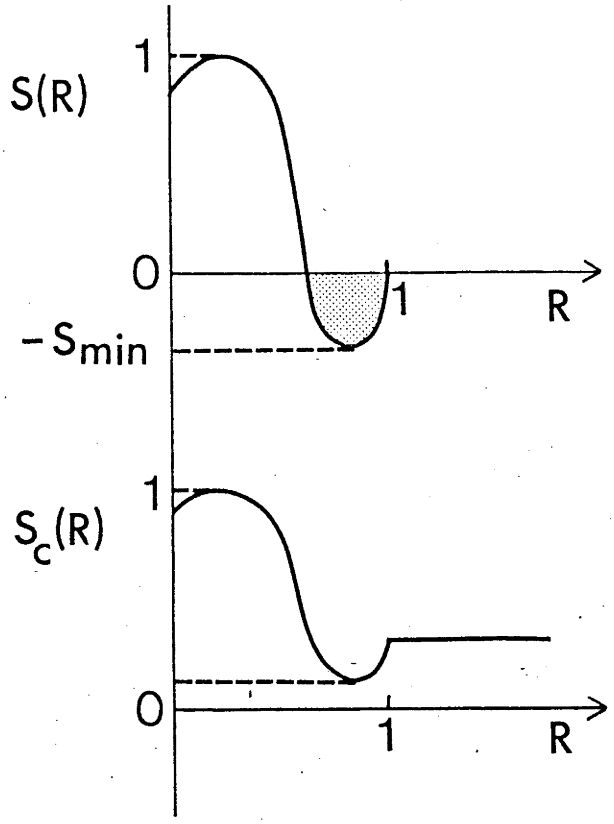

Fig. 4: Example of a normalization process which converts s(R) in (a) to $s_c(R)$ in (b) such that the shape function remains positive.

$$-\frac{d^2\psi}{dR^2} - \frac{1}{R}\frac{d\psi}{dR} + W_c^2\psi = V_c^2\, s_c(R)\psi\,, \tag{32}$$

where

$$V_c^2 = (1+\gamma\, s_{min})\, V^2 \tag{33}$$

and

$$W_c^2 = W^2 + \gamma\, s_{min}\, V^2\,, \tag{34}$$

The Green's function for this problem is now written as

$$G(R,\xi) = I_0(W_cR)\, F(W_c\xi) \qquad R<\xi \tag{35a}$$

$$= F(W_cR)\, I_0(W_c\xi) \qquad R>\xi \tag{35b}$$

where

$$F(W_cR) = \alpha I_0(W_cR) + K_0(W_cR) \tag{36}$$

and α must be chosen to fit the boundary conditions, Eq. (8b,c), i.e.

$$\frac{F'(1)}{F(1)} = -\kappa\,. \tag{37}$$

Therefore

$$\alpha = \frac{W_c\ K_1(W_c) - \kappa\ K_0(W_c)}{W_c\ I_1(W_c) + \kappa\ I_0(W_c)} . \tag{38}$$

Equations (32) and (37) define an equation for V_c^2 which we write schematically as

$$V^2 = f(W_c^2) . \tag{39}$$

Equations (33) and (34) also define an equation for V_c^2, i.e.

$$V_c^2 = \left\{\frac{1+\gamma\ s_{min}}{\gamma\ s_{min}}\right\} (W_c^2 - W^2) . \tag{40}$$

These two equations can be written as a non-linear equation to be solved for W_c:

$$W_c^2 = \left\{\frac{\gamma\ s_{min}}{1+\gamma\ s_{min}}\right\} f(W_c^2) + W^2 . \tag{41}$$

Equation (41) is now in a form suitable for solution by a process of linear iteration [29]. If we write this equation in the form $x = g(x)$ where $x = W_c^2$, then convergence of the linear iteration process is assured if $|dg/dx| \leq 1$.

While a general proof of this condition is not available for the above problem, we can give an argument to show that there is always a region for which the condition holds. We have also established, by solving them on a computer, that the above condition is fulfilled for all profiles of practical interest. The argument is as follows: Differentiating Eq. (41) we get

$$\frac{dg}{dx} = \left(\frac{\gamma\ s_{min}}{1+\gamma\ s_{min}}\right) \frac{df}{dW_c^2} = \left(\frac{\gamma\ s_{min}}{1+\gamma\ s_{min}}\right) \frac{dV_c^2}{dW_c^2} . \tag{42}$$

From the Hellman-Feynman theorem [30] we find

$$\frac{dW_c^2}{dV_c^2} = \frac{\int_0^1 s_c \, \psi^2 \, RdR}{\int_0^1 \psi^2 \, RdR} \tag{43}$$

and we can say that

$$\xi \leq \frac{dW_c^2}{dV_c^2} \leq 1 \tag{44a}$$

or

$$1 \leq \frac{dV_c^2}{dW_c^2} \leq \frac{1}{\xi} , \tag{44b}$$

where ξ is the minimum value that the expression on the R.H.S. of Eq. (43) can assume. Substituting (44b) into (42) we have

$$\frac{\gamma \, s_{min}}{1 + \gamma \, s_{min}} \leq \frac{dg}{dx} \leq \frac{\gamma \, s_{min}}{1 + \gamma \, s_{min}} \frac{1}{\xi} \tag{45}$$

so that, since $\frac{\gamma \, s_{min}}{1 + \gamma \, s_{min}} < 1$, we *can* have $dg/dx < 1$, and our assertion is proven.

Results using the above procedure have been plotted in Fig. 3(b) for the profiles in Fig. 2(b). The profile in Fig. 2(b) case 3 is an example where $\Omega_0 = 0$, so that the cutoff of the fundamental mode is just still zero. The fundamental mode cutoff of the two other profiles of Fig. 2(b) are as indicated by the arrows in Fig. 3(b).

For those profiles for which $\Omega_0 > 0$, it is clear that waveguide dispersion, which is proportional to the second derivative of the eigenvalue, remains approximately zero over a wider and wider range of V values as the negative portion goes more negative and hence produces the important characteristics described earlier.

Profiles with $\Omega_0 < 0$ have cutoff values of the fundamental mode which are very sensitive to the "inner cladding" refractive index. If the cutoff V is small then the above characteristics can still hold.

Design criteria [25,26] which optimize the range of low

dispersion, however, suggest a W fibre where Ω_0 is very much greater than zero. Typical experimental profiles have Ω_0 which is just negative. In practice then most "W" profiles still comply with the characteristics described earlier.

5.4 RESUMÉ

We have stressed the necessity of characterizing single mode fibres in order to provide workable expressions for fibre design. By outlining previous characterization attempts we have laid the basis for the new methods to be developed in the following chapters.

Since *a priori* estimates of the accuracy of characterization schemes are not possible we also produced two numerical techniques for solving the scalar wave equation. The first was based on the infinite set of moments of the refractive index profile and produced simple analytic formulae when only the first three moments were known. The second was a Green's function method which could also be applied to the class of W fibres — for which case the exact moment scheme breaks down and the techniques to be developed later have not been applied.

REFERENCES

1. Sammut, R.A., Pask, C.: "Simplified numerical analysis of optical fibres and planar waveguides", *Electron. Lett.* 17, 105-106 (1981).

2. Rose, J.W., Mitra, S.S.: "Numerical solution of the scalar wave equation for inhomogeneous cylindrical dielectric waveguides", *Opt. Lett.* 6, 446-448 (1981).

3. Marcuse, D.: "Gaussian approximation of the fundamental modes of graded-index fibers", *J. Opt. Soc. Am.* 68, 103-109 (1978).

4. Snyder, A.W.: "Understanding monomode optical fibers", *Proc. I.E.E.E.* 69, 6-13 (1981).

5. Snyder, A.W., Sammut, R.A.: "Fundamental (HE_{11}) modes of graded optical fibers", *J. Opt. Soc. Am.* 69, 1663-1671 (1979).

6. Matsumura, H., Sugamura, T.: "Normalization of single-mode fibers having an arbitrary index profile", *Appl. Opt.* 19, 3151-3158 (1980).

7. Stewart, W.J.: "Simplified parameter-based analysis of single-mode optical guides", *Electron. Lett.* 16, 380-382 (1980).

8. Gambling, W.A., Matsumura, H., Ragdale, G.M.: "Wave propagation in a single mode fibre with dip in the refractive index", *Opt. & Quantum Electron.* 10, 301-309 (1978).

9. Sugimura, D., Diakoku, K., Imoto, N., Miya, T.: "Wavelength dispersion characteristics of single-mode fibres in low-loss region", *I.E.E.E.* QE-16, 215-225 (1980).

10. Brinkmeyer, E.: "Profile-independent representation of near- and far-field characteristics of single-mode fibers and its use for the determination of fiber parameters", *Proc. Opt. Comm. Conf.* paper 17-2, Amsterdam (1979).

11. Brinkmeyer, E.: "Spot size of graded-index single-mode fibers: profile-independent representation and new determination method", *Appl. Opt.* 18, 932-937 (1979).

12. Millar, C.A.: "Direct method of determining equivalent-step-index profiles for monomode fibres", *Electron. Lett.* 17, 458-460 (1981).

13. Gambling, W.A., Matsumura, H.: "Propagation in radially-inhomogeneous single-mode fibre", *Opt. & Quantum Electron.* 10, 31-40 (1978).

14. Gambling, W.A., Matsumura, H., Ragdale, C.M.: "Mode dispersion, material dispersion and profile dispersion in graded index single mode fibres", *Microwaves, Optics & Antennas* 3, 239-246 (1979).

15. Gambling, W.A., Matsumura, H., Ragdale, C.M.: "Zero mode dispersion in single mode fibres", *Electron. Lett.* 14, 618-620 (1978).

16. Snyder, A.W., Sammut, R.A.: "Dispersion in graded single-mode fibres", *Electron. Lett.* 15, 269-271 (1979).

17. Imoto, N., Kawana, A., Machida, S., Tsuchiya, H.: "Characteristics of dispersion free single-mode fiber in the 1.5 μm wavelength region", *I.E.E.E.* QE-16, 1052-1058 (1980).

18. Pask, C., Sammut, R.A.: "Experimental characterization of graded index single-mode fibres", *Electron. Lett.* 16, 310-311 (1980).

19. Yeh, C., Ha, K., Dong, S.B., Brown, W.P.: "Single-mode optical waveguides", *Appl. Opt.* 18, 1490-1504 (1979).

20. Anderssen, R.S., DeHoog, F.R., Love, J.D.: "A numerical technique for solving the scalar wave equation for Gaussian and smoothed-out profiles", *Opt. & Quantum Electron.* 13, 217-224 (1981).

21. Love, J.D.: "Power series solutions of the scalar wave equation for cladded, power-law profiles of arbitrary exponent", *Opt. & Quantum Electron.* 11, 464-466 (1979).

22. Hildebrand, F.B.: *Methods of Applied Mathematics* (Prentice Hall, New York, 1952), pp.144, 187.

23. Baker, C.T.H.: *The Numerical Treatment of Integral Equations* (Clarendon Press, Oxford, 1977), pp.222-227.

24. Kokubun, Y., Iga, K.: "Formulas for TE_{01} cutoff in optical fibers with arbitrary index profile", *J. Opt. Soc. Am.* 70, 36-40 (1980).

25. Okamoto, K., Edahiro, T., Kawana, A., Miya, T.: "Dispersion minimization in single mode fibres over a wide spectral range", *Electron. Lett.* 15, 729-731 (1979).

26. Miya, T., Okamoto, K., Ohmori, Y., Sasaki, Y.: "Fabrication of low dispersion single-mode fibers over a wide spectral range", *I.E.E.E.* QE-17, 858-861 (1981).

27. Kawakami, S., Nishida, S.: "Characteristics of doubly clad optical fiber with a low-index inner cladding", *I.E.E.E.* QE-10, 879-887 (1974).

28. Sammut, R.A.: "Range of monomode operation of W-fibres", *Opt. & Quantum Electron.* 10, 509-514 (1978).

29. Conte, S.D.: *Elementary Numerical Analysis* (McGraw-Hill, Kogakusha, 1965).

30. Merzkacher, E.: *Quantum Mechanics* (Wiley, New York, 1970).

CHAPTER 6

MOMENTS DESCRIPTION OF SINGLE MODE FIBRES

PREAMBLE

We describe the theory of characterizing single mode optical fibres in terms of the moments of the refractive index profile. Using reduced profile data in the form of the first three moments Ω_0, Ω_2 and Ω_4, we find that light propagation along such fibres can be accurately described. In this formalism the average or effective waveguide parameter $\bar{V}$, which incorporates Ω_0, emerges naturally and universal formulae are given in terms of $\bar{V}$, $\bar{\Omega}_2 = \Omega_2/\Omega_0$ and $\bar{\Omega}_4 = \Omega_4/\Omega_0$. These formulae cover the fundamental mode eigenvalue, group velocity and dispersion parameters, field spot size and fraction of power propagating within the core, and the cutoff parameter for the second waveguide mode. They are simple to apply and their good accuracy, which is demonstrated for a wide variety of examples, indicates that they are suitable for use in fibre design studies. The formulae also naturally lead to a qualitative description of waveguide behaviour: different fibres have similar properties when these are considered as functions of $\bar{V}$, and a residual magnitude scaling can be attributed to profile shape which enters principally through $\bar{\Omega}_2$.

6.1 INTRODUCTION

In this chapter we present a new approach to describing the properties of single mode optical fibres. The objective is to isolate

a few basic parameters which adequately characterize such fibres and allow their properties to be simply quantified and analysed with a high degree of accuracy. The concepts of light guidance and profile shape can be defined and examined in simple terms. For continuity and clarity of argument and for the readers' convenience we will redefine certain parameters and reintroduce certain concepts which have already been considered in previous chapters.

An optical fibre consists of a cylindrical, uniform cladding material of refractive index n_{cl} with a core region of higher refractive index embedded in it. We assume a circular core region, radius ρ, a refractive index profile with maximum n_o, and light with wavenumber $k = 2\pi/\lambda$ where λ is the wavelength. When the waveguide parameter

$$V = k\rho\sqrt{(n_o^2 - n_{cl}^2)} \tag{1}$$

takes on values $V < V_{co}$ the fibre supports only one bound mode. The magnitude of V_{co}, the cutoff V for the HE_{21} or second mode, depends considerably on the index profile. A first attempt at including profile effects can be made by using $\bar{V}$, an average or effective V, defined by [1,2]

$$\bar{V}^2 = 2k^2 \int_0^\rho [n^2(r) - n_{cl}^2]\, r dr . \tag{2}$$

Then the values of $\bar{V}_{co}$ are much more nearly the same for a variety of profiles and [2]

$$\bar{V}_{co} \simeq 2.405 . \tag{3}$$

Note that $\bar{V} = V$ of Eq. (3) is exact for a step index fibre. Equation (3) defines the single mode limit and we take as the practical domain of interest fibres with $1 \lesssim \bar{V} \lesssim 2.405$. There are some proposals for opeating with $\bar{V}$ larger than this and we comment further in Section 8.

If we observe that in practice n_o^2 differs little from n_{cl}^2, so that $n_o^2 - n_{cl}^2 \simeq 2n_{cl}(n_o - n_{cl})$, and also that $n_o - n_{cl}$ is roughly proportional to the density of dopant used in forming the core [3], then Eq. (2) indicates that $\bar{V}^2$ is proportional to the total amount of dopant used [2]. Fibres will differ because the dopant is deliberately distributed in various ways and because diffusion effects in the manufacturing process will alter the profile. In order to go beyond a fibre characterization based on $\bar{V}$ we need information about the profile shape function s(r), where

$$n^2(r) = n_{cl}^2 + (n_o^2 - n_{cl}^2)\ s(r)\ . \tag{4}$$

If s(r) is completely specified, then all properties of the fibre can be calculated exactly using numerical methods. However, it is not easy to obtain s(r) in exact detail and exact numerical methods can be tiresome to implement for irregular profiles. A more important point is that *complete details of s(r) are not required for obtaining modal properties to a high degree of accuracy*, a claim which we substantiate in the subsequent sections and discuss in Section 7. In this chapter we attempt to isolate the key distinguishing aspects of s(r), which are important for determining modal parameters, but which require only limited information about s(r). In Chapter 7 [4] we explore the possibility of measuring these factors directly and of using them for fibre design.

We follow Stewart [1] and characterize the profile by using the moments of s(r), which we define by

$$N_\ell = \int_0^\rho [n^2(r) - n_{cl}^2]\ r^{\ell+1}\ dr \tag{5a}$$

$$= (n_o^2 - n_{cl}^2) \int_0^\rho s(r)\ r^{\ell+1}\ dr \tag{5b}$$

$$= (n_o^2 - n_{cl}^2)\ \rho^{\ell+2}\ \Omega_\ell\ , \tag{5c}$$

where

$$\Omega_\ell = \int_0^1 s(R)\ R^{\ell+1}\ dR\ . \tag{5d}$$

We have introduced $R = r/\rho$ and Ω_ℓ, the moments of the shape function s. We note that

$$\bar{V}^2 = 2k^2 N_0 = 2V^2\Omega_0\ . \tag{6}$$

In this chapter we shall use the even moments Ω_0, Ω_2, Ω_4, ... and show that single mode fibres are accurately described when only the first three are given. The reasons, theoretical and experimental, for choosing these particular moments are explained in the next section, where a few relevant properties and some pertinent examples of moments are given to orientate the readers' thinking.

The rest of the chapter is organized as follows: Section 3 examines a perturbation method of solving the wave equation which, as in the variational scheme described in Chapter 5, relies on only profile moments. This method is applied in Section 4 to produce analytical formulae for the fundamental modal properties, the accuracy of which are demonstrated in Section 5. In Section 6 the same approach is used for the second mode cutoff parameter $\bar{V}_{co}$. In Section 7 the derived formulae are used to provide a qualitative discussion of waveguide modal behaviour and Section 8 comprises the Conclusion.

6.2 PROFILE SHAPE FUNCTION AND MOMENTS

The usual definition of n_o leads to a shape function s, Eq. (4),

which always has a maximum of 1. The finite core, uniform cladding assumption means that we take

$$\begin{aligned} 0 \le s(R) &\le 1, \qquad 0 \le R \le 1, \\ s(R) &= 0, \qquad R \ge 1. \end{aligned} \tag{7}$$

A typical shape function is shown in Fig. 1 where we see that the step provides bounds.

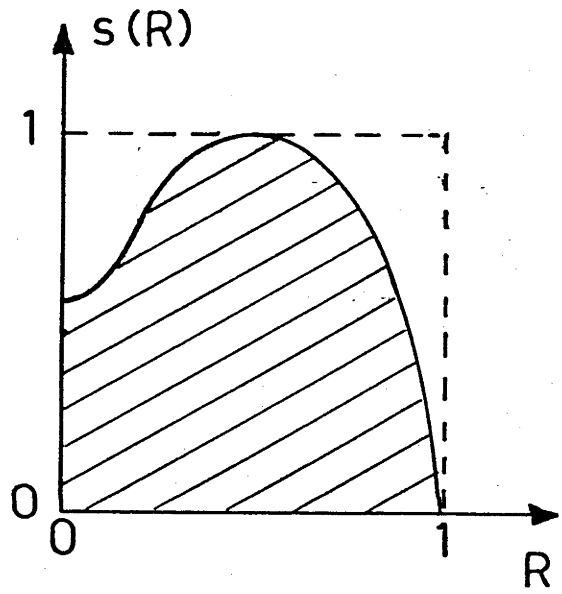

Fig. 1: Typical profile function s(R) considered in this chapter. $R = r/\rho$ and s is related to the refractive index through Eq. (4).

The restricted region in which s is non-zero implies that only the even moments Ω_0, Ω_2, Ω_4, ... are required for its full specification [5]. This fact is also refected in S(t), the Hankel transform of s, which has the moment expansion [6]

$$S(t) \equiv \int_0^\infty J_0(tR)\ s(R)\ RdR \tag{8}$$

$$= \sum_{\ell=0}^{\infty} \frac{(-1)^\ell}{(\ell!)^2}\, \Omega_{2\ell} \left(\frac{t}{2}\right)^{t\ell}. \tag{9}$$

Note that S(t) is a directly measurable quantity [7,8]. For the above reasons only the even moments $\Omega_{2\ell}$ are used in this work.

From their definition, Eq. (5d), and Eq. (7), we deduce that the moments form a monotonically decreasing series: $\Omega_0 \geq \Omega_2 \geq \Omega_4 \geq \ldots$. For example, the moments of the step profile, which of course yields the maximum moments, are

$$\Omega_{2\ell} = \frac{1}{(2\ell+2)} . \tag{10}$$

It is clear that any smoothing near the core-cladding boundary will rapidly decrease the higher moments, while on the other hand any dips in the profile near the fibre axis will only show up strongly in the lower moments. We define the normalized quantity $\bar{\Omega}_\ell$, where

$$\bar{\Omega}_\ell = \Omega_\ell/\Omega_0 , \tag{11}$$

as these are required explicitly in the expressions derived in Section 3.

In order to further acquaint the reader with moments we now present some examples in which trends can be easily appreciated.

6.2.1 Examples

As a first example we use the familiar power law profiles, shown in Fig. 2, to illustrate the effects of: (i) profile rounding of the core-cladding interface, (ii) the effects of on-axis dips, and (iii) the combined effects of the above, on the first three moments Ω_0, Ω_2, Ω_4 and their corresponding normalized quantities $\bar{\Omega}_2$ and $\bar{\Omega}_4$. The power law profiles are defined as follows:

$$s_1(R) = 1 - R^{q_1} , \qquad 0 \leq R \leq 1 , \tag{12a}$$

$$s_2(R) = 1 - (1-R)^{q_2} , \qquad 0 \leq R \leq 1 , \tag{12b}$$

$$\begin{aligned} s_3(R) &= 1 - (1-2R)^{q_3} , & 0 \leq R \leq \tfrac{1}{2} , \\ &= 1 - (2R-1)^{q_3} , & \tfrac{1}{2} \leq R \leq 1 , \end{aligned} \tag{12c}$$

and

$$s_1(R) = s_2(R) = s_3(R) = 0 , \qquad 1 \leq R \leq \infty . \tag{12d}$$

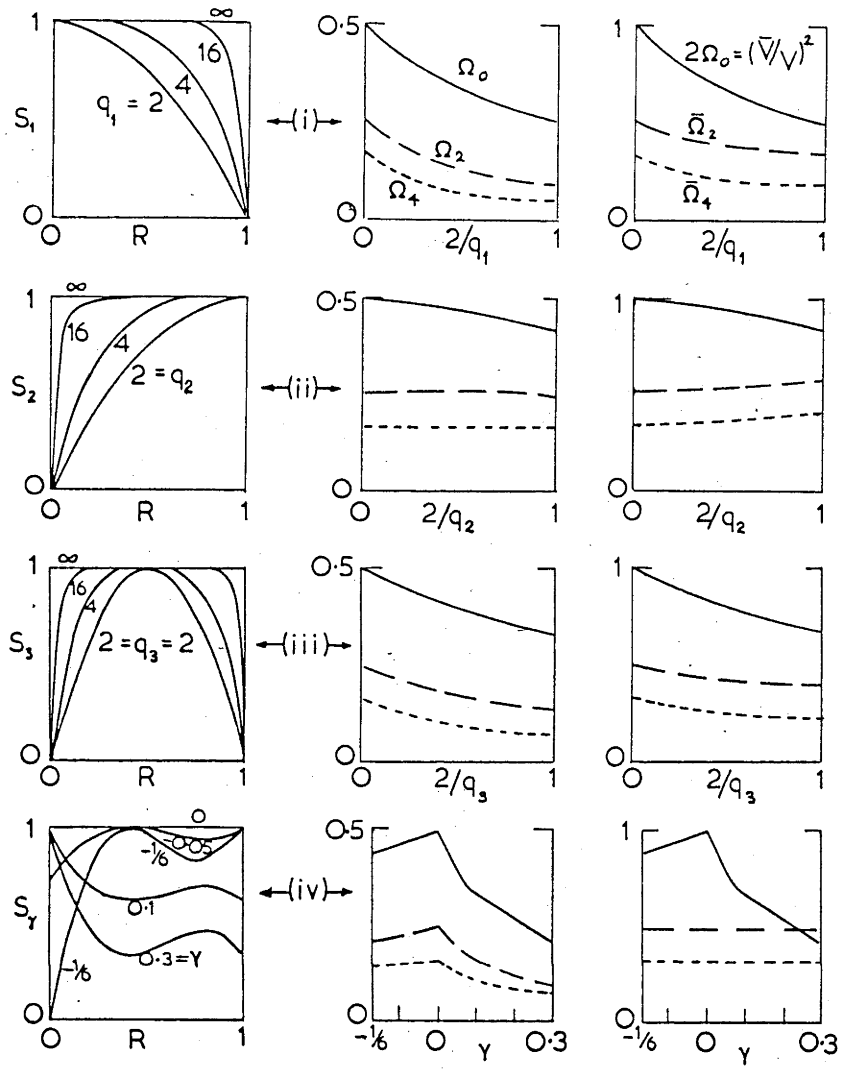

Fig. 2: Examples of profiles and their moments. The profile function s defined in Eq. (4) and $R = r/\rho$. The power law profile s_1, s_2 and s_3 are defined in Eq. (12) and the γ-profiles s_γ are given by Eq. (13). The moments Ω_ℓ and normalized moments $\bar{\Omega}_\ell$ are defined by Eqs. (5) and (11). Solid and broken curves all refer to moments as labelled in case (i).

Note that the dips in s_2 and s_3 go to zero on-axis and are therefore a severe test of the effects of dips on the moments.

The curves in Fig. 2 show how Ω_0, hence $\bar{V}$, Ω_2 and Ω_4 decrease as the profile departs from a step. It is noticeable that the dips decrease Ω_0 somewhat, but have only a minor effect on Ω_2 and Ω_4. It

is instructive to look at the normalized quantities in Fig. 2. We now observe that $\bar{\Omega}_2$ and $\bar{\Omega}_4$ decrease for shoulders, but increase for dips. Thus the normalized moments become indicators of profile shape. The dips and shoulders have a compensating effect on $\bar{\Omega}_2$ and $\bar{\Omega}_4$, but these moments still decrease in case (iii) because of the greater influence of the shoulders.

The results which we generate later depend on $\bar{\Omega}_2$ and $\bar{\Omega}_4$ so it is interesting to consider sample profiles which all have the same values for these parameters. We choose the step profile parameters $\bar{\Omega}_2 = 1/2$ and $\bar{\Omega}_4 = 1/3$. One set of profiles is obtained by modifying the step profile using a suitable polynomial, the magnitude of the change being determined by a parameter γ. Hence, we define the "γ profiles":

$$s_\gamma(R) = \frac{1+\gamma\, s_p(R)}{1+\gamma\, s_{pmax}}, \tag{13}$$

where

$$s_p(R) = 6 - 35R + 64R^2 - 35R^3 \tag{14}$$

and the normalization is needed to keep the maximum of s_γ at unity. We find

$$\begin{aligned} 1+\gamma\, s_{pmax} &= 1 + 0.0041843\,\gamma, \qquad \gamma < 0 \\ &= 1 + 6\,\gamma \qquad\qquad\quad , \qquad \gamma > 0 . \end{aligned} \tag{15}$$

In order to satisfy Eq. (7) we must take $-1/6 \le \gamma < \infty$. A selection of these profiles is shown in Fig. 2, case (iv). We can now see how large a dip is required (the negative γ examples) to balance a small amount of distortion nearer the core-cladding boundary. Clearly profiles which are characterized by the same values of $\bar{\Omega}_2$ and $\bar{\Omega}_4$ can appear to be quite different in other respects.

6.2.2 Bounds on the Moments

In the above discussion we related the moments to particular features of profile shape. It now remains to specify the range of values which Ω_0, Ω_2 and Ω_4 can assume.

The restrictions on s(R), Eq. (7), imply that

$$0 \leq \Omega_0 \leq 0.5 . \tag{16}$$

When Ω_0 is given it becomes a mathematical question to specify the possible range of Ω_2 and Ω_4 values and we find

$$\Omega_0^2 \leq \Omega_2 \leq \Omega_0 (1 - \Omega_0) \tag{17}$$

and

$$\frac{4}{3} \Omega_0^3 \leq \Omega_4 \leq \Omega_0 \left[1 - 2\Omega_0 + \frac{4}{3} \Omega_0^2 \right] . \tag{18}$$

These bounds are shown plotted in Fig. 3 together with the profiles corresponding to these extreme values. The lower limits occur when a whole block of the profile is removed from near R = 1 and are not representative of the profile shoulders we consider in practice. The broken curves showing Ω_2 and Ω_4 versus Ω_0 for the power law profiles of Eq. (12) show how close to the extremes the values of the moments might be expected to fall.

A similar approach can be used to obtain the mathematically possible range of values of Ω_4 when Ω_0 and Ω_2 are *both* specified, and we find

$$\frac{\Omega_0}{3} \left\{ \Omega_0^2 + \frac{3\Omega_2^2}{\Omega_0^2} \right\} \leq \Omega_4 \leq \left\{ \Omega_2 - \Omega_0^2 - 2\Omega_0\Omega_2 - \frac{2}{3} \Omega_0^3 \right\}$$
$$- \frac{2}{(1 - 2\Omega_0)} \{ \Omega_0^4 - 2\Omega_0\Omega_2 + 2\Omega_0^2\Omega_2 + \Omega_2^2 \} . \tag{19}$$

We illustrate these bounds in Fig. 3(b) using the power law profiles of Eq. (12) to define a set of Ω_0, Ω_2 values, and then applying Eq. (19) to map out the area of all possible Ω_4 values. The curves for

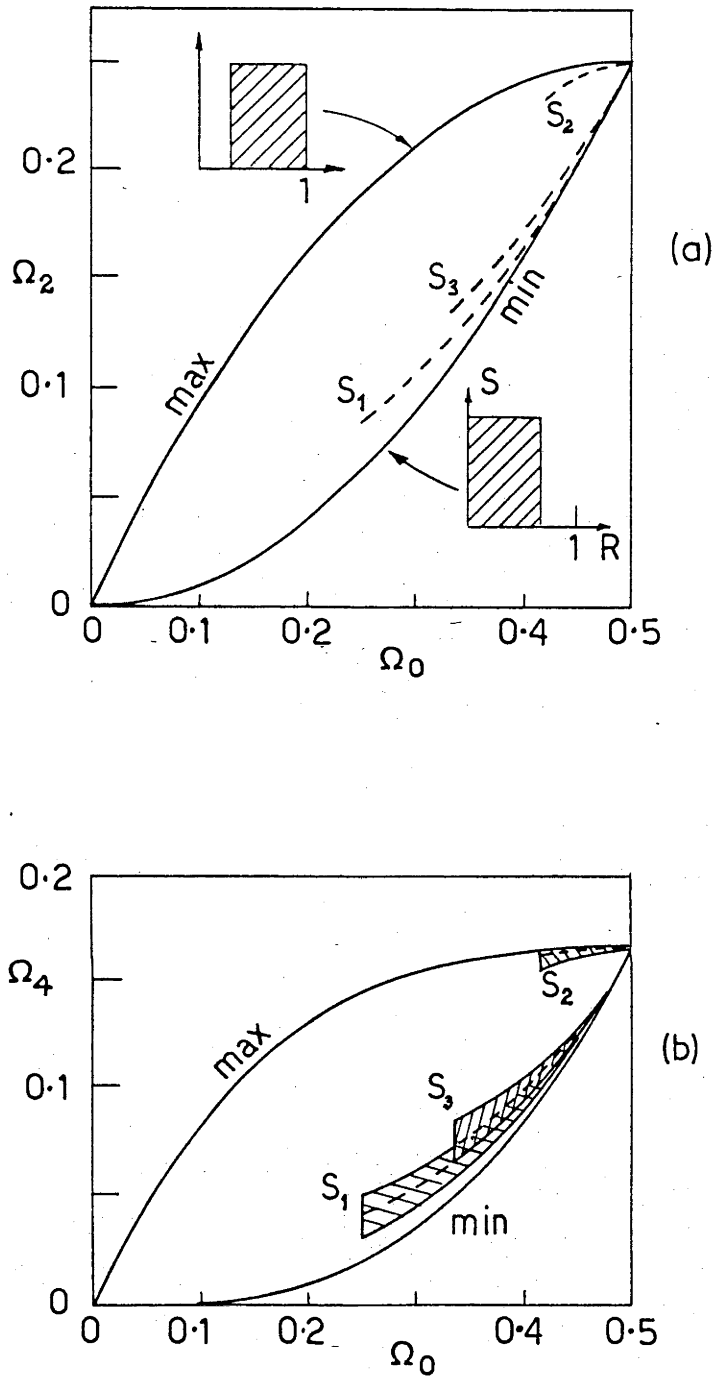

Fig. 3: Bounds on moment values. The solid curves indicate the maximum and minimum values which Ω_2 (a) and Ω_4 (b) can attain for a given Ω_0, in accordance with Eq. (18). The profiles corresponding to these extremes are also shown. The dashed lines plot the Ω_2 vs Ω_0 and Ω_4 vs Ω_0 for the power law profiles s_1, s_2 and s_3 shown in Fig. 2. In (b) the shaded areas show possible values of Ω_4, as given by Eq. (19), when Ω_0 and Ω_2 take on their power law profile values.

the power law profiles lie in this area of course. The variation of Ω_4, given Ω_0 and Ω_2, is very small. This fact is important when variations of Ω_4 are treated as perturbations in later sections.

6.3 SOLVING THE WAVE EQUATION

With the fibre now specified we turn to the calculation of modal properties. We can rewrite the scalar wave equation (2.21) [9] in terms of V (Eq. 1), shape function s (Eq. 4) and $R = r/\rho$, as

$$-D_\ell \psi + V^2 \; s(R)\psi \;=\; W^2 \psi \,, \tag{20}$$

where

$$D_\ell \;=\; \left\{ -\frac{d^2}{dR^2} - \frac{1}{R}\frac{d}{dR} + \frac{\ell^2}{R^2} \right\} \tag{21}$$

and the modal eigenvalue W (or U) is given by

$$W^2 \;=\; V^2 - U^2 \,. \tag{22}$$

The result concerning cutoff, (Eq. 3), suggests that single mode waveguides with the same $\bar{V}$ behave similarly and particular examples [10] plus the further general results in this chapter strongly reinforce that idea. Thus we begin by converting Eq. (20) to

$$-D_0 \psi + \tfrac{1}{2}\bar{V}^2 \; \bar{s}(R)\psi \;=\; W^2 \psi \,, \tag{23}$$

where

$$\bar{s}(R) \;=\; s(R)/\Omega_0 \,. \tag{24}$$

The moments of $\bar{s}$ are $\bar{\Omega}_2, \bar{\Omega}_4, \ldots$ as in Eq. (11). The similar behaviour mentioned above also suggests that a perturbation scheme should work well for Eq. (23). We assume a reference profile $\bar{s}_{ref}$ and field ψ_{ref},

$$-D_0 \; \psi_{ref} + \tfrac{1}{2}\bar{V}^2 \; \bar{s}_{ref}(R) \; \psi_{ref} \;=\; W^2_{ref} \; \psi_{ref} \tag{25}$$

and then first order perturbation theory gives

$$\frac{W^2}{\bar{V}} \simeq \frac{W^2_{ref}}{\bar{V}} + \frac{\bar{V}}{2} \frac{\int_0^\infty (\bar{s} - \bar{s}_{ref})\ \psi^2_{ref}\ RdR}{\int_0^\infty \psi^2_{ref}\ RdR} . \tag{26}$$

We do not calculate the upper integral in Eq. (26) directly since only moments are to be used, but we can express it as

$$\int_0^\infty (\bar{s} - \bar{s}_{ref})\ \psi^2_{ref}\ RdR = \sum_{i=1}^{\infty} a_i (\bar{\Omega}_{2i} - \bar{\Omega}_{2i,ref}) , \tag{27}$$

where the a_i are the coefficients resulting from an expansion of ψ^2_{ref} as a polynomial in R^2. The treatment of the sum in Eq. (27) rests on two points: we can choose our reference fibre so that one term is zero, and we can truncate the sum so that only a few moments are involved but sufficiently accurate answers are obtained. (The reader may see here an analogy with the methods of asymptotic expansions, although in fact our sum always finally converges.) We also remind the reader that only a small spread in higher moment values can occur once the lower moments are fixed (see the discussion in Section 2), and so higher terms in Eq. (27) do ultimately become very small and the series converges.

It is convenient to choose some step index fibre as a reference because its field and other modal properties are well known. The reference parameter to be fixed is the step radius ρ_s and then

$$\begin{aligned} \psi_{ref}(R) &= \frac{J_o(U_{st}\ r/\rho_s)}{J_o(U_{st})} = \frac{J_o(U_{st}\ R[\rho/\rho_s])}{J_o(U_{st})} \qquad r \le \rho_s \\ &= \frac{K_o(W_{st}\ r/\rho_s)}{K_o(W_{st})} = \frac{K_o(W_{st}\ R[\rho/\rho_s])}{K_o(W_{st})} \qquad r > \rho_s \end{aligned} \tag{28}$$

with U_{st} and W_{st} being the step fibre eigenvalues for $V = \bar{V}$. The coefficients a_i in Eq. (27) are readily available [11]. Investigation

reveals that the best choice of ρ_s depends on the parameter x,

$$x = 1 - [2\bar{\Omega}_2/\sqrt{3\bar{\Omega}_4}] \tag{29}$$

which is an indicator of profile type. For example, x is zero for a step profile, positive when shoulders occur (e.g. as in Fig. 2, case (i)) and negative for dip profiles (e.g. as in Fig. 2, case (ii)). When $x < 0$, we choose ρ_s so that $\bar{\Omega}_{2,ref} = \bar{\Omega}_2$ and ignore all higher order terms in Eq. (27), while for $x > 0$ we match $\bar{\Omega}_{4,ref} = \bar{\Omega}_4$ and keep only the perturbation term in $(\bar{\Omega}_2 - \bar{\Omega}_{2,ref})$. A little manipulation leads to the following results:

$$x \le 0: \quad \rho_s/\rho = (2\bar{\Omega}_2)^{\frac{1}{2}} \tag{30a}$$

$$W^2 \simeq W_{st}^2(\bar{V})/2\bar{\Omega}_2 , \tag{30b}$$

$$x > 0: \quad \rho_s/\rho = (3\bar{\Omega}_4)^{\frac{1}{4}} \tag{30c}$$

$$W^2 \simeq \frac{W_{st}^2(\bar{V})}{\sqrt{3\bar{\Omega}_4}} \left\{ 1 + x \frac{U_{st}^2}{4J_1^2(U_{st})} \right\} . \tag{30d}$$

Note that the $\bar{V}$ dependence enters through the step index fibre parameters $U_{st} = U_{st}(\bar{V})$ and $W_{st} = W_{st}(\bar{V})$, i.e. the eigenvalue at $V = \bar{V}$. (The zealous reader might note that we have taken a_i in Eq. (27) from the expansion of $J_0^2(U_{st} R\rho/\rho_s)$ in all cases; this involves a small approximation when $x > 0$ and $\rho_s < \rho$ so that part of the approximate field in the core comes from the K_o term in Eq. (28). The error involved is of no consequence.)

Equations (28) and (30) enable us to evaluate all relevant modal properties and we gather these together in a concise form in the next section deferring considerations of accuracy until Section 5.

6.4 FUNDAMENTAL MODE PARAMETERS

We are now in a position to derive expressions for all quantities of importance when describing propagation in single mode fibres. We begin with pulse propagation which can be analysed, including the effects of material dispersion [12-14], in terms of the three parameters

$$b(V) = W^2/V^2 , \tag{31a}$$

$$b_1(V) = d(Vb)/dV , \tag{31b}$$

$$b_2(V) = Vdb_1/dV . \tag{31c}$$

Writing these in terms of $\bar{V}$ leads to normalized expressions:

$$b(V) = 2\Omega_0 W^2/\bar{V}^2 = 2\Omega_0 \bar{b}(\bar{V}) \tag{32a}$$

$$b_1(V) = 2\Omega_0 d(\bar{V}\bar{b})/d\bar{V} = 2\Omega_0 \bar{b}_1(\bar{V}) \tag{32b}$$

$$b_2(V) = 2\Omega_0 \bar{V} d(\bar{b}_1)/d\bar{V} = 2\Omega_0 \bar{b}_2(\bar{V}) . \tag{32c}$$

Equation (30) can now be more conveniently written as

$$\bar{b}(\bar{V}) \simeq b_{st}(\bar{V})/(2\bar{\Omega}_2) \quad , \quad x \le 0 \tag{33a}$$

$$\bar{b}(\bar{V}) \simeq \frac{b_{st}(\bar{V})}{\sqrt{3\bar{\Omega}_4}} \left\{ 1 + \frac{xU_{st}^2}{4J_1^2(U_{st})} \right\} , \quad x > 0 . \tag{33b}$$

Note that for the step fibre $V = \bar{V}$ and $\bar{b}_{st}(\bar{V}) = b_{st}(\bar{V})$. It is then a matter of straightforward differentiation to obtain $\bar{b}_1(\bar{V})$ and $\bar{b}_2(\bar{V})$ in terms of $b_{1,st}(\bar{V})$ and $b_{2,st}(\bar{V})$. Hence for an arbitrary fibre, the calculation of pulse dispersion can be made using only a knowledge of Ω_0, Ω_2, Ω_4 and the parameters for a step index fibre evaluated at $V = \bar{V}$. The step index fibre data is well known, e.g. see Ref. 12 and the appendix of Chapter 7 for analytic formulae and numerical data.

Questions about source coupling into the fibre, fibre-fibre splicing, and bending and microbending losses can be simply addressed

when a measure of the modal spot size is given. The field in Eq. (28) enables us to express the spot size ω in terms of the reference step. We always use Eq. (30a), irrespective of the sign of x, as the expression obtained is simple as well as being very accurate, and

$$\left(\frac{\omega}{\rho}\right)_{\bar{V}} \simeq (2\bar{\Omega}_2)^{\frac{1}{2}} \left(\frac{\omega}{\rho}\right)_{st,V=\bar{V}} \tag{34}$$

so that spot size is expressed in terms of the step index fibre spot size evaluated at $V=\bar{V}$. There are various definitions of ω, but for later considerations of accuracy we use the one given by Petermann [15] in connection with microbending theories:

$$\left(\frac{\omega}{\rho}\right)^2 = \int_0^\infty \psi^2 R^3 dR \Big/ \int_0^\infty \psi^2 R dR . \tag{35}$$

For this definition, there is a simple analytical expression for the step index fibre spot size [16].

The fraction η of power propagating within the core,

$$\eta = \int_0^\rho \psi^2 r dr \Big/ \int_0^\infty \psi^2 r dr , \tag{36}$$

is of interest when absorbing waveguides are involved [17], and again the use of the approximate field gives $\eta(\bar{V})$ for an arbitrary fibre in terms of its moments and the step fibre parameters evaluated at $V=\bar{V}$:

$$\eta(\bar{V}) \simeq \eta_{st}(\bar{V}) \left\{1 + \frac{J_0^2(U_{st})[h(W_{st}) - y\, h(y W_{st})]}{K_0^2(W_{st})\; j(U_{st})}\right\}, \qquad 2\bar{\Omega}_2 \le 1 \tag{37a}$$

and

$$\eta(\bar{V}) \simeq \eta_{st}(\bar{V})\; y\, j(y U_{st})/j(U_{st}) \qquad , \qquad 2\bar{\Omega}_2 > 1 \tag{37b}$$

where

$$y = 1/\sqrt{(2\bar{\Omega}_2)}$$

and

$$h(z) = K_1^2(z) - K_0^2(z) ,$$

$$j(z) = J_0^2(z) + J_1^2(z) .$$

6.5 ACCURACY

The expressions given in the previous section are straightforward to apply once the profile moments are known and these are trivial to calculate either analytically or numerically. However, we have no way of knowing *a priori* how accurate the modal parameters are given and so in this section we compare approximate and exact answers for a representative range of profiles. These are gathered together for convenience in Fig. 4 and include three experimental cases [18,19].

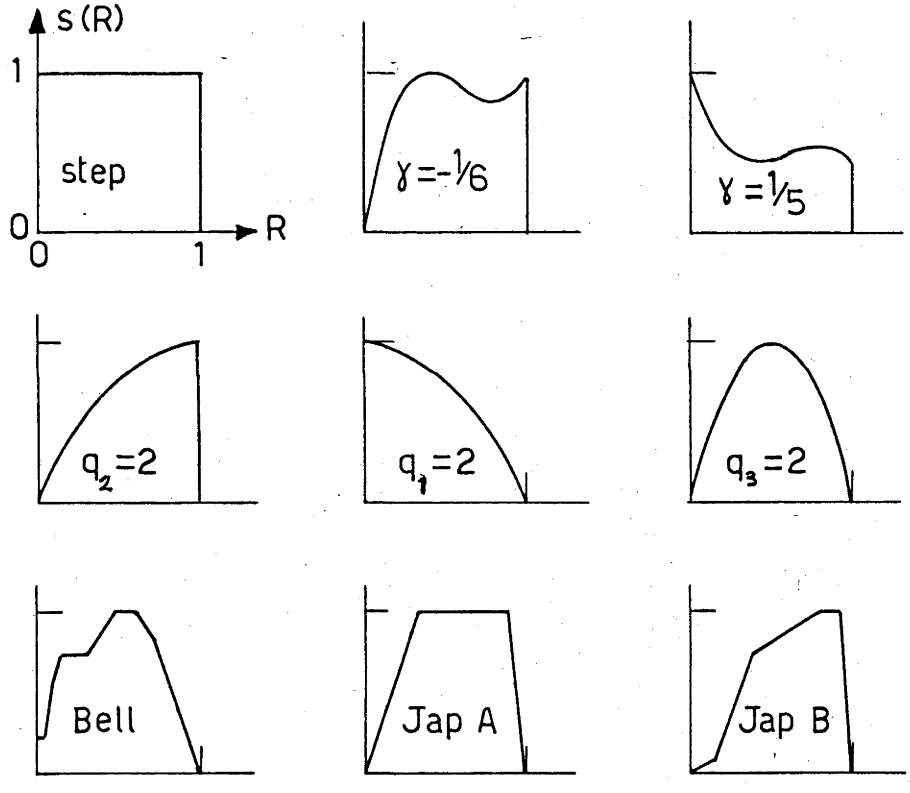

Fig. 4: Collection of profiles used to examine the accuracy of approximate formulae. The γ profiles are defined in Eq. (13) and q_1, q_2, q_3 refer to the power law profiles defined in Eq. (12) and Fig. 2. The $q_1 = q_2 = q_3 = 2$ cases are plotted. Bell $\equiv$ experimental profile in [18], JapA, JapB $\equiv$ experimental profiles in [19].

Table 1 lists the percentage errors in $\bar{b}$, $\bar{b}_1$ and $\bar{b}_2$ when Eq. (33) and its derivatives are used at $\bar{V} = 1.2$, 1.8 and 2.4. We observe that the errors are generally $\lesssim$ 1% for $\bar{b}(V)$, but increase as we go to $\bar{b}_1$ and to $\bar{b}_2$. However, even for $\bar{b}_2$ we have accuracy to a few per cent which is adequate for many purposes.

The sign of the profile parameter x (Eq. 29) is shown in Table 1 since it controls which formula applies in Eq. (33). The errors shown in brackets refer to quantities calculated using Eq. (33a), the $x \leq 0$ formula, even when $x > 0$. The point of this is that Eq. (33a) is an extremely simple formula requiring only $\bar{V}$ and $\bar{\Omega}_2$ for its evaluation. Table 1 indicates that the simple formula may be used with good accuracy in most reasonable cases, the errors becoming large only when extreme shoulder type profiles, e.g. $q_1 = 2$, are considered.

The results for the γ profiles, Fig. 4, are particularly interesting since those profiles have the same $\bar{\Omega}_2$ and $\bar{\Omega}_4$ values as the step profile (see Section 2). Hence, according to Eq. (33a), the $\bar{b}$, $\bar{b}_1$ and $\bar{b}_2$ values are just those of a step at the same $\bar{V}$, i.e. $b_{st}(\bar{V})$, $b_{1,st}(\bar{V})$ and $b_{2,st}(\bar{V})$. The errors in Table 1 indicate the accuracy of that result and we see that fibres characterized by the same $\bar{\Omega}_2$ and $\bar{\Omega}_4$ do indeed behave similarly.

The field properties approximated by Eqs. (34) and (37) are also accurate to around 1% as shown in Table 2. The spot size uses Petermann's definition [15], Eq. (35), and is very reliably given by Eq. (34). The spot size used here can of course be used to generate a Gaussian field approximation [15] if that is required for producing simple excitation and splicing formulae [20].

The results presented here obviously do not cover every conceivable type of profile, but we believe that they cover a wide

Table 1: Percentage errors in the normalized propagation constants, $\bar{b}$, $\bar{b}_1$ and $\bar{b}_2$ defined by Eq. (32), when the approximate formulae, Eq. (33), are used for the three $\bar{V}$ values in the single mode region. Parameter x is defined in Eq. (29) and its sign governs which of Eqs. (33a) and (33b) should be used. The errors in brackets refer to the $x \leq 0$ formula result when applied in cases where x is actually positive. The profiles are all illustrated in Fig. 4 for ease of reference and the q profiles are shown in detail in Fig. 2. Bell $\equiv$ profile in [18]. JapA and JapB $\equiv$ profiles from [19].

Table 1

Profile	Sign of x	% error in $\bar{b}$			% error in $\bar{b}_1$			% error in $\bar{b}_2$		
		$\bar{V}=1.2$	1.8	2.4	$\bar{V}=1.2$	1.8	2.4	$\bar{V}=1.2$	1.8	2.4
step	o	0	0	0	0	0	0	0	0	0
$\gamma=-1/6$	o	0.07	0.1	0.2	0.08	0.15	0.3	0.1	0.5	3.8
$\gamma=+1/5$	o	0.07	0.15	0.25	0.1	0.25	0.5	0.2	1.1	6.4
$q_1=16$	+	0.0 (0.2)	0.05 (0.32)	0.1 (0.42)	0.01 (0.25)	0.1 (0.44)	0.2 (0.6)	0.06 (0.41)	0.54 (1.3)	2.46 (3.54)
$q_1=4$	+	0.5 (1.5)	0.4 (2.5)	0.3 (3.3)	0.4 (2.0)	0.3 (3.4)	1.0 (4.6)	0.4 (3.0)	0.5 (9.0)	3.3 (23.0)
$q_1=2$	+	1.6 (3.0)	1.8 (5.2)	2.0 (6.8)	1.7 (4.0)	2.0 (7.0)	2.3 (9.6)	2.0 (6.0)	3.3 (18.0)	7.0 (41.0)
$q_2=16$	-	0.1	0.2	0.3	0.14	0.26	0.37	0.3	0.8	2.1
$q_2=4$	-	0.4	0.8	1.0	0.6	1.13	1.18	1.2	2.5	3.1
$q_2=2$	-	0.3	0.8	0.8	0.6	1.08	1.1	1.3	1.1	16.0
$q_3=16$	+	0.00 (0.02)	0.01 (0.03)	0.03 (0.03)	0.01 (0.02)	0.03 (0.04)	0.46 (0.42)	0.02 (0.03)	0.13 (0.08)	0.54 (0.16)
$q_3=4$	+	0.07 (0.16)	0.05 (0.22)	0.04 (0.3)	0.07 (0.2)	0.04 (0.3)	0.05 (0.42)	0.04 (0.25)	0.03 (0.8)	1.16 (4.0)
$q_3=2$	+	0.26 (0.3)	0.32 (0.5)	0.44 (0.7)	0.3 (0.4)	0.4 (0.67)	0.75 (1.13)	0.31 (0.55)	1.4 (2.26)	10.0 (12.6)
Bell	-	0.2	0.2	0.4	0.2	0.2	0.35	0.1	0.5	6.0
JapA	-	0.3	0.6	0.7	0.5	0.9	0.7	1.0	1.4	9.1
JapB	-	0.2	0.6	0.5	0.45	0.8	0.06	1.1	0.4	23

Table 2: Percentage errors in η, Eq. (36), and spot size (ω/ρ), Eq. (35), when the approximate formulae Eqs. (34) and (37) are used for three relevant $\bar{V}$ values. The profiles are all shown together in Fig. 4.

Profile	% error in η			% error in (ω/ρ)		
	$\bar{V}=1.2$	1.8	2.4	$\bar{V}=1.2$	1.8	2.4
step	0	0	0	0	0	0
$\gamma=-1/6$	0.35	0.16	0.12	0.3	0.15	0.1
$\gamma=+1/5$	0.3	0.2	0.3	0.1	0.2	0.5
$q_1=16$	0.52	0.45	0.36	0.22	0.4	0.6
$q_1=4$	1.42	1.4	1.2	1.0	2.05	3.5
$q_1=2$	2.4	2.1	1.72	2.0	3.9	6.9
$q_2=16$	0.3	0.1	0.09	0.05	0.1	0.4
$q_2=4$	0.3	0.85	1.10	0.25	1.0	2.3
$q_2=2$	0.55	1.6	2.05	0.28	1.55	3.6
$q_3=16$	0.4	0.25	0.2	0.12	0.18	0.1
$q_3=4$	0.45	0.3	0.2	0.2	0.22	0.02
$q_3=2$	0.5	0.35	0.2	0.3	0.25	0.15
Bell	0.7	0.3	0.2	0.7	0.2	0.5
JapA	0.2	0.9	1.04	0.05	1.0	2.3
JapB	0.2	0.2	1.8	0.25	1.35	3.45

range of possibilities and encompass most types of profile likely to be of interest in practice and consistent with our basic formalism (Sections 1 and 2). We conclude that the simple expressions given in Section 4 may be used to calculate modal properties with a good working accuracy.

6.6 SECOND MODE CUTOFF

The waveguide parameter for the second mode cutoff, $\bar{V}_{co}$, is comparatively insensitive to shape and Eq. (3) is an accurate, working formula for most profiles of interest. This formula can be improved

by applying the methods of Section 3 to the second mode ($\ell = 1$) at cutoff ($W = 0$). We find

$$\bar{V}_{co}^2 \simeq - \frac{2 \int_0^\infty \psi_{ref} \, D_1 \, \psi_{ref} \, RdR}{\int_0^\infty \psi_{ref}^2 \, \bar{s} \, RdR},$$

which leads to

$$\frac{1}{\bar{V}_{co}^2} \simeq \frac{1}{\bar{V}_{co,ref}^2} \left\{ 1 + \frac{\int_0^\infty \psi_{ref}^2 (\bar{s} - \bar{s}_R) \, RdR}{\int_0^\infty \psi_{ref}^2 \, \bar{s}_R \, RdR} \right\}. \tag{38}$$

We again use a step index fibre as the reference so that ψ_{ref} is as in Eq. (28), except that J_0 and K_0 are replaced by J_1 and K_1 now that we are dealing with the $\ell = 1$ mode, and since we are at cutoff $U_{st} = \bar{V}_{co,st} = 2.405$. The field expansion procedure follows that described in Section 3, and in this case we find it profitable to choose ρ_s by matching $\bar{\Omega}_{4,ref} = \bar{\Omega}_4$ so that $\bar{\Omega}_2$ enters the perturbation term. We then arrive at the expression

$$\bar{V}_{co} = \bar{V}_{co,st} / \{1 - 2.683 \, x\}^{\frac{1}{2}}, \tag{39}$$

where x is defined in Eq. (29). We point out that after ignoring higher moments, setting $x = 0$, Eq. (39) reduces to Eq. (3) which had previously only been obtained empirically. This formula is not particularly accurate, which is obviously a result of having to use the reference field and not the actual field itself. We overcome this by assuming the above *form* for $\bar{V}_{co}$, in terms of $\bar{V}_{co,st}$ and x, but determine the multiplicative factor for x by matching the value of $\bar{V}_{co}$ to that of a suitable known profile. We choose this profile by observing that the second mode is highly influenced by the shape of the profile at the core-cladding boundary, but is virtually unaffected

by the presence of on-axis dips. From Fig. 2 we can expect the s_1 profiles to affect the value $\bar{V}_{co}$ more than the s_2 or s_3 profiles. These s_1 profiles also lie close to the extreme bounds for the moments (see Fig. 3). For these reasons we choose the $q_1 = 2$ profile which has $V_{co} = 3.518$ and $\bar{V}_{co} = 2.4876$. Using this as a match we then obtain

$$\bar{V}_{co} = \bar{V}_{co,st}/\{1 - 1.1419\ x\}^{\frac{1}{2}}$$

$$= 2.405/\{1 - 1.1419\ x\}^{\frac{1}{2}}. \qquad (40)$$

This formula is highly accurate; for example, for the profiles considered in Fig. 4 it leads to results with errors of less than 1%.

6.7 QUALITATIVE FEATURES OF MODAL GUIDANCE

Our simple formulae for modal properties relate to general profiles, so that we can now extract the *qualitative* behaviour of those properties without recourse to many different kinds of profiles and examples, which previously has been the only possible approach.

The initial basic parameter for the *fibre* is the first moment Ω_0, which is the *degree of guidance* introduced by Gambling, Matsumura and Ragdale [2], who called it G and observed that it was a measure of the number of doping or guiding ions used to form the profile. Ω_0 is used to define $\bar{V}$ (Eq. 6) which directly indicates the guiding abilities of an optical fibre: for a multimode fibre the number of bound modes is given by $\bar{V}^2/2$ [1,21] and this also measures the light collected and guided from a Lambertian source [22]; for smaller guides $\bar{V}$ still indicates the numbers of guided modes and for $\bar{V} < 2.405$ only the fundamental bound mode propagates (Sections 1 and 6). If we go beyond the class of profiles considered in this chapter and allow $s(r) < 0$, then we have the possibility of negative values for Ω_0 as is the case

for some doubly clad or W-fibres. In this case Ω_0 tells us whether even the first mode can always propagate: if $\Omega_0 < 0$ then as $V \to 0$ the first mode will cease to propagate. This result is proved for the analogous quantum mechanical, Schrödinger equation in [23] and is confirmed for various examples in [24,25].

We now concentrate on the *guiding of the fundamental mode*. For two fibres with the same V value, manipulation of the wave equations (Eq. 20) leads to

$$W_1^2 - W_2^2 = V^2 \int_0^1 \psi_1\psi_2 [s_1(R) - s_2(R)] \, RdR / \int_0^1 \psi_1\psi_2 \, RdR . \tag{41}$$

From this equation and the integral calculus mean value theorem [26], we readily deduce that when $s_1(R) \geq s_2(R)$,

$$W_1^2 - W_2^2 = \xi(\Omega_{0,1} - \Omega_{0,2}) , \tag{42}$$

where ξ is a positive constant. Thus removing material from a profile decreases W: for the profiles in Fig. 5, $\Omega_{0,3} < \Omega_{0,2} < \Omega_{0,1}$ and $W_3 < W_2 < W_1$. The field in the cladding is $K_0(WR)$ so that removing material to decrease Ω_0 means a decrease in W, a more slowly decaying cladding field and a more weakly guided mode.

After incorporating Ω_0 into $\bar{V}$, Eqs. (30) and (34) indicate that W decreases and spot size increases as $\bar{V}$ decreases (ignoring higher moment effects to be discussed below). In fact for small $\bar{V}$, variational or other methods [23,27] give W becoming extremely small and $W \sim \exp(-2/\bar{V}^2)$. This is further evidence of the fact that reduction in the degree of guidance Ω_0 leads to a more extended modal field, greater susceptibility to bending losses [15] and weaker guidance. There is a residual dependence on profile shape, or the higher moments, which we now examine in detail for some important modal properties. For this purpose we use Eqs. (30), (33a) and (34)

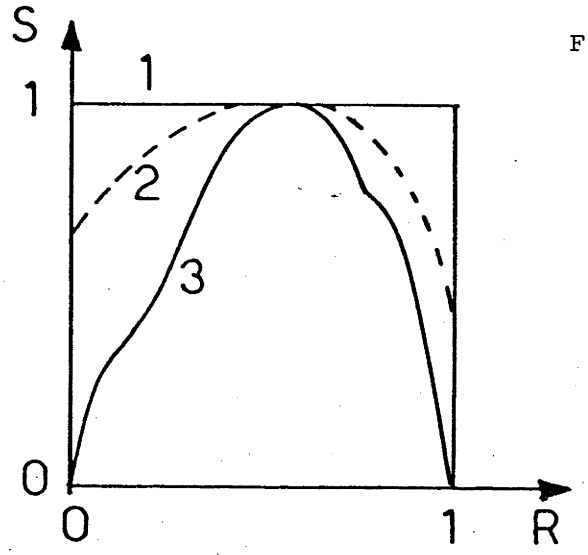

Fig. 5: Step profile and two profiles obtained when some doping material is removed from the step profile.

so that shape enters in the form of the parameter $\bar{\Omega}_2$ (ignoring the errors made when $x > 0$ as discussed in Section 5 on accuracy).

Equation (30b) says that $W(\bar{V}) \simeq W_{st}(\bar{V})/\sqrt{(2\bar{\Omega}_2)}$ and for our main region of interest ($1.2 \lesssim \bar{V} \lesssim 2.4$) we can couple this with the Rudolph-Neumann [28] step fibre formula to give the simplest of results

$$W \simeq -(0.704/\sqrt{\bar{\Omega}_2}) + 0.808/\sqrt{\bar{\Omega}_2})\ \bar{V}\,, \tag{43a}$$

$$W \simeq -(0.704/\sqrt{\bar{\Omega}_2}) + (1.1428\sqrt{[\Omega_0/\bar{\Omega}_2]})\,V\,. \tag{43b}$$

Our formulae reveal that

10% variation in $\bar{V}$ around $\bar{V} = 1.5 \rightarrow \sim 23\%$ variation in W,

10% variation in $\bar{V}$ around $\bar{V} = 2 \rightarrow \sim 18\%$ variation in W,

for fixed $\bar{V}$, 10% change in $\bar{\Omega}_2 \rightarrow \sim 5\%$ change in W,

for fixed $\bar{V}$, 20% change in $\bar{\Omega}_2 \rightarrow \sim 10\%$ change in W.

The behaviour of W is dominated by Ω_0 and extreme changes of shape only affect W slightly through $\bar{\Omega}_2$. For example, see Fig. 2 and note that the complete change from step to $q_2 = 2$ dip or $q_3 = 2$ hump causes $\bar{\Omega}_2$ to change by $\leq 20\%$.

Sample graphs of W plotted in various ways are shown in Fig. 6. The plot of $W(\bar{V})\sqrt{(2\bar{\Omega}_2)} = W_{st}(\bar{V})$ versus $\bar{V}$ is the universal curve; the graphs of $W(\bar{V})$ versus $\bar{V}$ show how the values of W simply scale with the shape parameter $\bar{\Omega}_2$; while resorting to V again, the graphs of W versus V show the complication present when the appropriate profile parameters are not isolated. The ordering with respect to $\bar{\Omega}_2$ values is lost in going from Fig. 6(b) to 6(c).

The spot size ω/ρ can be treated similarly and the results are shown in Fig. 7. The change from V to $\bar{V}$ aligns the curves and shows that there is a scaling, due to the shape parameter $\bar{\Omega}_2$, which can be eliminated by introducing the universal quantity $(\omega/\rho)\sqrt{(2\bar{\Omega}_2)}$ = step index fibre (ω/ρ).

As another example we examine the dispersion parameter b_2, Eq. (31c), for the familiar power law profiles Fig. 2, case (i). Figure 8a shows the *exact* results for b_2 versus V. We now extract out the Ω_0 dependence by noting Eq. (32c) and therefore plotting $\bar{b}_2(\bar{V}) = b_2/2\Omega_0$ versus $\bar{V}$. Once again we produce an alignment of the curves with a scaling which we interpret as due to profile shape factors. Equation (33a) would suggest that the shape again enters through $\bar{\Omega}_2$ and in Fig. 8c we show $b_2\bar{\Omega}_2/\Omega_0 = 2\bar{\Omega}_2\bar{b}_2$ versus $\bar{V}$. We stress that these are the *exact* results and they reveal that, while the shape factor $\bar{\Omega}_2$ gives a major scaling, there is still some spread in the curves. But this is to be expected since the power law shoulder profiles have x (Eq. 29) > 0 and Eq. (33b) rather than (33a) should be used with a more complicated shape correction depending on $\bar{\Omega}_2$ and $\bar{\Omega}_4$. For many profiles, $x < 0$ and dispersion parameters are almost exactly scaled according to $\bar{\Omega}_2$ values and the accuracy of this scaling is shown by the errors in Table 1. For example, if the exercise in Fig. 8 were

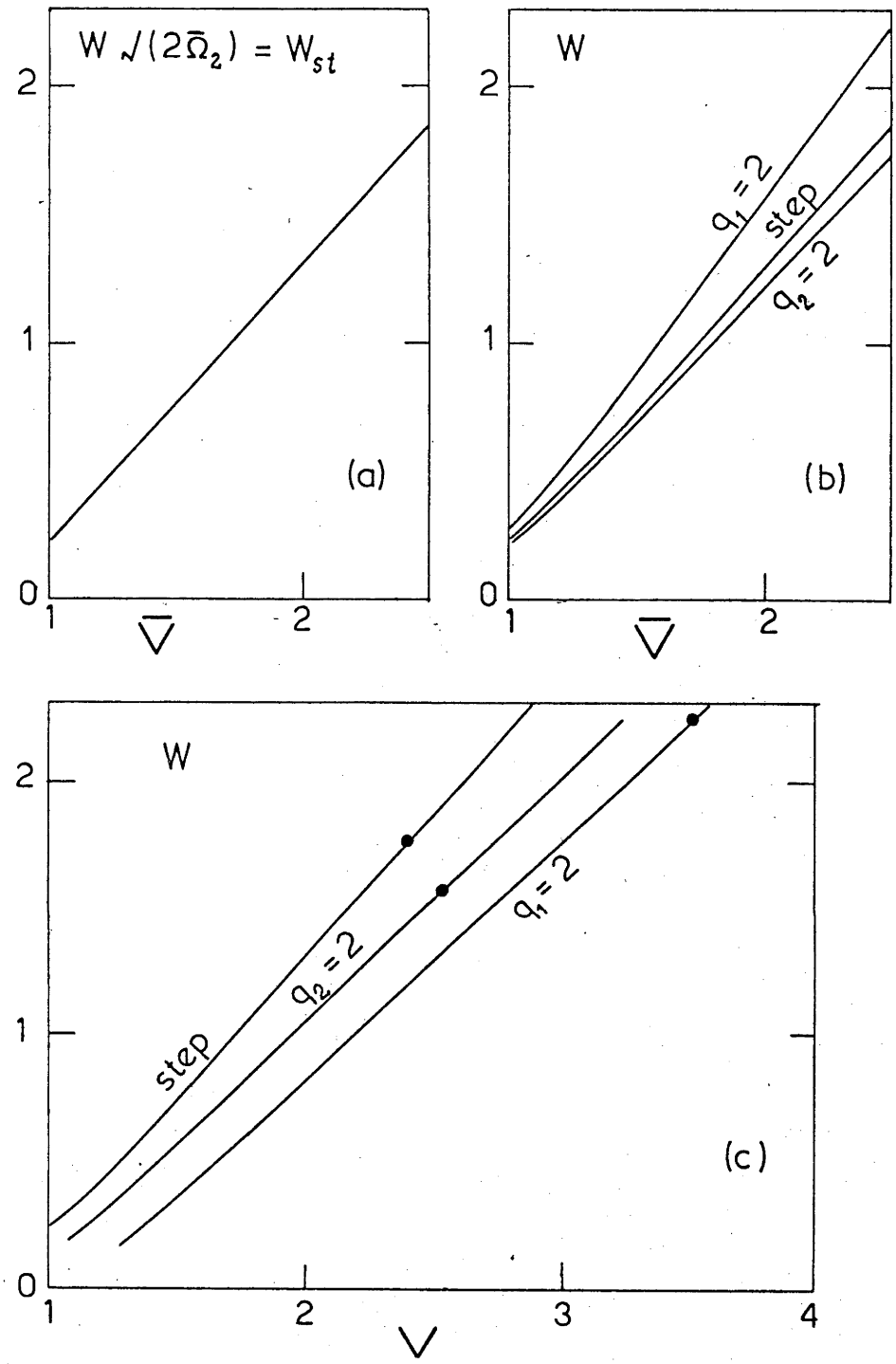

Fig. 6: Graphs of modal eigenvalue W. (a) The universal curve $W/(2\bar{\Omega}_2)$ vs. $\bar{V}$ which is just W_{st} vs. $\bar{V}$ according to Eq. (30b). (b) W vs. $\bar{V}$ for the step, parabolic shoulder, $q_1 = 2$, and parabolic dip, $q_2 = 2$, profiles. (c) As in (b) but now versus V. The dots indicate limit of monomode operation. Note that $\bar{\Omega}_2 = 0.5$ for the step, 1/3 for $q_1 = 2$ and 0.56 for $q_2 = 2$ so that the curves in (b) are ordered according to $\bar{\Omega}_2$ values.

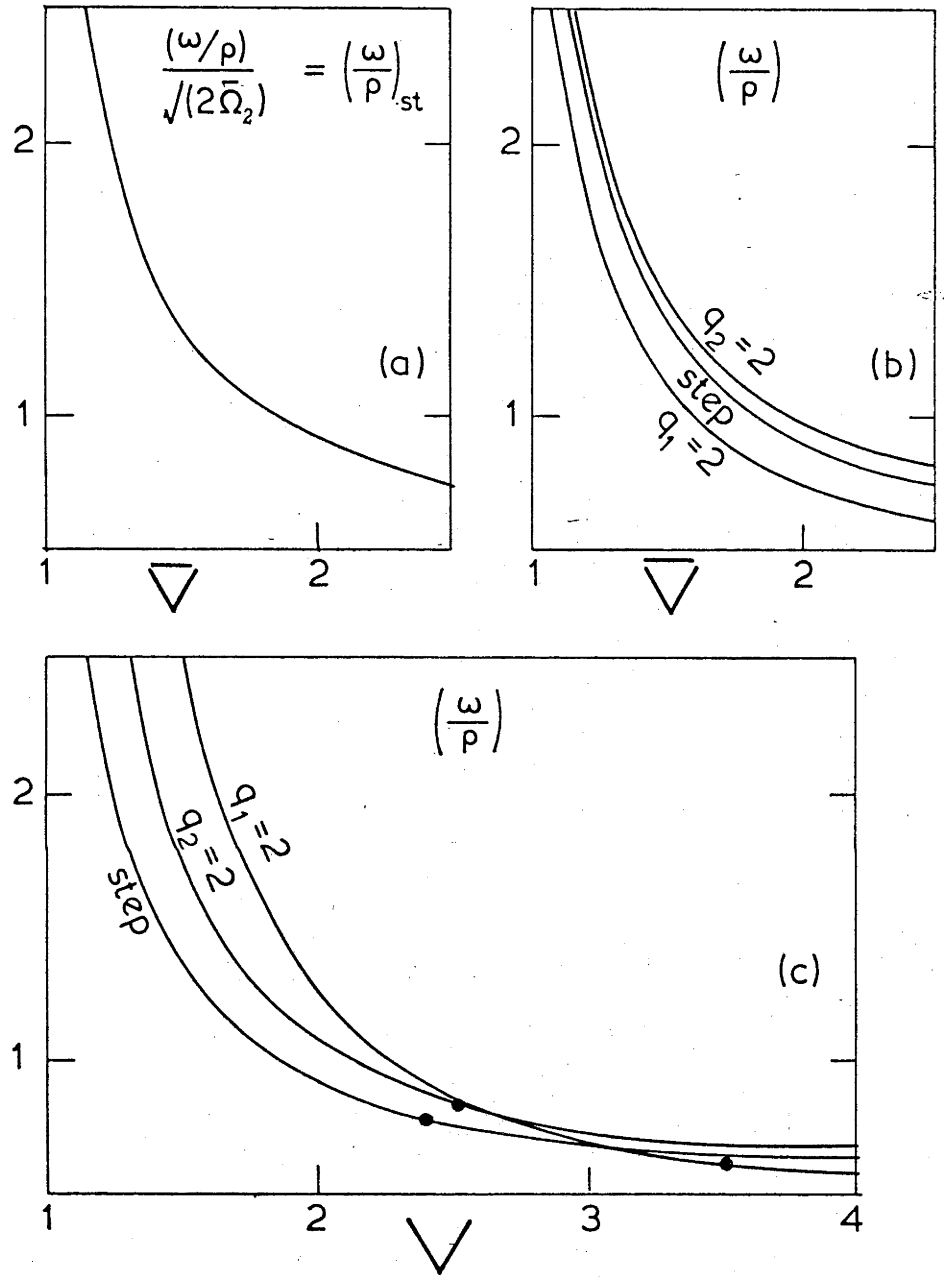

Fig. 7: Graphs of spot size (ω/ρ). Definition by Eq. (35) is used. (a) The universal curve $(\omega/\rho)/\sqrt{(2\bar{\Omega}_2)}$ vs. $\bar{V}$ which is just $(\omega/\rho)_{st}$ vs. $\bar{V}$ according to Eq. (34). (b) (ω/ρ) vs. $\bar{V}$ for the step, parabolic shoulder $q_1 = 2$ and parabolic dip, $q_2 = 2$, profiles. (c) as in (b) but now versus V. The limits of monomode operation are indicated by spots and the curves are a little less accurate for larger V, but the crossover is correctly described.

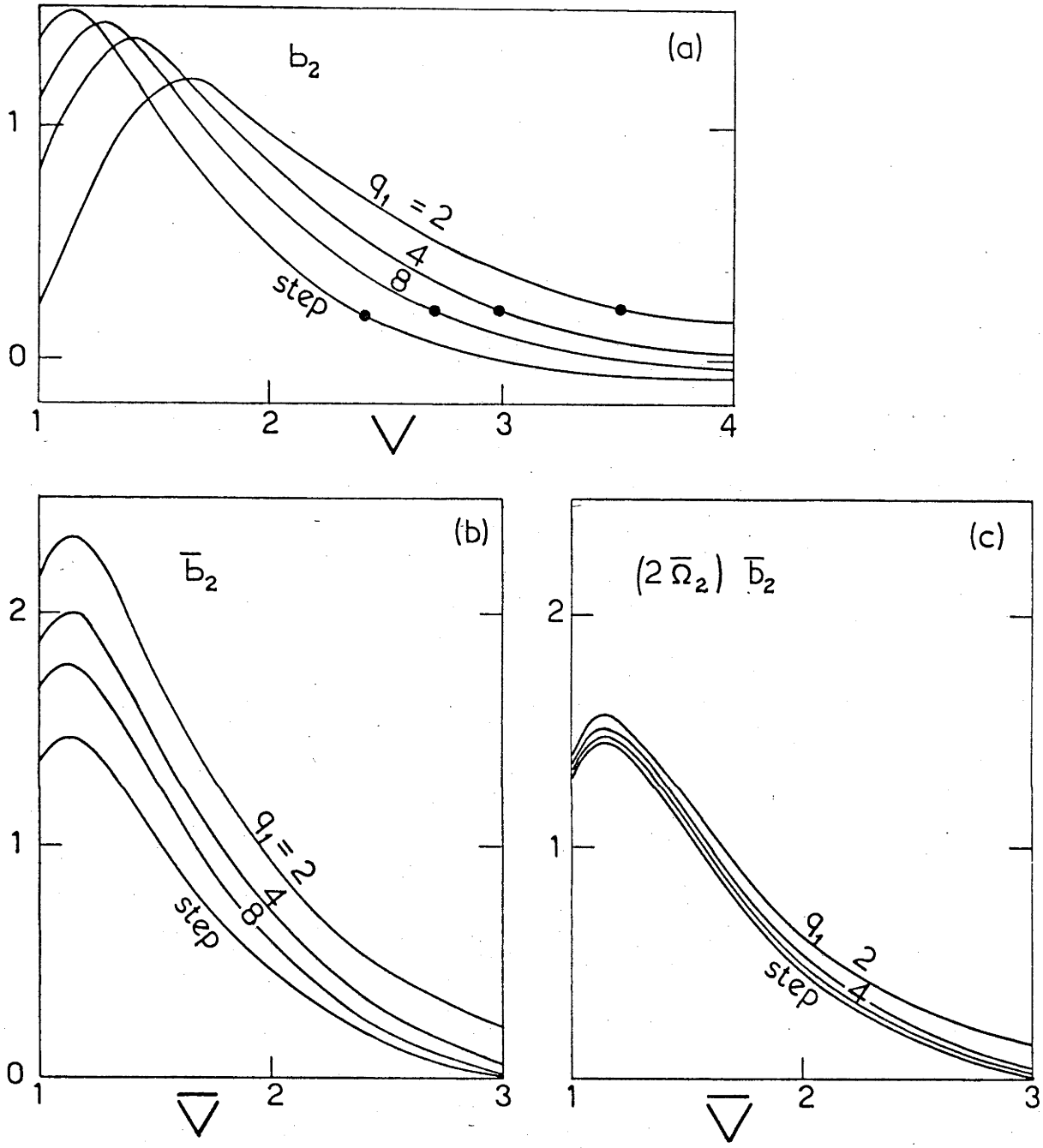

Fig. 8: Fundamental mode dispersion parameters. Power law shoulder profiles are used and curves are labelled by q_1 (Eq. 12a and Fig. 2, case (i)). (a) b_2 (Eq. 31c) versus V. Dots mark limit of monomode operation. (b) Normalized parameter $\bar{b}_2$ (Eq. 32c) versus $\bar{V}$. (c) $2\bar{\Omega}_2\bar{b}_2$ versus V. All fibres are monomode for $\bar{V} \lesssim 2.405$. (Curves are shown here for $\bar{V} > 2.4$ since exact results not approximate formulae are being used.)

repeated for the power law dip curves the final $2\bar{\Omega}_2\bar{b}_2$ versus $\bar{V}$ curves would be almost exactly coincident. In Fig. 9 we show $\bar{b}_2$ versus $\bar{V}$ for a variety of profiles all having $\Omega_0 = 5/12$ so that only profile shape orders the curves. This example vividly demonstrates the power of $\bar{V}$ and the way in which seemingly very different profiles can have similar waveguide properties.

The second mode cutoff $\bar{V}_{co}$ is almost entirely an Ω_0 effect with a small shape correction entering through x as in Eq. (40). Ranging over all the profiles shown in Fig. 4, the shape factor has to account for only ~ 3% changes in $\bar{V}_{co}$ from the step profile value 2.405.

We conclude that single mode fibres have very similar modal properties when the degree of guidance is used to normalize them through $\bar{V}$. A remaining scaling factor can be largely attributed to shape through the second profile moment $\bar{\Omega}_2$. The underlying reason for this simplicity is that all fibres in the single mode region have smooth, similarly shaped modal fields, a fact which has been stressed by many authors and used to rationalize Gaussian approximations, e.g. [1,15,16,20,29]. This smooth modal field does not sense the fine details of the profile, but only its broad, integrated properties which in our work are described by the profile moments. This contrasts with multimode fibres over the core of which modal fields rapidly oscillate, sensing the profile details and leading to dramatic pulse dispersion changes for small profile perturbations, e.g. [30].

6.8 CONCLUSION

We have developed a general, profile independent description of single mode fibres by isolating suitable parameters, Ω_0, Ω_2 and Ω_4. These parameters lead to analytical formulae for modal properties.

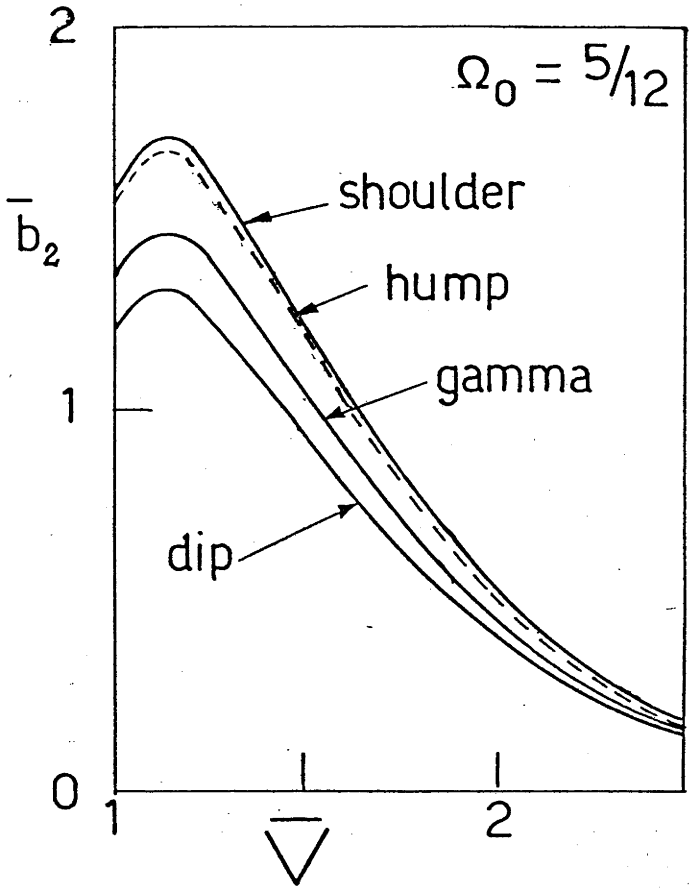

Fig. 9: Effect of shape on fundamental mode dispersion parameters. The normalized dispersion parameter $\bar{b}_2$, Eq. (32c), is plotted vs. $\bar{V}$ for fibres with $\Omega_0 = 5/12$ but different profile shapes. Shoulder: $q_1 = 10$; dip: $q_2 = 2$; hump: $q_3 = 5$; gamma: $\gamma \simeq 0.04$, where these profiles are given in Eqs. (12) and (13) and in Fig. 2. The curves scale principally in accordance with the $\bar{\Omega}_2$ values which can be read off Fig. 2.

The formulae are simple because the complexity of waveguide behaviour enters them through the appropriate step index fibre results which are known in complete detail.

The average or effective waveguide parameter $\bar{V}$ emerges naturally in this work and it is shown quite generally that when modal properties are considered as a function of $\bar{V}$, all single mode fibres exhibit similar behaviour, although magnitude scaling due to profile shape factors may also occur. This explains why almost coincident curves are found in graphs of waveguide quantities plotted against V/V_{co} (e.g. see [8,14]): Eqs. (3) and (6) give $V/V_{co} = \bar{V}/2.405$ and so plotting against V/V_{co} is approximately equivalent to using $\bar{V}$. The effects of profile shape are largely specified by the normalized

moment $\bar{\Omega}_2$.

Further uses of $\bar{V}$ and the approximations in Section 3 are straightforward to make: the near field of Eq. (28) can be used to obtain the modal diffraction or far field and its properties in terms of $\bar{V}$, $\bar{\Omega}_2$ and $\bar{\Omega}_4$; the theories of radiation from single mode fibres can be related to $\bar{V}$ as we discuss in Chapter 9. The eigenvalue correction term and the results for the birefringence properties as discussed in Chapter 4 and Reference [31] can also be related to $\bar{V}$. The theory can also be extended to cover variable fibres by letting $\Omega_m = \Omega_m(z)$, where z is measured along the fibre axis, and the effects of fibre perturbations on loss and dispersion calculated. The fact that the second mode cutoff is described so accurately by these methods suggests that for $\bar{V} < \bar{V}_{co}$ the leaky mode properties of the second mode should also relate to the fibre moments. The generality of the formulae further suggests that they may be applied in fibre design [4].

Throughout this chapter we have stuck strictly to the single mode domain $\bar{V} < 2.405$, which is appropriate for recently reported experimental systems, especially those using longer wavelength sources. It is known that operating above $\bar{V} = 2.405$ is feasible if some sort of filter is used to remove the second mode which is very susceptible to bending losses near to cutoff [32,33]. A characterization of fibres based on profile moments is still possible and as we describe in Chapter 8, proves to be very powerful when examining the interesting waveguide dispersion properties around $\bar{V} = 3$ [34], but the formulae presented in Sections 3 and 4 become less accurate as $\bar{V}$ increases and different methods for calculating the modal properties must be used.

REFERENCES

1. Stewart, W.J.: "Simplified parameter-based analysis of single-mode optical guides", *Electron. Lett.* 16, 380-382 (1980).

2. Gambling, W.A., Matsumura, H., Ragdale, C.M.: "Wave propagation in a single-mode fibre with dip in the refractive index", *Opt. & Quantum Electron.* 10, 301-309 (1978).

3. Gambling, W.A., Payne, D.N., Hammond, C.R., Norman, S.R.: "Optical fibres based on phosphosilicate glass", *Proc. I.E.E.* 123, 570-576 (1976).

4. Hussey, C.D., Pask, C.: "Characterization and design of single mode fibres", *Opt. & Quantum Electron.*

5. Richards, P,I.: *Manual of Mathematical Physics* (Pergamon, 1959), pp.286-289.

6. Papoulis, A.: *Systems and Transforms with Applications in Optics* (McGraw-Hill, 1968), Chap. 5.

7. Okoshi, T., Hotate, K.: "Refractive-index profile of an optical fiber: its measurement by the scattering pattern method", *Appl. Opt.* 15, 2756-2764 (1976).

8. Brinkmeyer, E.: "Spot size of graded-index single-mode fibers: profile independent representation and new determination method", *Appl. Opt.* 18, 932-937 (1979).

9. Snyder, A.W., Young, W.R.: "Modes of optical waveguides", *J. Opt. Soc. Am.* 68, 297-309 (1978).

10. Snyder, A.W.: "Understanding monomode optical fibers", *Proc. I.E.E.E.* 69, 6-13 (1981).

11. Abramowitz, M., Stegun, I.A.: *Handbook of Mathematical Functions* (NBS, Washington DC, 1980), Section 9.

12. Gambling, W.A., Matsumura, H., Ragdale, C.M.: "Mode dispersion, material dispersion and profile dispersion in graded-index single-mode fibres", *I.E.E. Microwaves, Opt. & Antennas* 3, 239-246 (1979).

13. Marcuse, D.: "Interdependence of waveguide and material dispersions", *Appl. Opt.* 18, 2930-2932 (1979).

14. Sigumura, A., Daikoku, K., Imoto, N., Miya, T.: "Wavelength dispersion characteristics of single-mode fibers in low-loss region", *I.E.E.E. J. Quantum Electron.* QE-16, 215-225 (1970).

15. Petermann, K.: "Fundamental mode microbending loss in graded-index and W-fibres", *Opt. & Quantum Electron.* 9, 167-175 (1977).

16. Gambling, W.A., Matsumura, H.: "Simple characterisation factor for practical single-mode fibres", *Electron. Lett.* 13, 691-693 (1977).

17. Snyder, A.W.: "Leaky-ray theory of optical waveguides of circular cross-sections", *Appl. Phys.* 4, 273-298 (1974).

18. Cohen, L.G., Mammel, W.L., Presby, H.M.: "Correlation between numerical predictions and measurements of single mode fiber dispersion characteristics", *Appl. Opt.* 19, 2007-2010 (1980).

19. Imoto, N., Kawana, A., Machida, S., Tsuchiya, H.: "Characteristics of dispersion free single-mode fiber in the 1.5 μm wavelength region", *I.E.E.E. J. Quantum Electron.* QE-16, 1052-1058 (1980).

20. Marcuse, D.: "Loss analysis of single-mode fiber splices", *Bell Sys. Tech. J.* 56, 703-718 (1977).

21. Pask, C., Snyder, A.W., Mitchell, D.J.: "Number of modes on optical waveguides", *J. Opt. Soc. Am.* 65, 356-357 (1975).

22. Pask, C.: "Equal excitation of all modes on an optical fiber", *J. Opt. Soc. Am.* 68, 572-576 (1978).

23. Simon, B.: "The bound state of weakly coupled Schrödinger operators in one and two dimensions", *Annals of Phys.* 97, 279-288 (1976).

24. Sammut, R.A.: "Range of monomode operation of W-fibres", *Opt. & Quantum Electron.* 10, 509-514 (1978).

25. Kumar, A., Chandra, R., Sammut, R.A., Ghatak, A.K.: "Cutoff frequencies of a parabolic-core W-type fibre", *Electron. Lett.* 14, 676-678 (1978).

26. Korn, G.A., Korn, T.M.: *Mathematical Handbook for Scientists and Engineers* (McGraw-Hill, New York, 1968), Section 4.7.

27. Landau, L.D., Lifshitz, E.M.: *Quantum Mechanics* (Pergamon Press, Oxford, 1965), Second Edition, Section 45, Problem 2.

28. Rudolph, H.D., Neumann, E.G.: "Approximations for the eigenvalues of the fundamental mode of a step index fiber waveguide", *Nachrichtentech Z.* 4, 328-329 (1976).

29. Snyder, A.W., Sammut, R.A.: "Fundamental (HE_{11}) modes of graded optical fibers", *J. Opt. Soc. Am.* 69, 1663-1671 (1979).

30. Marcuse, D., Presby, H.M.: "Effects of profile deformations on fiber bandwidth", *Appl. Opt.* 18, 3758-3763 (1979).

31. Sammut, R.A., Hussey, C.D., Love, J.D., Snyder, A.W.: "Modal analysis of polarization effects in weakly guiding fibres", *I.E.E. Proc. Part H* 128, 173-187 (1981).

32. Gambling, W.A., Matsumura, H., Ragdale, C.M.: "Zero mode dispersion in single mode fibres", *Electron. Lett.* 14, 618-620 (1978).

33. Katsuyama, Y.: "Single mode propagation in 2-mode region of optical fibre by using mode filter", *Electron. Lett.* 15, 442-444 (1979).

34. Hussey, C.D., Pask, C.: "Waveguide dispersion in single mode fibers with on-axis dips", *J. Opt. Soc. Am.*

CHAPTER 7

FIBRE DESIGN BY THE MOMENT METHOD

PREAMBLE

In this chapter we consider the application of the moment description of single mode fibres in some design examples. We relate the moments Ω_0, Ω_2, Ω_4 to experimentally-measurable quantities. Thus only a few parameters need be measured and simple formulae result for calculating microbending loss and dispersion in arbitrary fibres. These formulae are used to discuss various fibre design criteria. The use of preform data and the theoretical description of the preform-to-fibre process are considered. The method presented is compared with the equivalent step methods which were described in Chapter 5.

7.1 INTRODUCTION

Previous methods of studying single mode optical fibres, as we described in Chapter 5, have been based on specifying a particular refractive index profile [1-3], or class of profile such as the power laws [1,2], and then calculating their propagation properties using some form of exact numerical method for solving eigenvalue equations. The results are presented as series of curves which can be used to design fibres if the restricted class of profiles is used. In Chapter 6 [4,5] we presented a theory which applies to arbitrary profiles, characterizing them by only two or three parameters, and we gave

results as simple formulae which were used to draw qualitative, general conclusions about propagation in single mode fibres. In this chapter, we consider the design of single mode fibres and how these few profile parameters might be related to experiment. We are not aiming for the extreme theoretical accuracy which is possible when the exact refractive index profile is known. Rather we present a scheme which is generally valid while retaining accuracy of order one or two per cent for most quantities of interest [5] and provides a possible working basis for fibre design using only simple formulae.

Our approach then is to take the theoretical scheme developed in Chapter 6 and show how to implement it in practice, working on the premise that that scheme is adequate and sufficiently accurate for practical purposes. The two major steps in Chapter 6 are the description of waveguide properties in terms of the averaged or effective waveguide parameter $\bar{V}$ [6,7]

$$\bar{V} = k\left(2\int_0^\infty [n^2(r) - n_{cl}^2]\, r dr\right)^{\frac{1}{2}} \tag{1}$$

instead of the usual parameter

$$V = k\,\rho(n_o^2 - n_{cl}^2)^{\frac{1}{2}}, \tag{2}$$

and the specification of profiles in terms of two or three of their moments. In Eqs. (1) and (2), $k = 2\pi/\lambda$, where λ is wavelength in vacuum, $n(r)$ is the fibre refractive index which becomes equal to n_{cl} in the cladding, n_o is the maximum value of $n(r)$, and ρ is the core radius.

The second waveguide mode enters at the cutoff point $V = V_{co}$, or $\bar{V} = \bar{V}_{co}$, and to a very good approximation [5,6]

$$\bar{V}_{co} \simeq 2.405\,, \tag{3}$$

so that $\bar{V} \leq 2.405$ can be taken as defining our working single mode region (see the Conclusion). In passing, we note that normalizing V by V_{co} is equivalent to using $\bar{V}$ if Eq. (3) holds, since $V/V_{co} \simeq \bar{V}/2.405$, and plots of waveguide behaviour versus V/V_{co} were actually given for some specific profiles in [3,8,9].

The profile moments which we require in order to calculate waveguide properties are related to directly measurable refractive index properties in section 2. We thus isolate a few features of the fibre refractive index and in section 3 we consider the use of experiments on fibres and preforms for giving this basic data. The preform is relatively large and easy to experiment on, but we may need to account for the manufacturing process if we use preform data to describe the resulting fibres. Because we have reduced the problem to a few key parameters, there is some hope of including the manufacturing effects by simply modifying the preform parameter values. Similarly, we can estimate the effects of measurement errors on our method since only a few parameters and simple relationships are used — see section 4. We are then ready to suggest design procedures in section 5. We can manipulate our simple formalism so that such properties as zero total dispersion, second mode cutoff or particular modal spot size, and hence microbending loss, can be obtained at a given wavelength by arranging fabrication to produce our refractive index specification parameters. We emphasize that the manufacturer is not being ordered to produce a profile of some specific form, as in [1,2] for example, but to arrange that the profiles being produced comply with the general parameter specification.

The scheme in Chapter 6 [4,5] can be interpreted also in terms of an equivalent step fibre, as we explain in section 6, where we examine

how the moment method fits into recent attempts at producing equivalent steps as we reviewed in Chapter 5.

After the Conclusion, section 7, some useful analytical and numerical data for the step index fibre is given in an Appendix.

7.2 FORMALISM

Physical quantities relate to the refractive index through $n^2(r) - n_{cl}^2$ so we introduce the moments

$$N_m = \int_0^\infty [n^2(r) - n_{cl}^2]\ r^{m+1}\ dr \tag{4a}$$

and the normalized forms

$$\bar{N}_m = N_m/N_0 . \tag{4b}$$

The even moments $N_0, N_2, N_4, N_6, \ldots$ suffice for defining $n^2(r)$ completely since it only refers to $r \geq 0$, but in fact from Chapter 6 we know that we only require the first three of these moments. Note that N_0 is incorporated into the effective waveguide parameter, Eq. (1),

$$\bar{V} = k(2N_0)^{\frac{1}{2}} . \tag{5}$$

In Chapter 6 the refractive index profile $s(r/\rho)$ was defined by

$$\begin{aligned} n^2 &= n_{cl}^2 + (n_o^2 - n_{cl}^2)\ s(r/\rho) \\ &= n_{cl}^2[1 + 2\Delta\ s(r/\rho)] , \qquad r \leq \rho , \end{aligned} \tag{6}$$

where $\Delta \equiv (n_o^2 - n_{cl}^2)/2n_{cl}^2$ is as in [1]. The moments Ω_m of s,

$$\Omega_m = \int_0^1 s(R)\ R^{m+1}\ dR \tag{7}$$

as used in Chapter 6 can be converted into N_m terms by Eqs. (4) and (6).

In order to implement the moment scheme we require, apart from $\bar{V}$, the parameters

$$P_1 = N_0/\bar{N}_2 \tag{8}$$

$$P_2 = 2N_0/(3\bar{N}_4)^{\frac{1}{2}} \tag{9}$$

and

$$x = 1 - P_2/P_1 \ . \tag{10}$$

When pulse dispersion is discussed the parameter Δ is involved and we define

$$p_1 = P_1/2n_{cl}^2\Delta = \Omega_0/\bar{\Omega}_2 \tag{11}$$

$$p_2 = P_2/2n_{cl}^2\Delta = 2\Omega_0/(3\bar{\Omega}_4)^{\frac{1}{2}} \ . \tag{12}$$

Note that $p_1 = 1$ for the step index fibre and p_1, p_2 depend only on the profile shape function — see Eqs. (6) and (7). We know from Chapter 6 that for reasonable profiles of interest the moment values lead to $0.7 \lesssim p_1 \leq 1$.

The formulae to be used are listed below. They are in terms of the step fibre properties and the relevant numerical data and analytic expressions are collected together in the Appendix. The accuracy of the formulae is dealt with in detail in Chapter 6 [5].

7.2.1 Modal Field and Microbending

The most important quantity here is the field spot size ω which is given to an accuracy of $\sim$ 1% or better in cases of interest, see Table 6.2, by

$$\left(\frac{\omega}{\rho}\right) \simeq (2\bar{\Omega}_2)^{\frac{1}{2}} \left(\frac{\omega}{\rho}\right)_{st,\bar{V}} , \tag{13}$$

where the subscript $st,\bar{V}$ means the step index fibre formula with $V = \bar{V}$. We concentrate on the influence of spot size on loss through microbending, in which case ω is as defined in [10] and the loss increases as L_{mb} increase where

$$L_{mb} \equiv k\omega = k\rho(\omega/\rho) \ . \tag{14}$$

In terms of our parameters, Eqs. (5) and (8) and Eq. (13),

$$L_{mb} \simeq \frac{1}{\sqrt{P_1}} \bar{V}\left(\frac{\omega}{\rho}\right)_{st,\bar{V}} . \tag{15}$$

Figure 1 shows the $\bar{V}$ dependence of L_{mb} and we note that there is a minimum at

$$\bar{V} = \bar{V}_{mb} \simeq 2.03 . \tag{16}$$

Thus microbending loss is minimized by operating at $\bar{V} = \bar{V}_{mb}$.

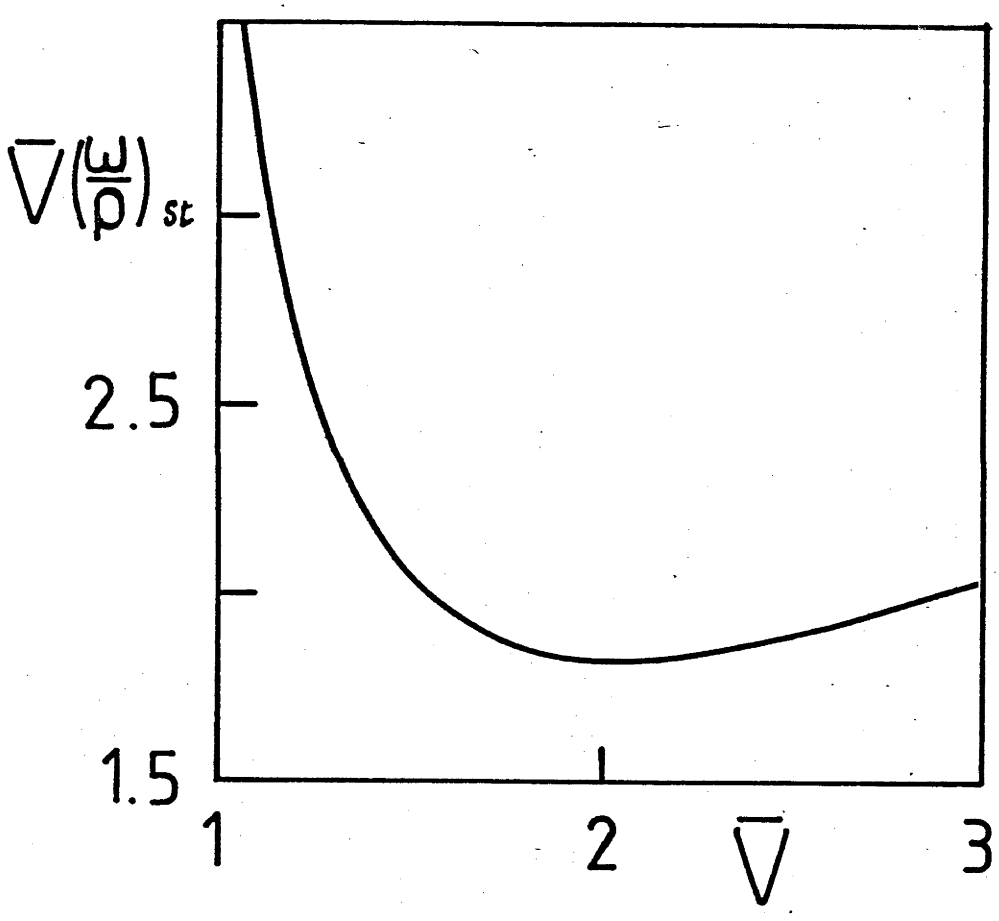

Fig. 1: Graph of $\bar{V}(\omega/\rho)_{st,\bar{V}}$. This indicates the $\bar{V}$ dependence of the parameter L_{mb}, Eq. (15), which controls the microbending loss.

7.2.2 Pulse Dispersion

In order to completely describe pulse dispersion, including material dispersion effects, we need to know [1,3] the parameters

$$b = \frac{W^2}{V^2}, \qquad b_1 = \frac{d(bV)}{dV}, \qquad b_2 = \frac{Vdb_1}{dV}, \tag{17}$$

where W is the modal eigenvalue. These are given for arbitrary fibres in Chapter 6 [4,5] and in terms of our parameters, Eqs. (5), (10)-(12),

$$b \simeq p_1\, b_{st}(\bar{V}), \qquad x \le 0 \tag{18a}$$

$$\simeq p_2\, b_{st}(\bar{V})\{1 + xU_{st}^2/4J_1^2(U_{st})\}, \qquad x > 0, \tag{18b}$$

where the subscript st denotes the step index fibre formula and $U_{st}^2 = \bar{V}^2 - W_{st}^2$. Then b_1 and b_2 follow by differentiation and are in terms of $b_{1st}(\bar{V})$, $b_{2st}(\bar{V})$ (see Appendix).

In many cases of practical interest $x < 0$ or $x \approx 0$ so that the simpler Eq. (18a) applies. In fact Eq. (18a) provides good accuracy in all cases except when extreme rounding occurs at the core-cladding boundary without an accompanying on-axis profile dip (see Table 6.1).

The total pulse dispersion T_{tot} per wavelength of source width is [1]

$$T_{tot} = T_{wd} + T_{cmd} + T_{cpd}, \tag{19}$$

where the terms are due to waveguide dispersion, composite material dispersion and composite profile dispersion. For the simple formula, Eq. (18a), we find

$$T_{wd} = \frac{n_{cl}\Delta}{c\lambda}\left(1 - \frac{\lambda}{n_{cl}}\, n'_{cl}\right)^2 p_1\, b_{2st}, \tag{20a}$$

$$T_{cmd} = \frac{\lambda}{c}\{\tfrac{1}{2}\, p_1 (b_{st} + b_{1st})(n_{cl}\Delta)'' + n''_{cl}\}, \tag{20b}$$

$$T_{cpd} = -\frac{n_{cl}}{c}\left(1 - \frac{\lambda}{n_{cl}}\, n'_{cl} - \frac{\lambda}{4\Delta}\,\Delta'\right)\Delta'\, p_1 (b_{2st} + b_{1st} - b_{st}), \tag{20c}$$

where c is the speed of light in vacuum and prime denotes differentiation with respect to λ. All the step index quantities are evaluated at $V = \bar{V}$. Recalling that $p_1 = 1$ for the step index fibre,

Eqs. (19) and (20) lead to

$$T_{tot} = p_1 \, T_{tot,st}(\lambda,\Delta,\bar{V}) + \frac{\lambda}{c} (1 - p_1) \, n''_{cl} \, . \tag{21}$$

Similar but slightly more involved formulae follow if the $x > 0$ result, Eq. (18b), is used.

7.3 REFRACTIVE INDEX DATA

The moments N_m are trivial to calculate when the refractive index profile $n(r)$ is given. The integrals in Eqs. (4a) and (7) are well behaved and a simple numerical method is adequate. Since weighted averages over $n(r)$ are being calculated there is also a data smoothing effect, errors in individual $n(r)$ values will cancel out and requirements of great accuracy in the input data would therefore be superfluous.

It would be advantageous to measure the moments N_m or Ω_m directly. For example, $f(\ell) \equiv \Omega_{\ell-2}$ is the Mellin transform [11] of $s(R)$, a measurement of which would give the moments for integer ℓ values. Although Mellin transforms are used in optical processing [12,13] they have not yet been used in profile measurements. However, the Hankel transform [11] is directly obtained when a fibre is illuminated transversely by a laser beam [8,14]. If $S(t)$ is the Hankel transform of $s(R)$, then [11]

$$S(t) = \sum_{m=0}^{\infty} \frac{(-1)^m}{(m!)^2} \Omega_{2m} \left(\frac{t}{2}\right)^{2m} \tag{22}$$

so that fitting S as a polynomial leads to coefficients giving the moments required. Alternatively, we note that

$$\left.\frac{d^{2m}S}{dt^{2m}}\right|_{t=0} = \frac{(-1)^m \, (2m)!}{(m!)^2 \, 2^{2m}} \Omega_{2m} \tag{23}$$

so that derivatives of S at $t = 0$ lead directly to the moments. Although this experiment has been successfully carried out [8,14] it requires elaborate equipment and extracting the moments may be inaccurate.

Rather than dwell on the above points, we wish to suggest a different approach and that is to use preform data. The advantages of this are that the preform is relatively large and easier to carry out measurements on than the fibre, and more importantly, there is still a stage left in fibre manufacturing, i.e. the drawing process, which can be used to obtain suitable fibre properties. This is elaborated on in detail in section 5. The disadvantages are that the preform-to-fibre process is not well documented and its details are dependent on the materials used in the glass. Nevertheless, we can make some basic assumptions which allow us to proceed and which can be modified or replaced when experimental tests are more complete.

The first assumption to make is that the fibre drawing process involves a simple scaling and we introduce a *first manufacturing parameter* m_1 by

$$m_1 = (\rho/\rho_p)^2 , \tag{24}$$

where ρ_p is the preform radius. Under a simple scaling

$$N_0 = m_1 N_{0p} \tag{25}$$

$$P_1 = P_{1p} \tag{26}$$

$$P_2 = P_{2p} \tag{27}$$

$$\Delta = \Delta_p , \tag{28}$$

where the subscript p refers to preform quantities.

It seems at first sight that the above assumption is unrealistic,

but in fact that need not be the case. Although the details of the profile and its irregular, distorted shape may change considerably during heating and diffusion processes, the gross parameters used in our theory are not greatly changed. Because N_0 is related to the degree of guidance and the total amount of material used to form the profile [5,6], Eq. (25) should always hold. The profile height parameter Δ may vary a little, although its exact definition may be difficult in practice where only small changes are recorded after the drawing process, e.g. [15]. Note also that when dispersion is considered, Eqs. (20) and (12) show that the time spread depends only on the ratios Δ'/Δ and Δ''/Δ and the moments-only parameters P_1 and P_2 of Eqs. (8) and (9). This leaves the moments N_2 and N_4, or $\bar{N}_2$ and $\bar{N}_4$, to be discussed.

At this point the examples in Fig. 2 may be enlightening. They show various perturbations superimposed on a step profile and in each case N_0, N_2 and N_4 are equal to the step profile values. Equally well the perturbations could be superimposed on any profile to leave its moments unchanged. These examples illustrate the point that profiles can appear to differ greatly before and after smoothing, but in fact the gross or integrated properties such as the moments can remain constant. (Mathematically inclined readers will recognize that additions to the profile function $s(r/\rho)$, Eq. (6), in the form of sums of $P_\ell[1-2(r/\rho)^2]$, where P_ℓ is the Legendre polynomial [11], will leave Ω_m or N_m unchanged for $m < 2\ell$.).

The second assumption which we can make involves a description of the profile changing or smoothing process. One approach is to observe that fluctuations may be removed by filtering [16,17], i.e. we take the Fourier transform of the profile and then filter out the higher

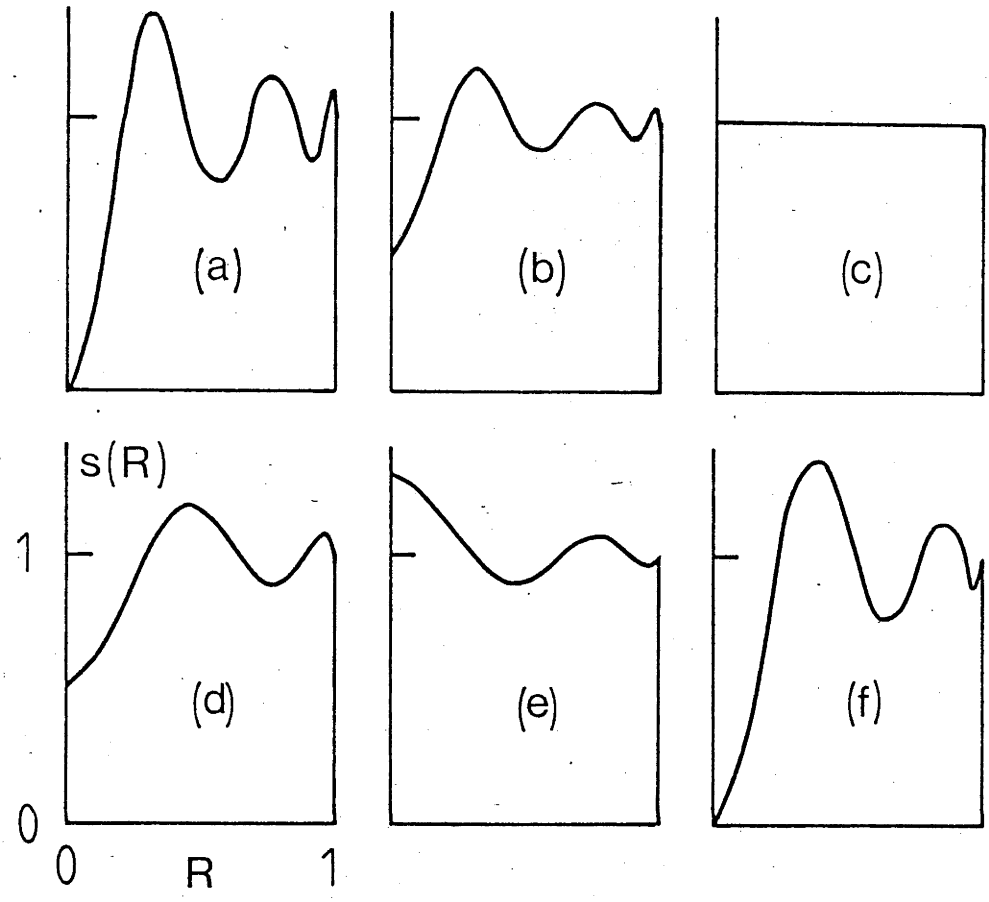

Fig. 2: Examples of refractive index profile shapes s(R), Eq. (6), showing fluctuations about the step profile which leave the moments N_0, N_2 and N_4 unchanged. The fluctuations in (a) are partially smoothed out in (b) and totally in (c). In (d) and (e) the distortion is of the same form but different magnitude and sign cases are illustrated.

frequency components. This approach has shown promise in certain examples, but the form of filter to be used needs further investigation. We can also achieve smoothing, and model the diffusion process, by using the convolution approach [16,17], which has the

advantage here that we can introduce a *second manufacturing parameter* m_2 to characterize the fibre drawing process. Letting $R = r/\rho$, the fibre profile n and preform profile after scaling n_{ps} are related by

$$n^2(R) - n_{cl}^2 = [n_{ps}^2 - n_{cl}^2] ** h , \tag{29}$$

where h(R) is the smoothing function and ** denotes the two-dimensional convolution [16,17]. If we insist that the amount of material involved remains constant, so that Eq. (25) holds, and define H_m to be the moments of h, then Eq. (29) links the fibre and preform moments according to

$$N_2 = m_1^2 (N_{2p} + H_2 N_0) \tag{30a}$$

$$N_4 = m_1^3 (N_{4p} + H_4 N_0 + 4H_2 N_{2p}) , \tag{30b}$$

where m_1 is the scaling parameter in Eqs. (24) and (25). The smaller the amount of the smoothing, the more peaked h(r) becomes and the more rapidly its moments H_m decrease as m increases. As a first approximation to this process we retain only H_2 which we define to be the second manufacturing parameter m_2. In this case the moment parameters P_1 and P_2 (Eqs. 8 and 9) become

$$P_1 = \frac{N_{op}}{\bar{N}_{2p} + m_2} \tag{31a}$$

$$P_2 = \frac{2N_{op}}{[3(\bar{N}_{4p} + 4m_2\bar{N}_{2p})]^{\frac{1}{2}}} \tag{31b}$$

or

$$\frac{1}{P_1} = \frac{1}{P_{1p}} + \frac{m_2}{N_{op}} \tag{32a}$$

$$\frac{1}{P_2^2} = \frac{1}{P_{2p}^2} + \frac{3m_2}{N_{op}} \frac{1}{P_{1p}} , \tag{32b}$$

where as usual the subscript p indicates the quantity for the preform.

7.4 ERROR ANALYSIS

In section 2 we have isolated a few necessary fibre parameters and shown how they can be used to calculate modal parameters. The relative simplicity of this scheme allows the effects of experimental errors in the fibre data to be assessed for the required waveguide parameters. We assume errors dP_1 and dN_0 in P_1 and N_0 and then the resultant errors in the calculated values of L_{mb}, Eq. (15), and the propagation parameters, Eqs. (17) and (18a), are

$$\left(\frac{dL_{mb}}{L_{mb}}\right) = -\frac{1}{2}\left(\frac{dP_1}{P_1}\right) + \left(\frac{1}{2} + \frac{\bar{V}}{2}\frac{d}{d\bar{V}}\left(\frac{\omega}{\rho}\right)_{st,\bar{V}} \Big/ \left(\frac{\omega}{\rho}\right)_{st,\bar{V}}\right)\left(\frac{dN_0}{N_0}\right)$$

$$\equiv -\frac{1}{2}\left(\frac{dP_1}{P_1}\right) + E_L\left(\frac{dN_0}{N_0}\right) \tag{33a}$$

$$\left(\frac{db}{b}\right) = \left(\frac{dP_1}{P_1}\right) + \left(\frac{b_{1st}}{2b_{st}} - \frac{1}{2}\right)\left(\frac{dN_0}{N_0}\right)$$

$$\equiv \left(\frac{dP_1}{P_1}\right) + E_b\left(\frac{dN_0}{N_0}\right) \tag{33b}$$

$$\left(\frac{db_1}{b_1}\right) = \left(\frac{dP_1}{P_1}\right) + \left(\frac{b_{2st}}{2b_{1st}}\right)\left(\frac{dN_0}{N_0}\right)$$

$$\equiv \left(\frac{dP_1}{P_1}\right) + E_1\left(\frac{dN_0}{N_0}\right) \tag{33c}$$

$$\left(\frac{db_2}{b_2}\right) = \left(\frac{dP_1}{P_1}\right) + \left(\frac{\bar{V}}{2b_{2st}}\frac{db_{2st}}{d\bar{V}}\right)\left(\frac{dN_0}{N_0}\right)$$

$$\equiv \left(\frac{dP_1}{P_1}\right) + E_2\left(\frac{dN_0}{N_0}\right). \tag{33d}$$

Thus the percentage error due to the error in P_1 is half the percentage error in P_1 for L_{mb} and equal to the percentage error in P_1 for b, b_1 and b_2. The dependence on N_0 is slightly more involved and depends on $\bar{V}$, but the percentage errors in the calculated quantities are always of the same order as or smaller than those in the measured values of N_0. More specifically, at $\bar{V} = 1.8$, 2 and 2.4 the error

proportionality constants are

$$E_L = .44,\ .45,\ .46 \tag{34a}$$

$$E_b = 1.0,\ 0.8,\ 0.6 \tag{34b}$$

$$E_1 = 0.4,\ 0.3,\ 0.1 \tag{34c}$$

$$E_2 = -0.16,\ -0.2,\ -0.3\ . \tag{34d}$$

7.5 FIBRE DESIGN

The formulae arrived at in section 3 allow us to devise a general design scheme independent of exact profile specification since only a few basic parameters are involved. We assume that the source is fixed so that wavelength λ is given. For the purposes of introducing the approach of this chapter we consider the simplest design scheme: the fibre is specified by its first moment N_0, or $\bar{V}$, and P_1, or p_1 (Eqs. (1), (5), (8) and (11)); the preform-to-fibre manufacturing process follows Eqs. (24)-(28) so that m_1 is the manufacturing parameter; and the fibre propagation properties $\bar{V}_{co}$, L_{mb}, $\bar{V}_{mb}$ and dispersion T are given by Eqs. (3), (15), (16) and (21).

This leaves us with two classes of design problems: the preform is made, but the drawing process can be used to give m_1 leading to suitable propagation requirements; the fibre parameters N_0 and P_1 or p_1 can be fitted to optimize two aspects of propagation behaviour.

7.5.1 Choosing m_1 when the Preform is Given

In this case N_{op} and P_1 are given, but m_1 may be arranged to give a suitable fibre first moment N_0 according to Eq. (25). This in turn means that we can choose the operating $\bar{V} = \bar{V}_{op}$, say, by Eq. (5). Thus, given λ and a preform with first moment N_{op}, in order to operate at

$\bar{V}_{op}$ Eqs. (5) and (25) require the manufacturing parameter m_1 to satisfy

$$m_1 = 8\pi^2\lambda^2\bar{V}_{op}^2/N_{op} . \tag{35}$$

Eq. (35) tells us how to arrange $\bar{V} = \bar{V}_{op}$ for any kind of profile and our other formulae suggest how to choose $\bar{V}_{op}$. If we are satisfied with the generally good bandwidths which single mode fibres automatically provide, then we can optimize other factors. The theory in section 2.1 indicates that setting $\bar{V}_{op} = 2.03$ will minimize the effects of microbending losses. If we require large fibre radius ρ for ease of handling and jointing, then for a given preform radius ρ_p Eq. (24) says that m_1 should be made as large as possible. This is achieved by substituting the largest possible value of $\bar{V}_{op}$ into Eq. (35) and in order to remain single-moded, the largest $\bar{V}$ value for any type of fibre is $\bar{V}_{co} \simeq 2.405$ (Eq. 3).

If bandwidth is at a premium, then the prime consideration will be to reduce pulse dispersion. In order to do this we use Eq. (21) to obtain $\bar{V}_{op}$ so that $T_{tot} = 0$, and then

$$T_{tot,st}(\lambda,\Delta,\bar{V}_{op}) = \frac{\lambda}{c}\left(1 - \frac{1}{p_1}\right) n''_{cl} . \tag{36}$$

For given materials data, source wavelength and preform, we solve Eq. (36) for $\bar{V}_{op}$ and arrange the manufacturing parameter by Eq. (35).

Eq. (36) is straightforward to solve as $T_{tot,st}$ is a well known function, e.g. [1]. As an example, we take the data given in [1] and assume sources at $\lambda = 1.4$ μm and 1.5 μm. The right hand side of Eq. (36) requires $\lambda n''_{cl}/c$ which is given in [1,18] and $T_{tot,st}$ is calculated for the germanosilicate glass as in [1]. Reading the results from curves, we find for two fibres with $p_1 = 0.9$ or 0.8,

$$\bar{V}_{op} \simeq 1.97 \quad \text{for } \lambda = 1.5\ \mu m,\ p_1 = 0.9, \tag{37a}$$

$$\simeq 2.32 \quad \text{for } \lambda = 1.4\ \mu m,\ p_1 = 0.9, \tag{37b}$$

$$\simeq 1.90 \quad \text{for } \lambda = 1.5\ \mu m,\ p_1 = 0.8, \tag{37c}$$

$$\simeq 2.26 \quad \text{for } \lambda = 1.4\ \mu m,\ p_1 = 0.8. \tag{37d}$$

The parameter $p_1 \leq 1$ and practical fibres would usually have p_1 around 0.8 or 0.9 [5].

7.5.2 Two Parameter Designs

We now assume that fibre parameters N_0 and p_1, or P_1, are free to be chosen (so that the preform must be constructed with $N_{op} = N_0/m_1$ and the same p_1). For any given wavelength this means that $\bar{V}$ (by Eq. 5) and p_1 may be specified. We could choose both these parameters to reduce microbending as much as possible by using Eq. (15). However, a more interesting case is to say we wish to have T_{tot} zero and also specify the operating point. Thus $\bar{V}$ and p_1 are given by

$$\bar{V} = \bar{V}_{op} \tag{38}$$

$$T_{tot,st}(\lambda,\Delta,\bar{V}_{op}) = \left(1 - \frac{1}{p_1}\right) \frac{\lambda}{c}\, n''_{cl}\ . \tag{39}$$

Eq. (39) (which follows from Eq. 21) gives p_1 and Eqs. (38) and (5) give N_0 as the required values for the fibre to be constructed.

As an example, suppose we choose to maximize core size by setting $\bar{V}_{op} = \bar{V}_{co}$ as discussed in section 2. Then for a given λ,

$$N_0 = \bar{V}^2_{co}\lambda^2/8\pi^2 = 0.073\ \lambda^2\ . \tag{40}$$

To find p_1 we next solve Eq. (39) with $\bar{V}_{op} = \bar{V}_{co} \simeq 2.405$. (We must point out here that the basic Eq. (21) is more prone to error for near cutoff $\bar{V}$ values especially if used with shoulder type profiles (see Table 6.1), but this is a simple example and does lead to an

interesting general point.) Assume that we have a source with wavelength around 1.35 μm, then for the germanosilicate core-silica cladding fibre described in [1], we can solve Eq. (39) to get

$$p_1 \simeq 0.73,\ 0.82,\ 0.91 \text{ and } 0.99 \tag{41}$$

for $\lambda = 1.3$ μm, 1.37 μm, 1.38 μm and 1.39 μm, respectively. Notice that once material properties are fixed only a small spread of wavelengths can be accommodated by variations of p_1 likely to be found in practice (all the fibres, including some extreme cases, referred to in Fig. 6.4 for example have p_1 in this range). Indeed, the accuracy of our formalism must cast doubt on the lower p_1 values in Eq. (41), but what we have confirmed is that when operating at cutoff, the profile shape does not greatly influence the wavelength leading to zero dispersion, a conclusion clearly demonstrated in [1] for the class of power law profiles.

7.6 THE MOMENT METHOD AND EQUIVALENT STEPS

The moment method in the form applied in this chapter can be thought of as an equivalent step method [19-22] since the formulae we used here were derived in Chapter 6 using a particular step index fibre field to approximate the real fibre field (although of course the moment method in its more accurate or elaborate form builds on corrections to the first approximation formulae and goes beyond an equivalent step method — see Chapter 6 and Eq. (18), for example). It therefore seems appropriate to briefly review equivalent steps to see where the moment method fits in.

Six recently reported approaches to the equivalent step index fibre, as outlined in Chapter 5, are summarized in Table 1. In cases

Table 1. Summary of some approaches to the definition of an equivalent step index fibre.

Author	Method for Finding Equivalent Step Fibre	Comments
(A) Brinkmeyer (1979) [8,9]	Fit to V_{co} and first zero in diffraction pattern of transverse fibre illumination.	Original limitation to power law profiles
(B) Snyder & Sammut (1979) [19]	Step field used in variational calculations of modal eigen-value.	Full profile required. Equivalent step parameters vary with λ.
(C) Pask & Sammut (1980) [20]	Fit to modal far field half width and first zero.	Equivalent step parameters vary with λ.
(D) Matsumura & Suganuma (1980) [21]	Best fit to modal spot size over a range of V values.	Least squares numerical fit to be computed.
(E) Millar (1981) [22]	Fit to V_{co} and modal spot size at cutoff.	Uses simple formula for spot size. Mathematically simple but cutoff hard to define experimentally.
(F) Hussey & Pask (1981) [5] [Chapter 6]	Fit step profile to moments of given fibre profile.	Limited profile data required.

C, D and E various properties of the step index fibre modal field are matched to the same properties of the fibre to be characterized. In B and F the equivalent fibre is obtained directly from the profile. In B the full profile is used in a complex variational calculation giving highly accurate results in the cases tested [19], but a different equivalent step for each wavelength, whereas in F the limited profile data in the form of moments leads directly to one step fibre to be used at all wavelengths. Case A is a hybrid: the modal property V_{co} is used together with profile information in the form of the first zero of its Hankel transform, which follows from the side-on illumination of the fibre. Because of leaky mode behaviour of the second waveguide mode, it is not simple experimentally to define V_{co} and this militates against its use.

The equivalent step fibre in the simplest moment scheme has the same $\bar{V}$ as the fibre being characterized ("N_0 fitting") and a radius ρ_s defined by $\rho_s/\rho = (2\bar{\Omega}_2)^{\frac{1}{2}}$ ("$\bar{\Omega}_2$ fitting", see Eq. (34a) in [5]). The formulae derived on this basis are for cutoff, Eqs. (3) and (5), and spot size, Eq. (13), and these could be used to implement the Millar [22] approach, case E in Table 1. Thus the moment equivalent step could be viewed also from the point of view of fitting modal properties, although the context in which we use it is that involving profile data to be used in predicting fibre modal properties.

7.7 CONCLUSION

We reiterate the point that the aim of this chapter is to present some new ideas for dealing with arbitrary profile fibres and to speculate on their use in fibre characterization and design. Absolute accuracy has been traded for a few parameter, general approach which

can be easily manipulated. The questions which (we hope) the reader will inevitably ask will probably require an experimental viewpoint to complement the theoretical approach presented here. The theoretical scheme can always be made more accurate as the need arises. Experimental questions concern methods of finding $[n^2(r) - n_{cl}^2]$, or better still of measuring directly its moments or Mellin transform, the characterization of the preform-to-fibre process and the trial of design schemes.

This work has been limited to the single mode region, $\bar{V} \lesssim 2.405$, deliberately since the basic formalism of Chapter 6 breaks down in its simplest, few moment form as $\bar{V}$ becomes larger. It is recognized that fibres can be operated effectively single-moded for $2.4 < \bar{V} \lesssim 3$ [23,24], but the trend to longer wavelength sources means that many fibres are in fact being used with $\bar{V} \sim 2$.

APPENDIX

FORMULAE AND NUMERICAL DATA FOR THE STEP INDEX FIBRE

The moment scheme in the form applied here enables properties of arbitrary fibres to be calculated once the step index fibre properties are known. For convenience, we gather together here the more useful analytical formulae for the step index fibre. Numerical data for these formulae and additional terms required by the moment scheme are presented in Table 2.

Table 2: Numerical data for the step parameters required by the moment scheme.

V	b	b_1	b_2	$\left(\frac{U}{J_1(U)}\right)^2$	$\left(\frac{\omega}{\rho}\right)$	η
1.0	.041	.302	1.346	5.109	4.140	.167
1.1	.071	.437	1.458	5.335	2.920	.255
1.2	.107	.564	1.440	5.568	2.239	.336
1.3	.146	.676	1.343	5.804	1.820	.411
1.4	.188	.771	1.209	6.041	1.544	.479
1.5	.230	.849	1.063	6.276	1.353	.539
1.6	.270	.913	.919	6.509	1.214	.592
1.7	.310	.965	.785	6.739	1.109	.637
1.8	.347	1.006	.664	6.964	1.028	.677
1.9	.383	1.039	.556	7.185	.965	.711
2.0	.416	1.065	.462	7.401	.913	.741
2.1	.448	1.085	.380	7.613	.871	.767
2.2	.477	1.102	.309	7.819	.835	.789
2.3	.504	1.114	.248	8.021	.806	.809
2.4	.530	1.124	.195	8.217	.780	.827
2.5	.554	1.131	.150	8.409	.758	.842
2.6	.576	1.136	.110	8.595	.739	.856
2.7	.597	1.139	.077	8.778	.722	.868
2.8	.616	1.141	.048	8.955	.707	.879
2.9	.635	1.143	.023	9.128	.694	.889
3.0	.651	1.143	.001	9.297	.682	.897

1. Spot Size (ω/ρ)

Using Petermann's definition of spot size [10] the following analytic formula is obtained [25]

$$\left(\frac{\omega}{\rho}\right)_{st} = \left(\frac{2}{3}\left(\frac{J_0(U)}{UJ_1(U)} + \frac{1}{2} + \frac{1}{W^2} - \frac{1}{U^2}\right)\right)^{\frac{1}{2}} . \tag{42}$$

An alternative definition of spot size corresponding to the spot size of an optimally exciting Gaussian beam can be expressed empirically,

to within a fraction of 1%, as follows [26]

$$\left(\frac{\omega}{\rho}\right)_{st} = (0.65 + 1.619\ V^{-3/2} + 2.879\ V^{-6})\ . \tag{43}$$

Note that some authors, e.g. [6,21,22] have an extra factor of 1/2 in their definition of Gaussians and for them the right hand side of Eq. (43) should be divided by $\sqrt{2}$.

2. Fraction of Power Propagating Within the Core (η) [27]:

$$\eta_{st} = 1 - \left(\frac{U}{VK_1(W)}\right)^2 [K_1^2(W) - K_0^2(W)] \tag{44a}$$

$$= \left(\frac{W}{VJ_1(U)}\right)^2 [J_1^2(U) + J_0^2(U)]\ . \tag{44b}$$

3. Dispersion Parameters [28]

$$b_{st} = W^2/V^2\ , \tag{45}$$

$$b_{1st} = 1 - \frac{U^2}{V^2}\left(1 - 2\ \frac{K_0^2(W)}{K_1^2(W)}\right), \tag{46}$$

$$b_{2st} = 2\ \frac{U^2}{V^2}\ \frac{K_0^2(W)}{K_1^2(W)}\left\{1 - 2\ \frac{K_0^2(W)}{K_1^2(W)} + \left(W + \frac{U^2}{W}\ \frac{K_0^2(W)}{K_1^2(W)}\right)\left(\frac{2}{W} - 2\ \frac{K_1(W)}{K_0(W)} + 2\ \frac{K_0(W)}{K_1(W)}\right)\right\}. \tag{47}$$

Graphs for b, b_{1st} and b_{2st} are given in [1]. The reader is cautioned that the graphs for b_{1st} and b_{2st} in [29] and [30] are wrong.

4. The Rudolph-Neumann Approximation [31]

$$W \simeq 1.1428\ V - 0.996\ . \tag{48}$$

This is the simplest expression for the eigenvalue of the step index fibre. It is very accurate, e.g. at V = 2 it has .05% error and at V = 2.4 it has .04% error. A discussion of the accuracy of using

the Rudolph-Neumann approximation in the analytic expressions for the dispersion parameters, Eqs. (45)-(47) is contained in [28].

REFERENCES

1. Gambling, W.A., Matsumura, H., Ragdale, C.M.: "Mode dispersion, material dispersion and profile dispersion in graded index single mode fibres", *I.E.E. Microwaves, Opt. & Antennas* 3, 239-246 (1979).

2. Paek, U.C., Peterson, G.E., Carnevale, A.: "Dispersionless single-mode lightguides with α index profiles", *Bell System Tech. J.* 60, 583-598 (1981).

3. Sugimara, A., Daikoku, K., Imota, N., Miya, T.: "Wavelength dispersion characteristics of single-mode fibres in low-loss region", *I.E.E.E.* QE-16, 215-225 (1980).

4. Hussey, C.D., Pask, C.: "Single mode fibres in a few moments", *Electron. Lett.* 17, 644-645 (1981).

5. Hussey, C.D., Pask, C.: "Theory of the profile moments description of single mode fibres", *I.E.E. Proc. Part H.*

6. Gambling, W.A., Matsumura, H., Ragdale, C.M.: "Wave propagation in a single mode fibre with dip in the refractive index", *Opt. & Quantum Electron.* 10, 301-309 (1978).

7. Stewart, W.J.: "Simplified parameter-based analysis of single mode optical guides", *Electron. Lett.* 16, 380-382 (1980).

8. Brinkmeyer, E.: "Spot size of graded-index single-mode fibers: profile independent representation and new determination method", *Appl. Opt.* 18, 932-937 (1979).

9. Brinkmeyer, E.: "Profile-independent representation of near- and far-field characteristics of single mode fibers and its use for the determination of fiber parameters", *Proc. Opt. Comm. Conf.* paper 17.2, Amsterdam (1979).

10. Petermann, K.: "Fundamental mode microbending loss in graded index and W-fibres", *Opt. & Quantum Electron.* 9, 167-175 (1977).

11. Korn, G.A., Korn, T.M.: *Mathematical Handbook for Scientists and Engineers* (McGraw-Hill, New York, 1968), Section 8.6.

12. Casasent, D., Psaltis, D.: "Scale invariant optical correlation using Mellin transforms", *Opt. Commun.* 17, 59-63 (1976).

13. Casasent, D., Psaltis, D.: "Scale invariant optical transform", *Opt. Engin.* 15, 258-261 (1976).

14. Okoshi, T., Hotate, K.: "Refractive-index profile of an optical fiber: its measurement by the scattering pattern method", *Appl. Opt.* 15, 2756-2764 (1976).

15. Saunders, M.J.: "Optical fiber profiles using the refracted near field technique: a comparison with other methods", *Appl. Opt.* 20, 1645-1651 (1981).

16. Bracewell, R.: *The Fourier Transform and Its Applications* (McGraw-Hill, New York, 1965).

17. Papoulis, A.: *Systems and Transforms with Applications in Optics* (McGraw-Hill, New York, 1968).

18. Payne, D.N., Gambling, W.A.: "Zero material dispersion in optical fibres", *Electron. Lett.* 11, 176-178 (1975).

19. Snyder, A.W., Sammut, R.A.: "Fundamental (HE_{11}) modes of graded optical fibers", *J. Opt. Soc. Am.* 69, 1663-1671 (1979).

20. Pask, C., Sammut, R.A.: "Experimental characterization of graded index single mode fibres", *Electron. Lett.* 16, 310-311 (1980).

21. Matsumura, H., Suganuma, T.: "Normalization of single-mode fibres having an arbitrary index profile", *Appl. Opt.* 19, 3151-3158 (1980).

22. Millar, C.A.: "Direct method of determining equivalent-step-index profiles for monomode fibres", *Electron. Lett.* 17, 458-460 (1981).

23. Gambling, W.A., Matsumura, H., Ragdale, C.M.: "Zero mode dispersion in single mode fibres", *Electron. Lett.* 14, 618-620 (1978).

24. Katsuyama, Y.: "Single mode propagation in 2-mode region of optical fibre by using mode filter", *Electron. Lett.* 15, 442-444 (1979).

25. Gambling, W.A., Matsumura, H.: "Simple characterization factor for practical single mode fibres", *Electron. Lett.* 13, 691-693 (1977).

26. Marcuse, D.: "Loss analysis of single-mode fiber splices", *Bell System Tech. J.* 56, 703-718 (1977).

27. Snyder, A.W.: "Asymptotic expressions for eigenfunctions and eigenvalues of a dielectric or optical waveguide", *I.E.E.E. Trans.* MTT-17, 1130-1138 (1969).

28. Huang, H., Wang, Z.: "An analytic approach to the prediction of dispersion properties of step-index single mode optical fibres", *Electron. Lett.* 17, 202-204 (1981).

29. Gloge, D.: "Dispersion in weakly guiding fibers", *Appl. Opt.* 10, 2442-2445 (1971).

30. Olshansky, R.: "Propagation in glass optical waveguides", *Rev. Mod. Phys.* 51, 341-367 (1979).

31. Rudolph, H.D., Neumann, E.G.: "Approximations for the eigenvalues of the fundamental mode of a step index glass fiber waveguide", *Nachrichtech. Z.* 4, 328-329 (1976).

CHAPTER 8

WAVEGUIDE DISPERSION AT $\bar{V} \simeq 3$

PREAMBLE

In this chapter we discuss a different moment scheme for examining the region $2.4 \leq \bar{V} \leq 3$. This is the region where the moment scheme developed in Chapter 6 breaks down. The method is applied to waveguide dispersion for the fundamental mode and results of widespread applicability are obtained. For step index fibres perturbed out to 0.4 of the fibre radius the dispersion behaviour is described in terms of two parameters encompassing all possible perturbations. It is argued that it is more appropriate to study waveguide dispersion at the point where the effective waveguide parameter $\bar{V} = 3$, rather than to concentrate on the point of zero dispersion.

8.1 INTRODUCTION

Many single mode optical fibres have refractive index profiles which are distorted around the fibre axis. In this chapter we characterize these profile perturbations using a new method which produces results independent of their detailed form. This method is again based on the moments of the perturbed profile but — unlike the methods of Chapters 6 and 7 — we now require the exact solution of a reference profile with the same extent of perturbation and the same moments. The approach is general, but initially we consider imperfect

step index fibres and our results encompass all possible perturbations contained in a specified region about the fibre axis. Other cases are discussed later. We focus on pulse dispersion to demonstrate our principles and suggest which dispersion parameters are most meaningful when comparing different fibres.

The modal group velocity in an optical fibre exhibits a wavelength dependence which leads to pulse dispersion proportional to the source spectral width. This fact has stimulated interest in the region where the fundamental mode's group velocity is relatively insensitive to wavelength [1-4]. The effects of material dispersion must finally be included [1-3], but here we concentrate on waveguide dispersion and its dependence on profile shape. To be more precise, consider a fibre with radius ρ, cladding index n_{cl}, maximum core index n_o and waveguide parameter

$$V = 2\pi\rho(n_o^2 - n_{cl}^2)^{\frac{1}{2}}/\lambda , \tag{1}$$

where λ is wavelength. Then, for a source of spectral width $\delta\lambda$, the pulse spread per unit length due to waveguide dispersion is as described in [2]

$$T = \delta\lambda\left(\frac{n_o - n_{cl}}{c\lambda}\right) V \frac{d^2(bV)}{dV^2} \tag{2a}$$

$$\equiv \delta\lambda\left(\frac{n_o - n_{cl}}{c\lambda}\right) b_2(V) . \tag{2b}$$

Profile shape determines the quantity of interest, $b_2(V)$, which was defined by Eq. (6.31) and is related to the modal propagation constant β through [2]

$$b = \rho^2(\beta^2 - 4\pi^2 n_{cl}^2/\lambda^2)/V^2 . \tag{3}$$

The values of b_2 for the fundamental mode are of special interest in the region $V \simeq 3$ where it has a zero for a step index fibre. Although

the second waveguide mode propagates in this region, it is highly susceptible to losses which make the guide effectively single moded in practice [5].

8.2 FIBRE PARAMETERIZATION

We define the profile shape function s(R) by

$$s(R) \equiv s(r/\rho) = [n^2(r) - n_{cl}^2]/(n_o^2 - n_{cl}^2) , \tag{4}$$

and the perturbed region is $0 \le R \le R_d$, so that

$$\begin{aligned} s(R) &= \text{arbitrary dips} && 0 \le R \le R_d , \\ &= 1 && R_d \le R \le 1 , \\ &= 0 && R \ge 1 . \end{aligned} \tag{5}$$

Rather than specify particular forms for s(R), we introduce its moments defined as in Chapter 6, by [6]

$$\Omega_m = \int_0^1 s(R)\, R^{m+1}\, dR . \tag{6}$$

Because s(R) is non-zero only in a restricted region, it is sufficient to give just the even moments Ω_0, Ω_2, Ω_4, ... in order to define s completely. Ω_0 is the degree of guidance defined in [7] and is related to the amount of material used to form the profile, while higher moments specify the profile shape.

For the fibres in question it is obvious from Eqs. (5) and (6) that

$$\Omega_m \simeq \Omega_{m,st} = 1/(m+2) , \qquad m > 2M , \tag{7}$$

where $\Omega_{m,st}$ are the step index fibre moments. The value of R_d fixes M so that *only* Ω_0, Ω_2, ..., Ω_{2M} *are needed to give a good working characterization of all profiles satisfying Eq. (5).* If exact equality is assumed in Eq. (7), an error of less than $100R_d^{m+2}$% is made.

In this chapter we chose $R_d = 0.4$ and then Ω_m differs from $\Omega_{m,st}$ by less than 0.41% for $m = 4$ and 0.066% for $m = 6$ for all profiles in question. *Therefore we conclude that only Ω_0 and Ω_2 need be given to quite accurately characterize any profile of the form in Eq. (5).*

When R_d and Ω_0 are given, we must have

$$\Omega_{2,min} \leq \Omega_2 \leq \Omega_{2,max} , \tag{8a}$$

where

$$\Omega_{2,max} = \Omega_0 (1 - \Omega_0) , \quad \Omega_{2,min} = \Omega_0^2 + (1 - R_d^2)(0.5 - \Omega_0) , \tag{8b}$$

and the profiles corresponding to the extreme values are shown in Fig. 1(c) and (d). Finally, then, we label our profiles by R_d (= 0.4) and Ω_0 and μ_2, $0 \leq \mu_2 \leq 1$,

$$\mu_2 = (\Omega_2 - \Omega_{2,min})/(\Omega_{2,max} - \Omega_{2,min}) . \tag{9}$$

To complete the fibre characterization, we must give V or the effective or averaged parameter

$$\bar{V} = V\sqrt{2\Omega_0} . \tag{10}$$

One advantage of the latter parameter is that certain results for the step index fibre become general when expressed in terms of $\bar{V}$; the second mode propagates for $\bar{V} \gtrsim 2.405$ and the effective single mode region may be taken as $\bar{V} \leq 3$ for all types of fibres, not just those with a step index profile [7]. (Note that $\Omega_0 = \frac{1}{2}$ and $\bar{V} = V$ for the step index fibre.) We take advantage of this generality and use $\bar{V}$, although profile dips do not greatly affect Ω_0 so that $\bar{V} \simeq V$ in these cases.

8.3 RESULTS

Before giving general results, consider the particular example of profiles as in Fig. 1(b) with $a = 0.4$. Results for b_2 are presented in

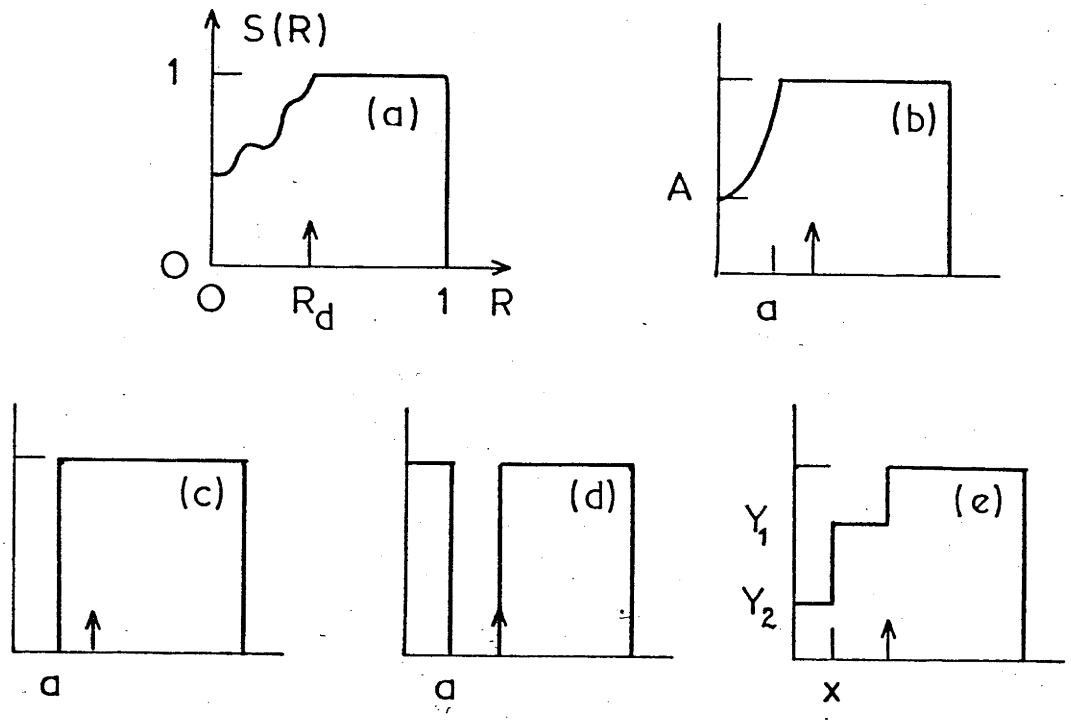

Fig. 1: Refractive index profiles. Eq. (4) defines s(R) where $R = r/\rho$ and ρ is fibre core radius. (a) Profiles are step index except for perturbations in $R \leq R_d$. (b) Parabolic dip, radius a, depth parameter A. The degree of guidance $\Omega_0 = (Aa^2 - a^2 + 2)/4$. (c) Square dip, radius a. This profile has $\Omega_2 = \Omega_{2,max}$, $\mu_2 = 1$ when $a^2 = 1 - 2\Omega_0$. (d) Profile giving $\Omega_2 = \Omega_{2,min}$, $\mu_2 = 0$, when $a^2 = R_d^2 + 2\Omega_0 - 1$. (e) Profile used for calculating general curves.

Fig. 2. Conventionally the value $\bar{V}_{zd}$ of $\bar{V}$ for which waveguide dispersion is zero, $b_2 = 0$, has been calculated. However, Fig. 2 demonstrates the point that small values of b_2 are present for profiles with wildly different $\bar{V}_{zd}$ values. We propose that $\bar{V} = 3$ is a useful reference or comparison point and consider b_2 at $V = 3$ as well as $\bar{V}_{zd}$.

We argued above that R_d, Ω_0 and Ω_2, or μ_2, are sufficient for parameterizing our fibres. *This implies that any convenient profile fitting* R_d, Ω_0 *and* μ_2 *values may be used to generate results which in fact will be valid to a good approximation for all possible profiles*

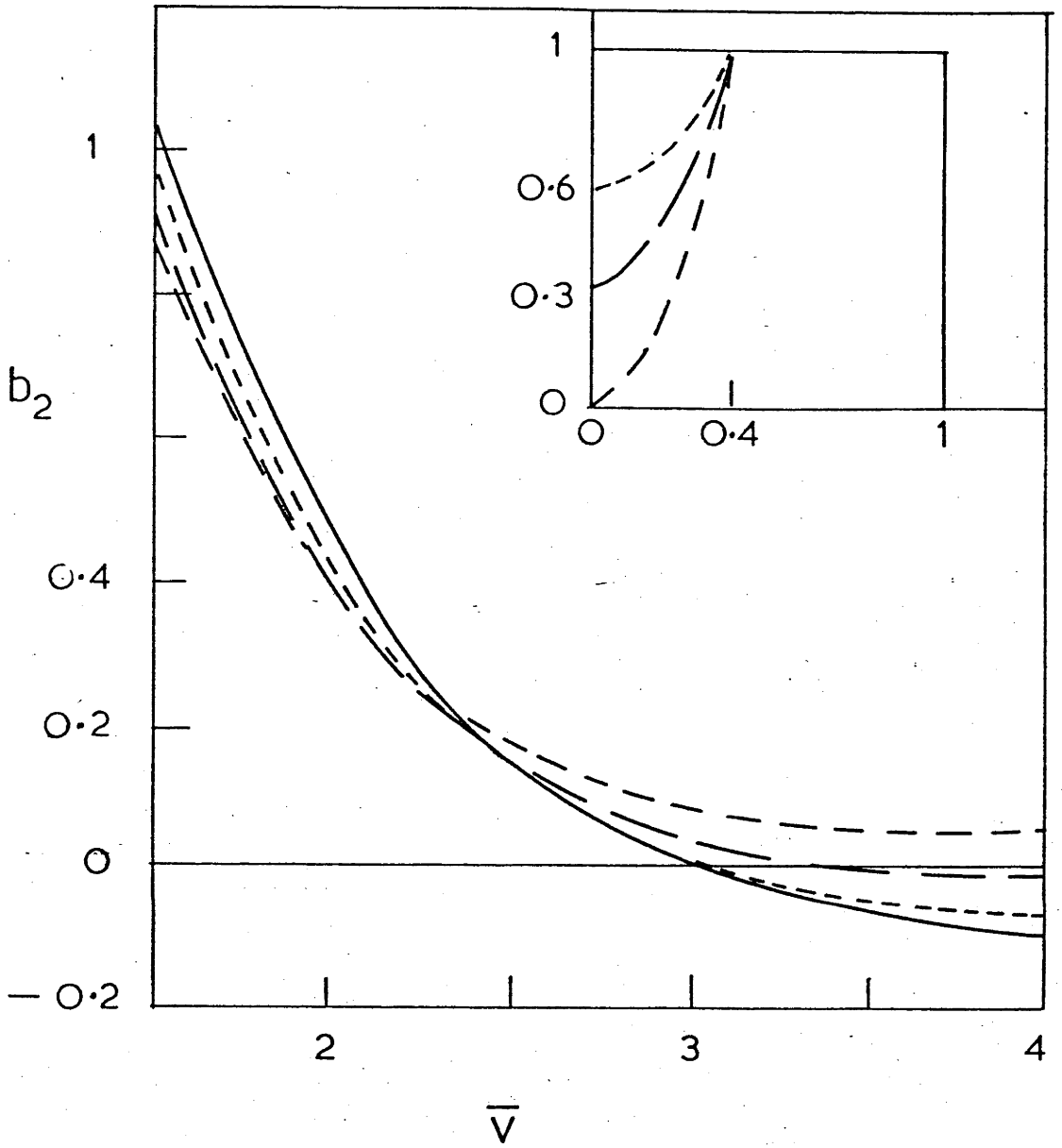

Fig. 2: Dispersion parameter b_2 vs. $\bar{V}$ for step index fibres with parabolic dips of width $R = 0.4$.

consistent with the given parameter values. To choose some sort of median for all these possible profiles, we note that, given R_d, Ω_0 and Ω_2, the next moment is also limited in range by $\Omega_{4,min} \leq \Omega_4 \leq \Omega_{4,max}$, and hence we use Ω_0, Ω_2 and $\Omega_4 = (\Omega_{4,min} + \Omega_{4,max})/2$ to calculate x, Y_1 and Y_2 in the profile of Fig. 1(e) which is then used to generate our

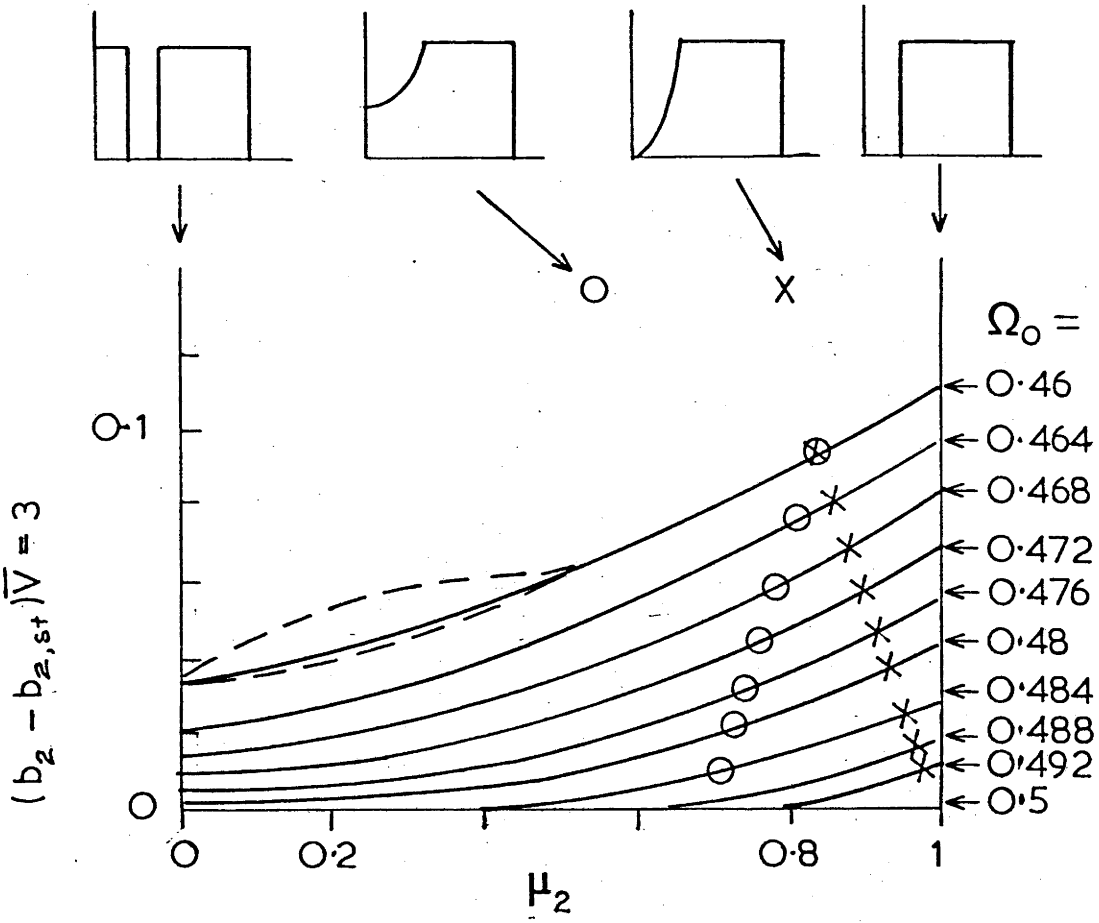

Fig. 3: Change in dispersion parameter b_2 from the step index value $b_{2,st}$ at $\bar{V} = 3$ vs. profile function normalized second moment μ_2. The curves are for fixed values of Ω_0 and can be used for any dips with $R_d \leq 0.4$. Special cases indicated are the extreme profiles having $\mu_2 = 0$ and 1 [see Fig. 1(c) and (d)], and parabolic dips of fixed width $R_d = 0.4$ and variable depth (the circles), or of fixed depth, $s(0) = 0$, and variable width (the crosses). The broken curves refer to profiles with $\Omega_0 = 0.46$ and extreme values for Ω_4.

results. (Note that the Ω_4 extremes depend only on Ω_0 and Ω_2 and we are taking $R_d = 0.4$.)

Figure 3 shows how b_2 at $\bar{V} = 3$ varies as a function of the shape parameter μ_2 for curves representing fixed Ω_0. These curves describe the behaviour of b_2 for all fibres perturbed in $0 \leq R \leq 0.4$ and with

$\Omega_0 \geq 0.46$. A parabolic shaped dip extending from the origin to $R = 0.4$ [$A = 0$, $a = 0.4$ in Fig. 1(b)] has $\Omega_0 = 0.46$. We observe that b_2 at $\bar{V} = 3$ increases as either μ_2 increases or Ω_0 decreases. These curves are relatively insensitive to the values of the higher moments Ω_4, Ω_6, ... as indicated by the dashed lines representing $\Omega_4 = \Omega_{4,max}$ and $\Omega_{4,min}$ for the $\Omega_0 = 0.46$ fibre. It should be noted that variations of b_2 with Ω_4 are associated with extreme and pathological profiles which are not really relevant in practice. The variation with Ω_4 decreases as Ω_0 increases. Thus we claim that Fig. 3 gives a good representation of the general behaviour of fibres.

For the reader who wishes to aid his appreciation of these results with some specific examples, we indicate in Fig. 3 the points referring to a square dip, and parabolic dips of fixed depth [$A = 0$, a varies in Fig. 1(b)] and fixed width [$a = 0.4$, A varies in Fig. 1(b)]. An increase in dip width or depth causes b_2 at $\bar{V} = 3$ to increase.

Figure 4 displays the variation of $\bar{V}_{zd}$ and in contrast to Fig. 3 we observe that the point of zero dispersion is highly dependent on profile parameters. Returning to Fig. 2, we see that for a parabolic dip of width 0.4, as the depth increases the b_2 vs. $\bar{V}$ curve shows a minimum around $\bar{V} \sim 4$, just touches the $\bar{V}$ axis and finally has no zero in the region of interest. This property of the b_2 vs. $\bar{V}$ curves is reflected in the abrupt ends to the curves in Fig. 4. The particular cases considered for Fig. 3 are also marked by the same symbols in Fig. 4.

The value of $\bar{V}_{zd}$ for smaller Ω_0 cases is quite sensitive to higher moments as the dashed lines in Fig. 4 show. However, we can say that $\bar{V}_{zd}$ increases as Ω_0 decreases or μ_2 increases. For a fixed Ω_0, the minimum value of $\bar{V}_{zd}$ occurs when $\mu_2 = 0$.

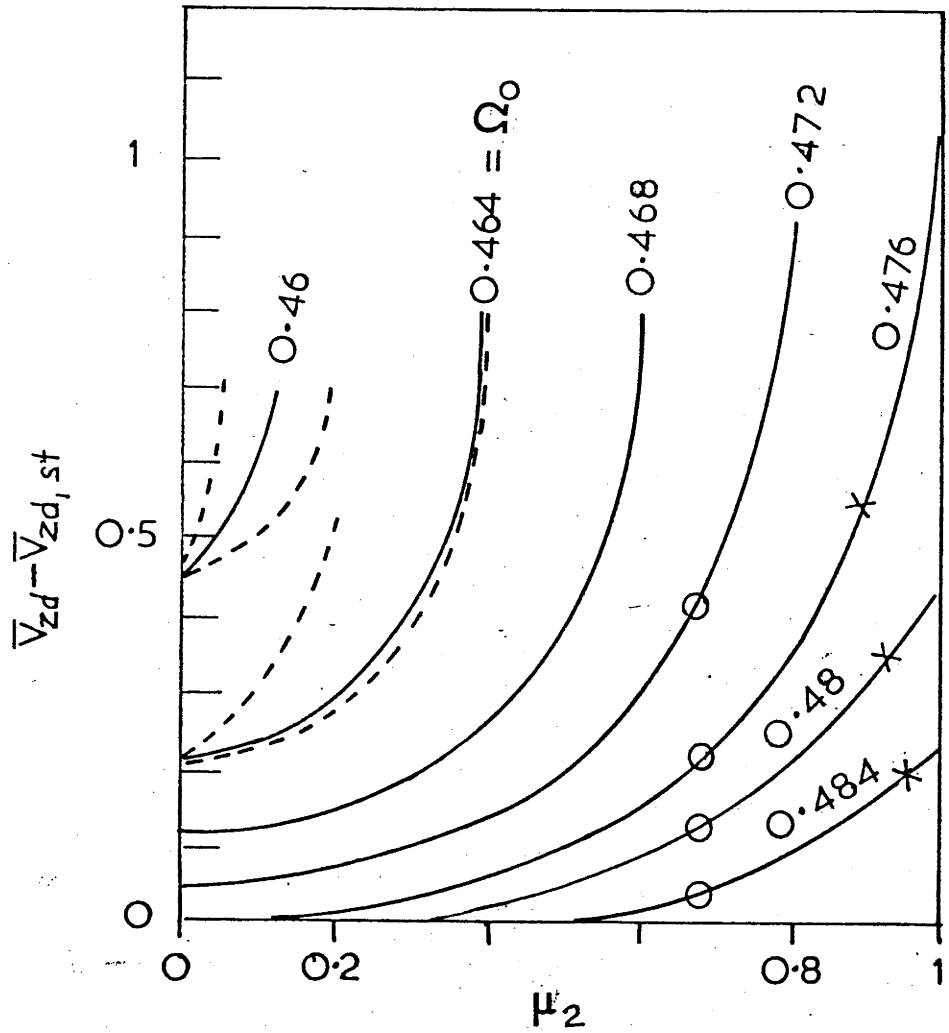

Fig. 4: Value $\bar{V}_{zd}$ of $\bar{V}$ for which $b_2 = 0$. The difference from $\bar{V}_{zd,st}$ is plotted vs. the profile function normalized second moment μ_2 with curves labelled by Ω_0 values. Circles and crosses are the special cases as in Fig. 3 and the broken curves refer to profiles with $\Omega_4 = \Omega_{4,max}$ or $\Omega_{4,min}$. Dip width $R_d = 0.4$.

8.4 CONCLUSION

The above arguments and numerical verifications lead to the conclusion that dips can be parameterized quite generally in terms of the moments Ω_0, which quantifies the total amount of material used to form the profile, and Ω_2, which is a shape related quantity. Figures 2, 3 and 4 strongly suggest that b_2 at $\bar{V} = 3$ is a more sensible

quantity to consider than $\bar{V}_{zd}$. The numerical results are obviously not exact for every conceivable profile, but they are highly accurate for most cases of interest and, probably more importantly, they demonstrate the effects of all dips on waveguide dispersion.

In this chapter we have chosen $R_d = 0.4$ and this embraces all fibres which would be obtained if a smaller value had been chosen. Clearly a similar program could be followed for a larger R_d, but the influence of Ω_4 and higher moments would grow as R_d is increased. Actually from practical considerations, $R_d = 0.4$ seems to be a reasonable choice.

We have also chosen the outer part of the profile, $R \geq R_d$, to be a step. Again the same type of program could be followed for any other form of perturbed profile, the difference being that $\Omega_{m,st}$ in Eq. (7) would be replaced by Ω_m for the new profile and the curve generating profile shown in Fig. 1(e) would be modified for $R \geq R_d$. The trends indicated in Figs. 3 and 4 are also found when there is rounding at the core-cladding boundary.

Because of its fundamental importance, we have chosen waveguide dispersion to illustrate the use and power of our fibre characterization method. However, the same approach could be followed for other quantities of interest, such as modal propagation constant or spot size, and general curves labelled by Ω_0 and μ_2 would apply.

REFERENCES

1. Gambling, W.A., Matsumura, H., Ragdale, C.M.: "Mode dispersion, material dispersion and profile dispersion in graded-index single-mode fibres", *I.E.E. Microwaves, Opt. & Antennas* 3, 239-246 (1979).

2. Marcuse, D.: "Interdependence of waveguide and material dispersions", *Appl. Opt.* 18, 2930-2932 (1979).

3. Sugimura, A., Daikoku, K., Imoto, N., Miya, T.: "Wavelength dispersion characteristics of single-mode fibers in low-loss region", *I.E.E.E. J. Quantum Electron.* QE-16, 215-255 (1980).

4. Snyder, A.W., Sammut, R.A.: "Dispersion in graded single-mode fibres, *Electron. Lett.* 15, 269-271 (1979).

5. Gambling, W.A., Matsumura, H., Ragdale, C.M.: "Zero mode dispersion in single mode fibres", *Electron. Lett.* 14, 618-620 (1978).

6. Hussey, C.D., Pask, C.: "Theory of profile moments description of single mode fibres", *I.E.E. Proc. Part H.*

7. Gamgling, W.A., Matsumura, H., Ragdale, C.M.: "Wave propagation in a single mode fibre with dip in the refractive index", *Opt. Quantum Electron.* 10, 301-309 (1978).

CHAPTER 9

RADIATION FROM GRADED INDEX OPTICAL FIBRES

PREAMBLE

In this chapter we take our first look at radiation from optical fibres. In particular we determine the radiation from tubular current sources with sinusoidal z dependence. We examine the effect of the presence of the perturbing graded index core on the free space (i.e. uniform cladding) radiation field of the fundamental HE_{11} mode. We approximate the radiation from the graded index monomode core to that of a step index with the same degree of guidance (i.e. the same Ω_0) for a given θ_c. We compare this and the W.K.B. approximation with the exact results for power law profiles.

9.1 INTRODUCTION

The weakly guiding optical fibre can be considered as a perturbing core embedded in a uniform cladding material. When solving radiation problems for weakly guiding fibres, Snyder has shown that it is more advantageous to use a direct Green's function type solution to Maxwell's equations [1] rather than the more conventional modal approach [2,3].

The advantage of Snyder's formalism, which we adopt here, is that the radiation field due to sources in weakly guiding fibres can be expressed in terms of a simple modification to the radiation field due to sources in free space.

For long distance communication purposes one is more interested in the order of magnitude of the radiation rather than a detailed description of the radiation pattern itself. For this reason we examine a simple equivalent step approximation and the W.K.B. asymptotic approximation for the graded index single mode fibre. These give excellent qualitative behaviour for all angles of radiation (although the W.K.B. method breaks down for on-axis radiation) and give exact quantitative results for large angles. The W.K.B. method can also be applied to multimode fibres.

9.2 THE MODIFICATION FACTOR FOR TUBULAR SOURCES WITH $\cos \ell\phi$ SYMMETRY

In the case of the tubular source described in Fig. 1, the Poynting vector can be written in terms of the free space Poynting vector as follows [1]

$$S = |C|^2 \, S^{FS} , \tag{1}$$

where C is the factor which corrects the free space radiation for the presence of the fibre.

We concentrate on fields of tubular sources since the fields of arbitrary sources can be synthesized from them [1].

9.2.1 The Step Profile

When the tubular source is in the core or on the core-cladding boundary (i.e. $R' \leq 1$, where $R = r/\rho$, ρ is the core radius and the prime denotes the position of the source) the correction factor C for the step index fibre is [1]

$$C(\theta) = J_\ell(UR') \, W_\ell(Q,Q)/J_\ell(QR') \, W_\ell(U,Q) \tag{2a}$$

$$\sim J_\ell(UR')/J_\ell(QR') \quad \text{when } U \cong Q \gg 1 . \tag{2b}$$

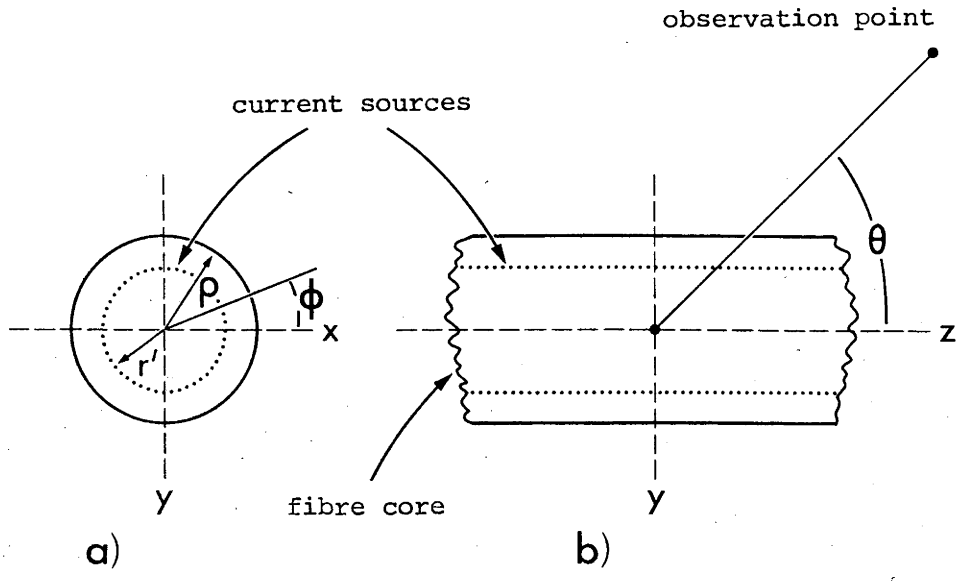

Fig. 1: Tubular current sources within the core of an optical fibre. The currents have $\cos\ell\phi$ symmetry and arbitrary z variation.

For sources in the cladding (i.e. $R' > 1$) the correction factor becomes

$$C(\theta) = 1 - H_\ell^{(1)}(QR')\{UJ_{\ell+1}(U)\ J_\ell(Q) - QJ_{\ell+1}(Q)\ J_\ell(U)\}/J_\ell(QR')\ W_\ell(U,Q) \tag{3a}$$

$$\sim 1, \qquad U \cong Q \gg 1. \tag{3b}$$

The function $W_\ell(U,Q)$ is defined as

$$W_\ell(U,Q) = UJ_{\ell+1}(U)\ H_\ell^{(1)}(Q) - QJ_\ell(U)\ H_\ell^{(1)}(Q) \tag{4a}$$

$$= \frac{2i}{\pi}, \qquad U = Q, \tag{4b}$$

where J_ℓ and H_ℓ are Bessel and Hankel functions. The parameters U and Q are related to the angle θ of Fig. 1(b) as

$$Q = \rho k_{cl} \sin\theta = (U^2 - V^2)^{\frac{1}{2}}, \tag{5}$$

where ρ is the fibre radius, V the usual fibre parameter

$$V = \rho(k_{co}^2 - k_{cl}^2)^{\frac{1}{2}} = \rho k_{co} \sin\theta_c \tag{6}$$

and θ_c, the complement of the critical angle, is

$$\theta_c \cong \mathrm{Sin}\theta_c = [1 - (k_{cl}^2/k_{co}^2)]^{\frac{1}{2}} . \tag{7}$$

9.2.2 The Graded Profile

Expressions for the correction factor C for graded index fibres take a similar analytical form as the equations for the step. We require only the equivalent of $J_\ell(UR)$ for the graded core medium. Since we assume a uniform cladding, the field solution in the cladding will be the same as for the step. Accordingly, if $F_\ell(UR)$ denotes the field solution in the core of the graded-fibre we can apply the following transformation to the step equations:

$$J_\ell(UR) \rightarrow F_\ell(UR) \tag{8a}$$

$$J_\ell(U) \rightarrow F_\ell(U) \tag{8b}$$

$$\left.\begin{array}{l} J_\ell(Q) \\ H_\ell(Q) \end{array}\right\} \text{unchanged} \quad \begin{array}{l} (8c) \\ (8d) \end{array}$$

and use the resultant expressions to determine radiation from graded core fibres.

Numerical methods are required, in general, to determine $F_\ell(UR)$ exactly for arbitrary profiles. For power law profiles of exponent q, however, we can use the power series solution defined in Chapter 3 [4,5]. We consider here the power law profiles with exponent $q = 1,2$ as shown in Fig. 2. These are examples which demonstrate the effects of severe grading in the core.

9.3 SOURCES WITH SINUSOIDAL z DEPENDENCE

We consider the case of sinusoidal perturbations of the core radius along the length of the fibre. This type of variation is of

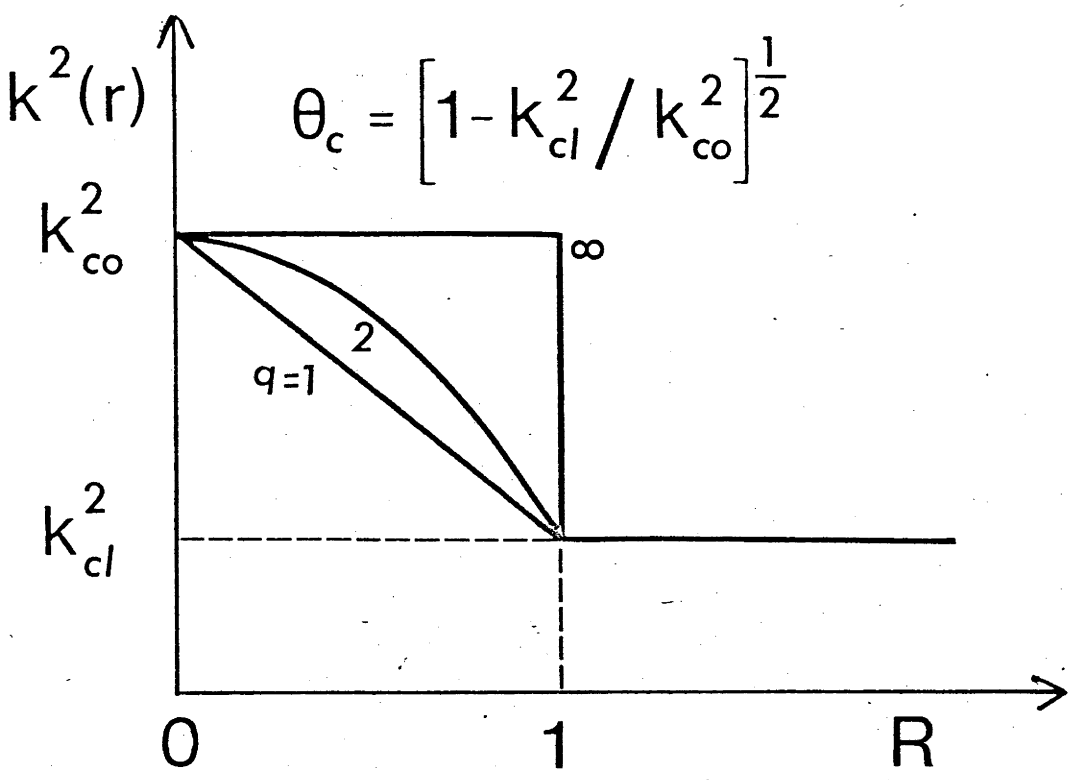

Fig. 2: Power law refractive index profiles considered in this chapter. The $q = 1$ and $q = 2$ are examples of profiles with severe grading.

practical importance since in fibre manufacture machine vibrations can introduce a small amplitude ripple of stable period. A perturbation of this type can be treated as a distribution of induced currents along the surface of the tubular cylinder and in its more general form has a spatial dependence $e^{i\alpha z}$ $\mathrm{Sin}\gamma z$. For this exceptional case all radiation is at one angle $\theta = \theta_o$ only [2,3,6], where θ_o is given by

$$\theta_o = \mathrm{Cos}^{-1}[(\alpha - \gamma)/k_{cl}] . \tag{9}$$

The radiated power than has the form

$$P = |C|^2 \, P^{FS} \tag{10}$$

which for current sources in the x direction becomes [1]

$$P = \kappa|C|^2 \ (1+\cos^2\theta_o) \ J_\ell^2(Q_o R') \tag{11a}$$

$$\sim \kappa(1+\cos^2\theta_o) \ J_\ell^2(U_o R') \ , \qquad R' \leq 1, \ U_o \cong Q_o >> 1 \tag{11b}$$

$$\sim \kappa(1+\cos^2\theta_o) \ J_\ell^2(Q_o R') \ , \qquad R' > 1, \ U_o \cong Q_o >> 1 \ . \tag{11c}$$

The constant κ depends on the length of the source and other constants related to P^{FS}, U_o and Q_o are given by eqns (5) and (6) with $\theta = \theta_o$.

9.4 RESULTS FOR THE FUNDAMENTAL HE_{11} MODE ($\ell = 0$)

In Fig. 3 P/κ is plotted for the fundamental mode ($\ell = 0$) of the three profiles shown in Fig. 2. We consider the case where the source position is at the core-cladding boundary ($R' = 1$), θ_c the complement of the critical angle has value 0.1 and $V = 2.4$, the cutoff value for the step profile. It is clear that the more graded the profile (i.e. the less core material present) the more "free space"-like the radiation pattern becomes.

In Figs. 4, 5 and 6 the radiation pattern is compared to that of free space for sources at (a) $R' = 1$ and (b) $R' = \frac{1}{2}$ at V values corresponding to cutoff for each profile considered. We find that the displacement from free space is similar in each case.

We can understand this behaviour in terms of $\bar{V}$, the average V, where

$$\bar{V} = \sqrt{2\Omega_0} \ V \ . \tag{12}$$

Ω_0 is the degree of guidance [7,8] as defined in Chapter 6, which is related to the amount of core material present in the fibre. Profiles with the same $\bar{V}$ have the same amount of material present in the core. At cutoff [7]

$$\bar{V}_{co} \cong 2.4 \tag{13}$$

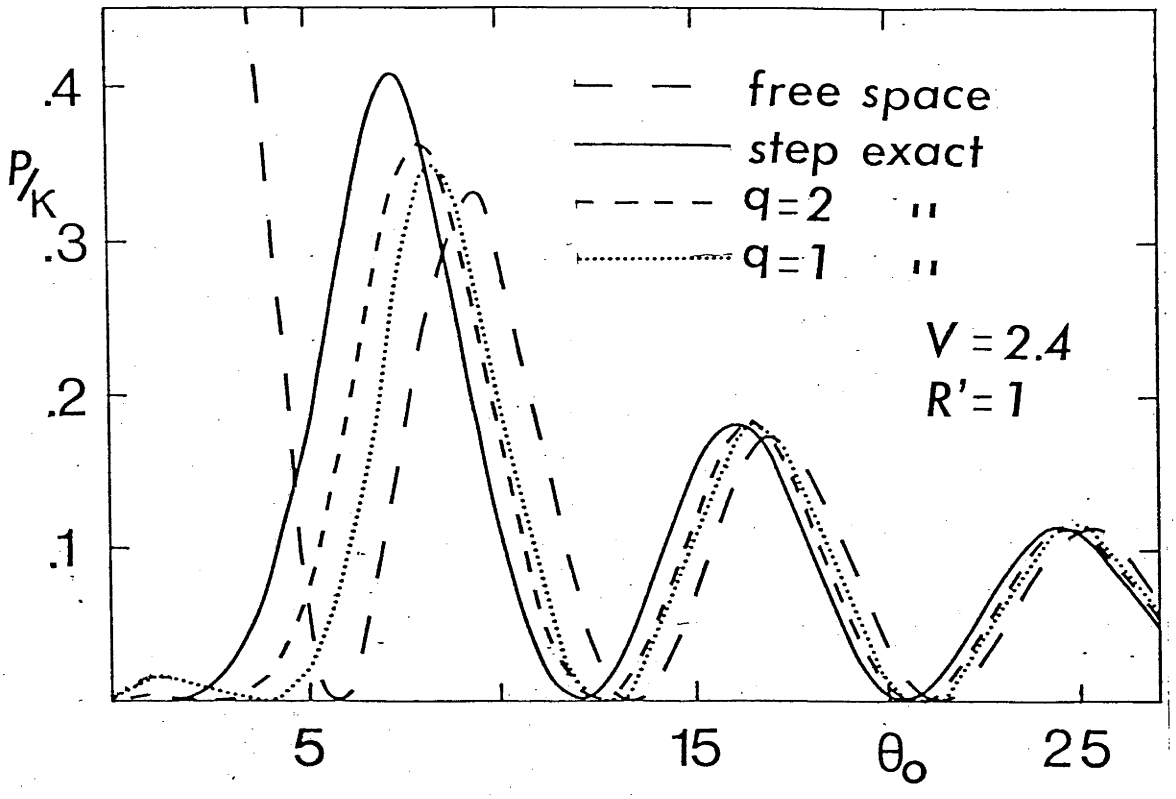

Fig. 3: Comparison of radiation for the three power law profiles $q = 1$, $q = 2$ and $q = \infty$ (step) with that of free space at $V = 2.4$ which is V_{co} for the step.

for arbitrary profiles. Therefore, for the plots in Figs. 4, 5 and 6, given the same θ_c and the same wavelength, similar amounts of core material are present; this results in similar distortions to the free space radiation.

9.5 APPROXIMATIONS

For arbitrary refractive index profiles the field solution in the core, $F_\ell(UR)$, requires numerical methods to be determined exactly. However, approximation techniques can be used which still provide accurate analytic solutions for the arbitrary profile.

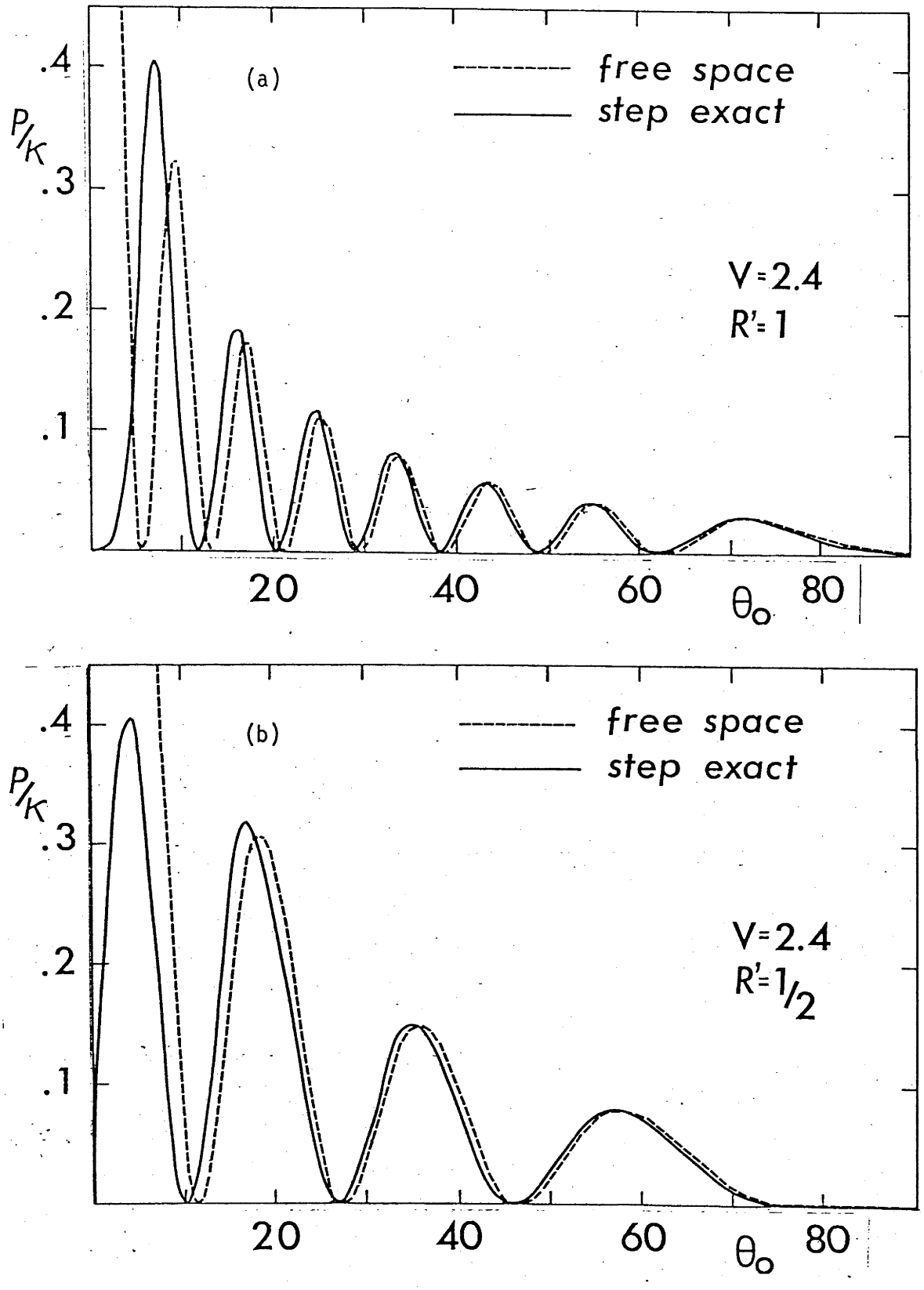

Fig. 4: Comparison of the exact radiation due to current sources, (a) on the core-cladding boundary ($R' = 1$) and (b) inside the core ($R' = \frac{1}{2}$), with the free space radiation for the step refractive index profile of $V = 2.4$ (i.e. of V_{co} for the step).

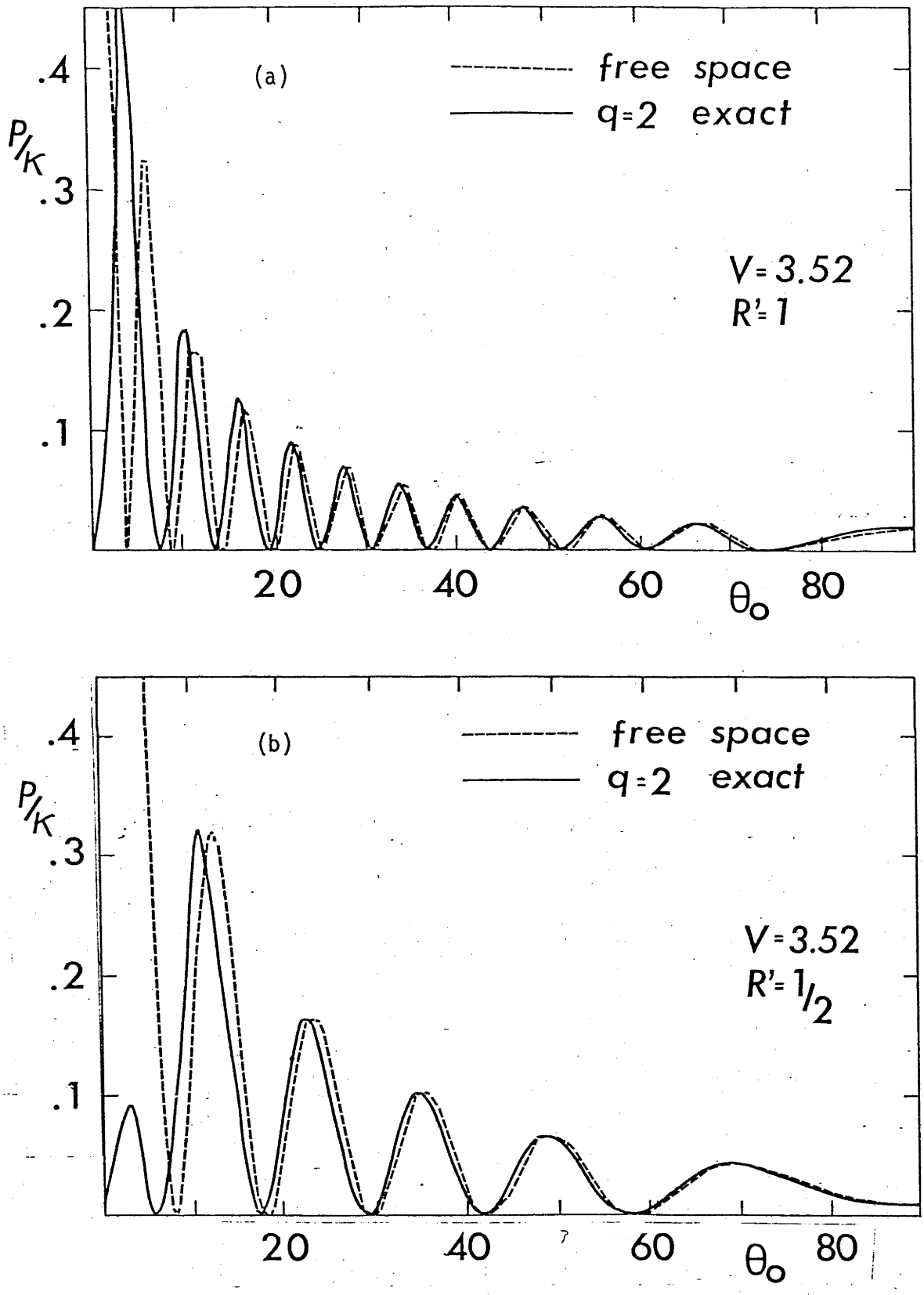

Fig. 5: As in Fig. 4 for the q = 2 profile of V = 3.52 (i.e. V_{co} for this profile.

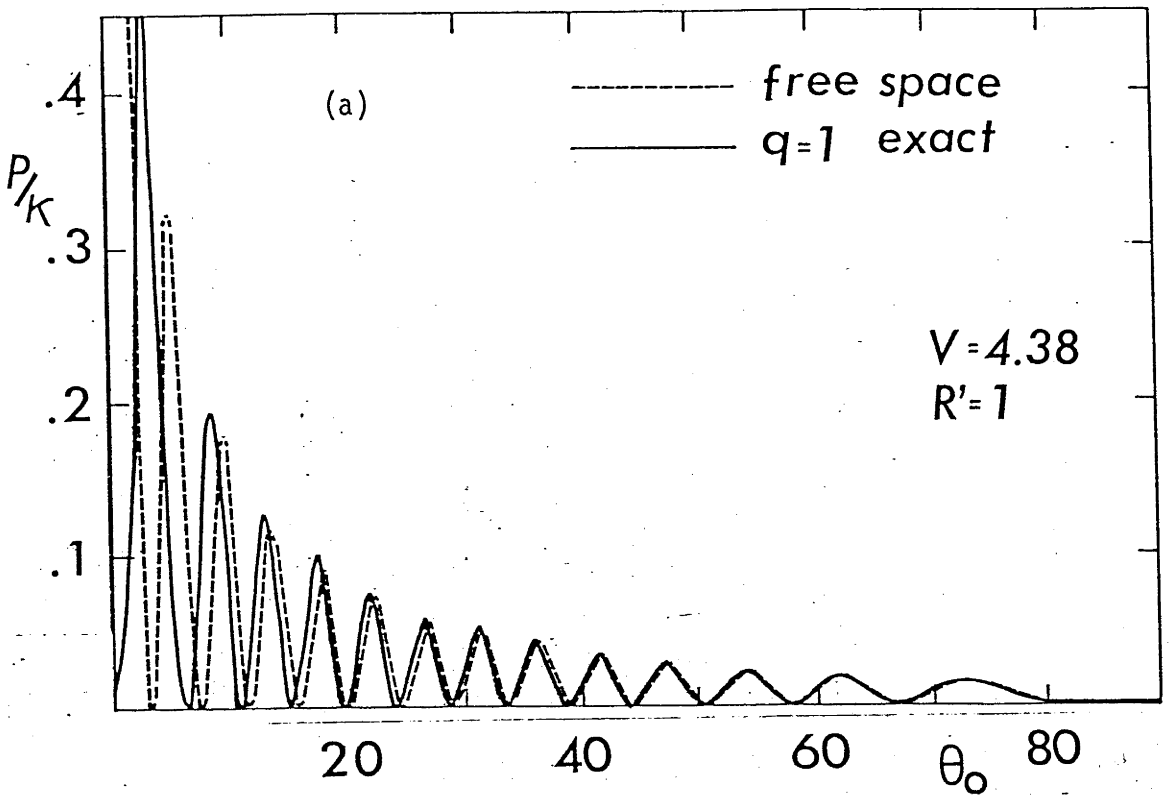

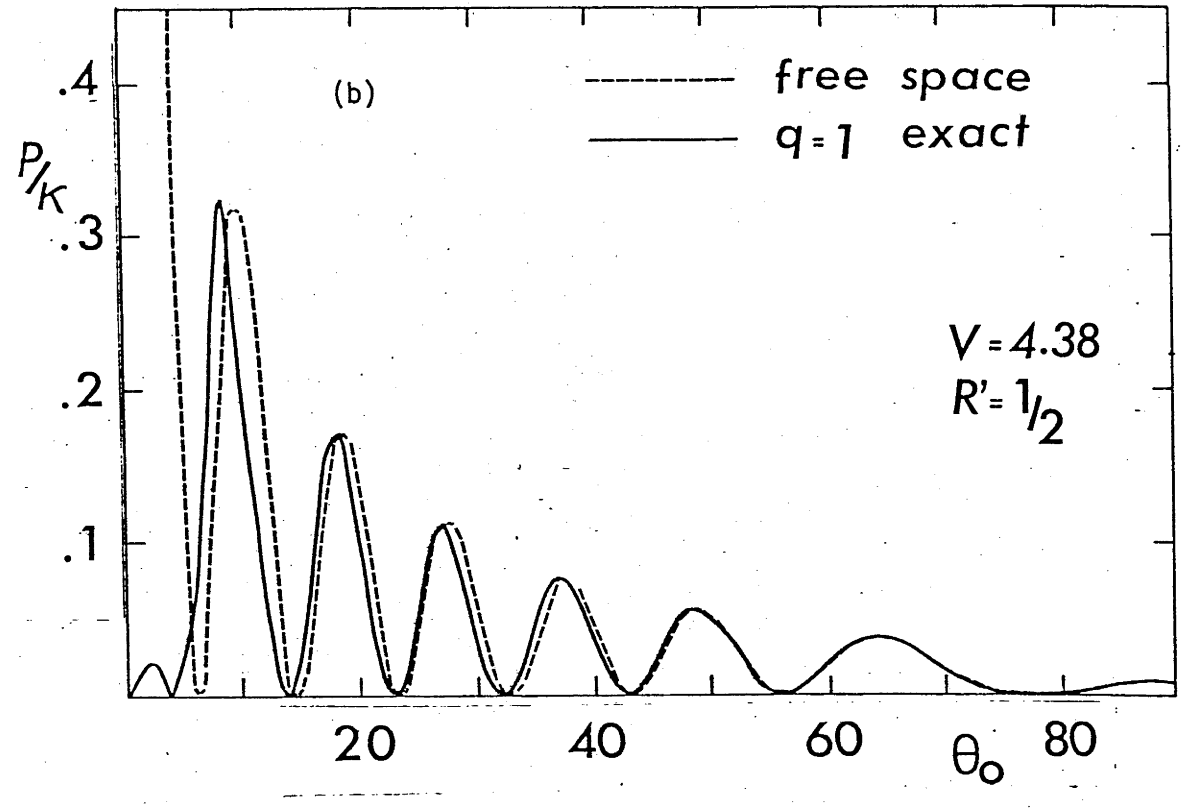

Fig. 6: As in Fig. 4 for the q = 1 profile at V = 4.38 (i.e. V_{co} for this profile).

9.5.1 The Equivalent Step Method

Following the earlier discussion that single mode fibres with the same θ_c and the same $\bar{V}$ can cause similar distortion to free space radiation, the graded fibre is approximated by a step fibre with the same θ_c but now with a core radius (ρ_s) determined such that its degree of guidance is the same as that of the graded fibre (i.e. $\rho_s = \sqrt{2\Omega_0}$). The source remains at the same position as in the graded case. The step equations, 2(a), 3(a), 4 and 11(a), then apply. The results, using this approximation are illustrated in Figs. 7 and 8 for the $q = 1,2$ profiles for sources at (a) $R' = 1$ and (b) $R' = \frac{1}{2}$. Correct behaviour is obtained for small θ_o and the approximation becomes exact as the angle θ_o gets large.

9.5.2 The W.K.B. Approximation

When the term (UR) is sufficiently large the W.K.B. asymptotic approximation for the field solution in the core, $F_\ell(UR)$, can apply. With U defined by eqn (5) we observe that $U >> 1$ except for on-axis ($\theta_o = 0$) radiation when $U = V$. We can then write [1]

$$F_\ell(UR') = \left(\frac{2}{\pi R' X(R')}\right)^{\frac{1}{2}} \operatorname{Cos}\left(\frac{\pi}{4} - \int_{R_{it}}^{R'} X(\xi)\, d\xi\right) \tag{14}$$

with $X(\xi)$ defined as

$$X(\xi) = [k^2(\xi) - \beta^2 - (\ell/\xi)^2]^{\frac{1}{2}} . \tag{15}$$

$\beta = k_{cl} \operatorname{Cos}\theta$ and $R_{it} < R' < R_{ot}$, where R_{it}, R_{ot} are solutions of the equation $X(R) = 0$.

This approximation holds for angles $\theta_o \geq \theta_c/V$. For angles smaller than this the expression $X(R)$ goes to zero independently of R and the W.K.B. approximation breaks down. We call this the "full W.K.B." in

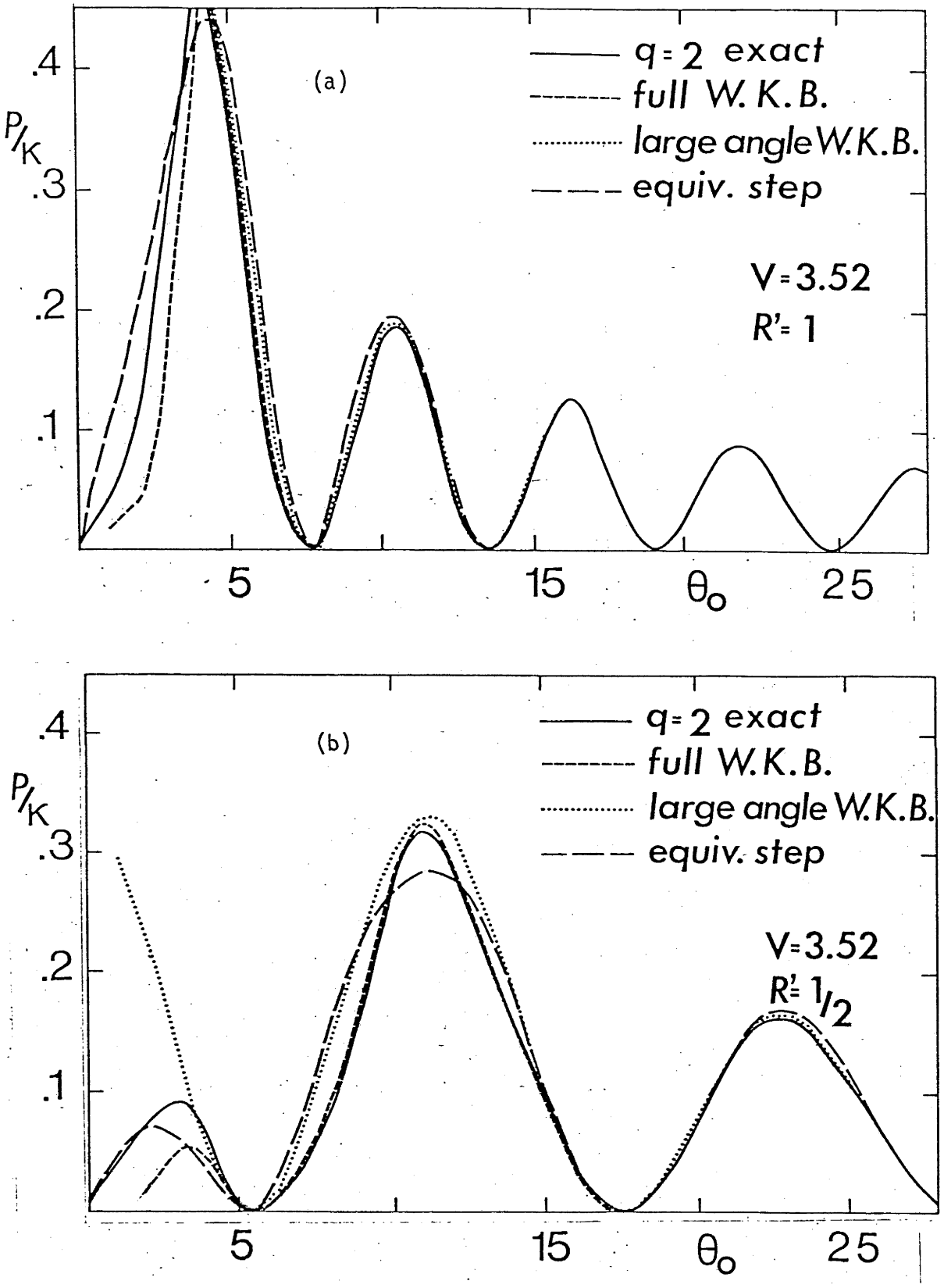

Fig. 7: Comparison of the equivalent step, full W.K.B. and large angle W.K.B. approximation with the exact radiation for the $q = 2$ profile at cutoff; for sources at (a) $R' = 1$ and (b) $R' = \frac{1}{2}$.

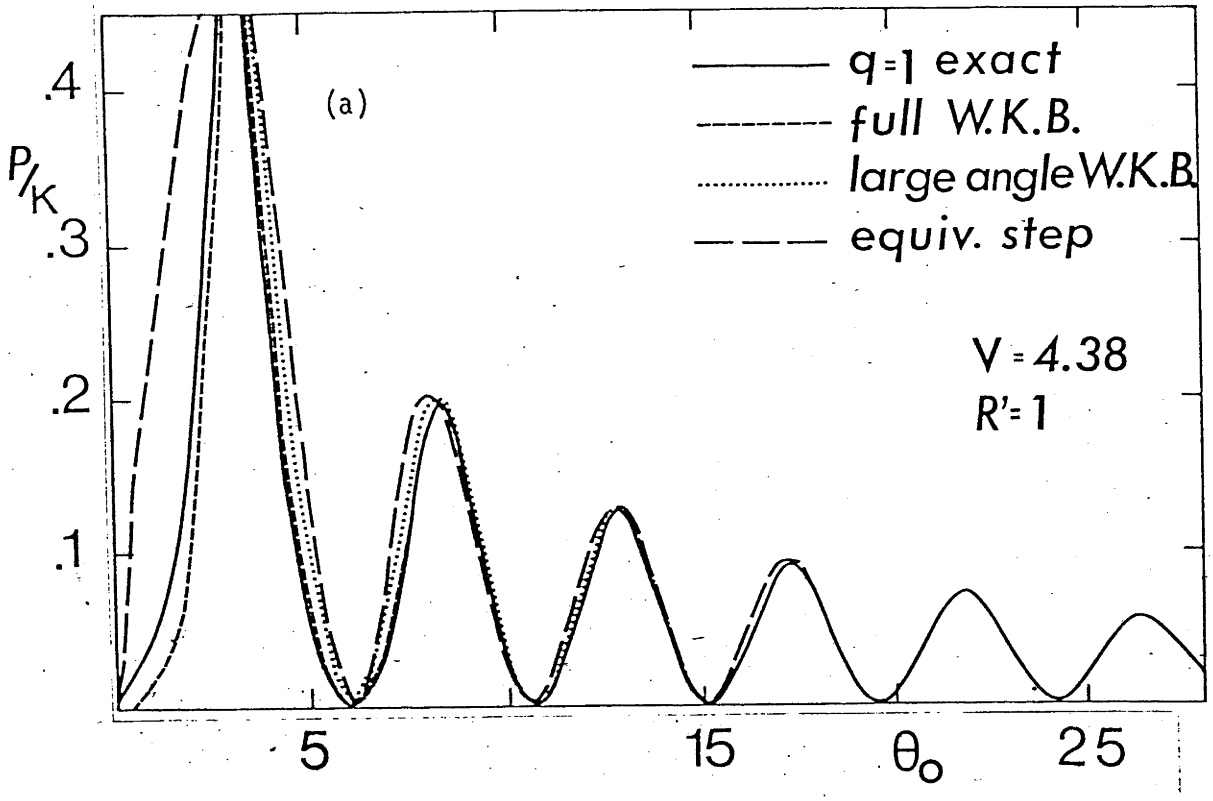

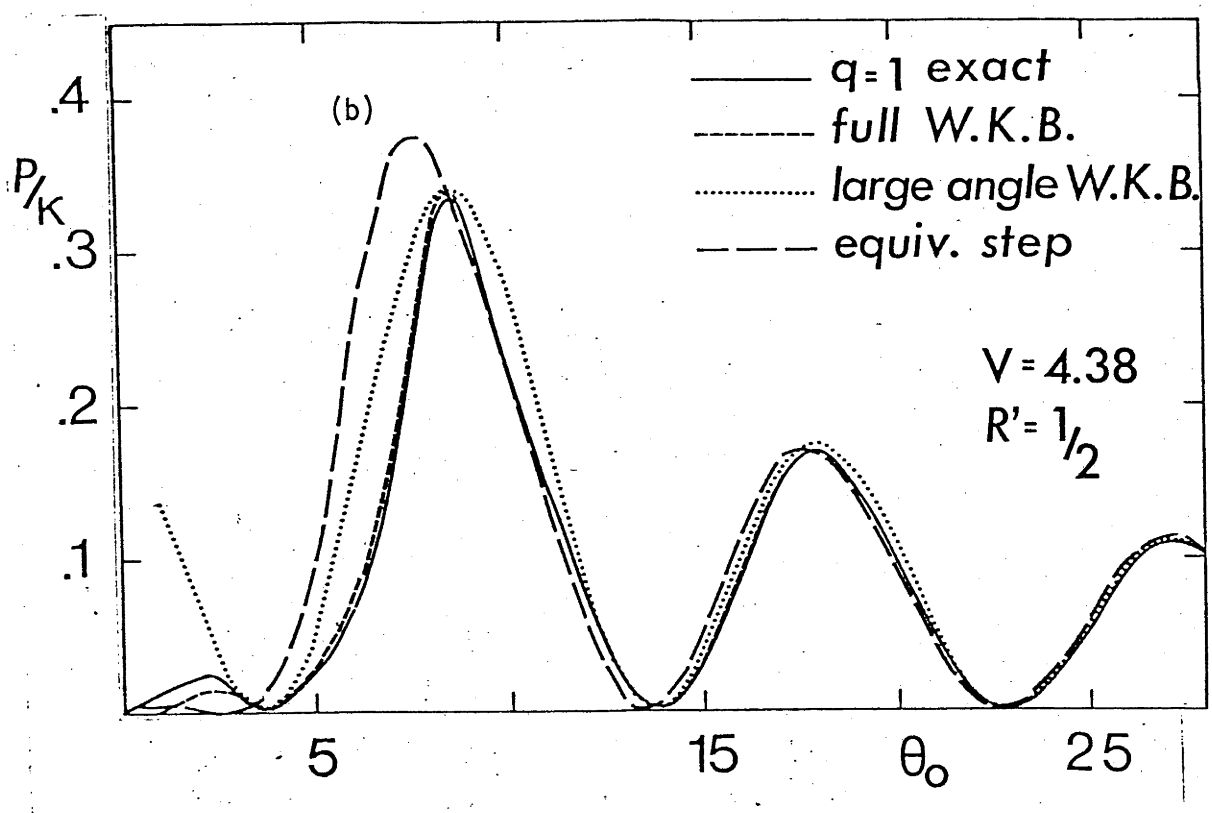

Fig. 8: As in Fig. 7 with q = 1.

Figs. 7 and 8 to distinguish it from the "large angle W.K.B." discussed later. Results shown in these figures are very good for small angles and become exact for large angles.

Unlike the equivalent step, the W.K.B. method applies for all modes and not only the fundamental mode.

9.5.3 Large Angle Approximation

For angles $\theta_o > \theta_c$, the parameters U_o and Q_o are large and approximately equal. In this case we can make the approximation $U_o \cong Q_o >> 1$, called the "large angle approximation".

9.5.3.1 Step index fibre

Using the large angle approximation, eqns 2(b), 3(b) and (11b,c) apply. Results for the step are plotted in Fig. 9. Results for (a) $R' = 1$ have already been considered by Snyder [1] and we also consider (b) $R' = \frac{1}{2}$. The lower "frequency" of zeros when the source is inside the core is due to the dominance of the $J_\ell(UR')$ term, whose variable is reduced as R' gets smaller. Excellent agreement is achieved for angles $\theta_o \geq \theta_c$.

9.5.3.2 Graded index fibre

Making the same approximation as for the step, the W.K.B. method is applied for the graded profile. These results are plotted in Figs. 7 and 8 and we again find that for angles $\theta_o \geq \theta_c$ the agreement with the exact field is very good.

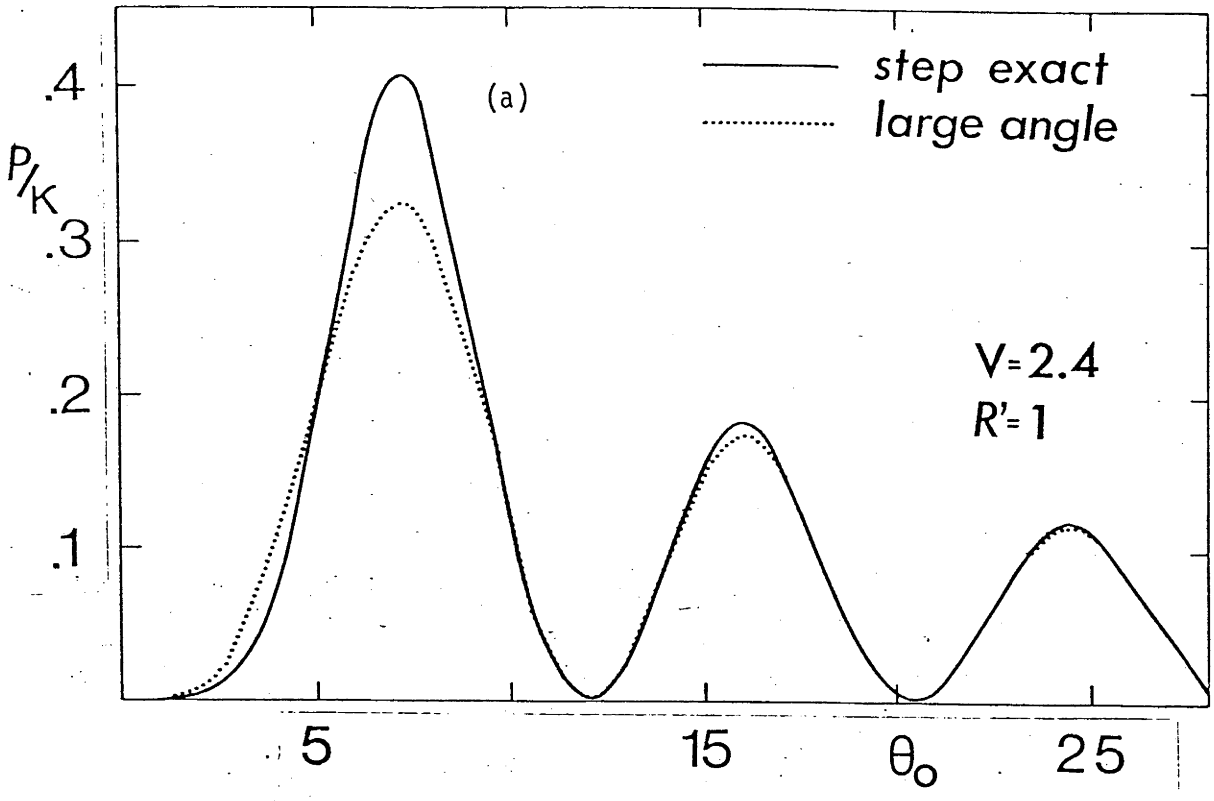

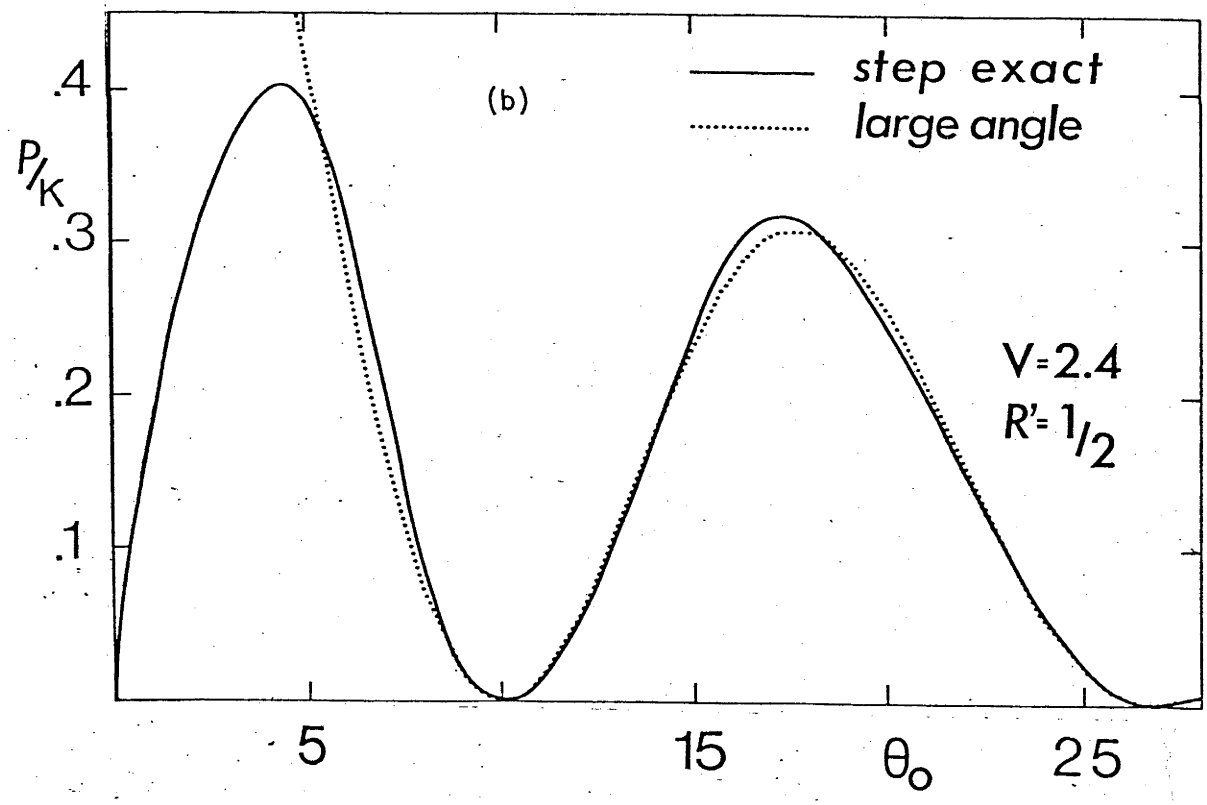

Fig. 9: Comparison of the large angle approximation for the step profile with exact radiation for sources at (a) R' = 1 and (b) R' = ½.

9.6 RESUMÉ

In this chapter we have examined radiation from graded index optical fibres. Using the point of view that the fibre can be considered as a uniform cladding region perturbed by the core, enabled us to examine radiation from sources in the fibre in terms of a "distortion" of the free space radiation pattern. We established that the extent of the distortion is closely related to the amount of core material present in the fibre.

For radiation from the fundamental mode of single mode fibres we exploited this fact, and, rather than solve for the exact field in the graded core, we approximated the graded core by a step index core with the same degree of guidance (i.e. with the same amount of core material). This provides excellent qualitative results for angles $\theta_o \cong 0$ and becomes exact for large angles.

We also examined the accuracy of the W.K.B. method for fields in the graded core. This provides excellent results except for on-axis radiation.

The W.K.B. method can, however, also be applied to multimode fibres and is not restricted to single mode fibres as is the equivalent step.

REFERENCES

1. Snyder, A.W.: 'Weakly guiding optical fibers', *J. Opt. Soc. Am.* 70, 405-411 (1980).

2. Marcuse, D.: *Theory of Dielectric Optical Waveguides* (Academic, New York, 1976).

3. Snyder, A.W., Sammut, R.A.: 'Radiation from optical waveguides — leaky mode interpretation', *Electron. Lett.* 15, 58-60 (1979).

4. Gambling, W.A., Matsumura, H.: 'Propagation in radially inhomogeneous single mode fibres', *Opt. & Quantum Electron.* 10, 31-40 (1978).

5. Love, J.D.: 'Power series solutions of the scalar wave equation for cladded, power-law profiles of arbitrary exponent', *Opt. & Quantum Electron.* 11, 464-466 (1979).

6. Snyder, A.W.: 'Radiation losses due to variations of radius on dielectric or optical fibres', *IEEE* MTT-18, 608-615 (1970).

7. Gambling, W.A., Matsumura, H., Ragdale, C.M.: 'Wave propagation in a single mode fibre with dip in the refractive index', *Opt. & Quantum Electron.* 10, 301-309 (1978).

8. Hussey, C.D., Pask, C.: 'Single mode fibres in a few moments', *Electron. Lett.* 17, 644-645 (1981).